Multizone Modeling of Airborne Quanta Transmission and CO_2-based Ventilation Designs

for Assessing Indoor Exposures

Shujie Yan

A Thesis

In the Department

of

Building, Civil, and Environmental Engineering

Presented in Partial Fulfillment of the Requirements

For the Degree of

Doctor of Philosophy (Building Engineering) at

Concordia University

Montreal, Quebec, Canada

September 2024

CONCORDIA UNIVERSITY

SCHOOL OF GRADUATE STUDIES

This is to certify that the thesis prepared

By: Shujie Yan

Entitled: Multizone Modeling of Airborne Quanta Transmission and CO_2-based Ventilation
Designs for Assessing Indoor Exposures

and submitted in partial fulfillment of the requirements for the degree of

DOCTOR OF PHILOSOPHY (*Department of Building, Civil and Environmental Engineering*)

complies with the regulations of the University and meets the accepted standards with respect
to originality and quality.

Signed by the final examining committee:

_____ Chair

Dr. Fariborz Haghighat

_____ External Examiner

Dr. Jianshun (Jensen) Zhang

_____ Examiner

Dr. Hua Ge

_____ Examiner

Dr. Xianming Zhang

_____ Thesis co-supervisor

Dr. Liangzhu (Leon) Wang

_____ Thesis co-supervisor

Dr. Zhiqiang (John) Zhai

Approved by _____

Dr. Mohamed Ouf

Month/Day/Year _____

Dr. Mourad Debbabi

Gina Cody School of Engineering and Computer Science

Abstract

Multizone Modeling of Airborne Quanta Transmission and CO_2-based Ventilation Designs for Assessing Indoor Exposures

Shujie Yan, Ph.D.
Concordia University, 2024

In indoor environments, ventilation is essential for diluting or removing contaminants, pathogens, excess heat, and moisture, thereby ensuring a healthy and comfortable space. The COVID-19 pandemic underscored the critical role of ventilation in controlling airborne respiratory infections indoors. During this period, inadequate ventilation systems and improper operations in densely populated public spaces were frequently linked to outbreaks and superspreading events, heightening concerns over indoor exposure risks for occupants. As COVID-19 restrictions begin to relax globally, the focus is transitioning to long-term management strategies for the virus. This transition necessitates a comprehensive understanding of the specific ventilation requirements for various indoor spaces. It is imperative to swiftly and accurately assess ventilation conditions and consistently ensure an adequate supply of clean air. This study focuses on mitigation strategies to reduce indoor exposure risks and prepare for the post-pandemic era. The multizone CONTAM modeling of aerosol transport under different mechanical mitigation strategies was investigated in five DOE prototype buildings. To utilize field evidence for improving indoor air quality, a novel approach integrating Bayesian inference and stochastic CO_2 grey-box models was applied. This approach was used to evaluate the ventilation conditions within two primary school classrooms in Montreal. The Equivalent Clean Airflow Rate (ECAi) was calculated following ASHRAE 241, revealing an insufficient clean air supply in both classrooms. To achieve a sufficient ECAi, an additional 0.38 m^3/s of clean air delivery rate (CADR) from air-cleaning devices is recommended. Finally, steady-state CO_2 thresholds (C_{limit}, C_{target}, and C_{ideal}) were established to indicate when ECAi requirements could be achieved under various mitigation strategies.

Acknowledgements

First and foremost, I would like to express my deepest appreciation to my supervisor, Professor Liangzhu (Leon) Wang for his guidance and support throughout my Ph.D journey. His enthusiasm, strong motivation, and immense knowledge have deeply inspired me. His support allowed me to deeply immerse myself in the built-environment field, engage in meaningful research projects, and develop skills in addressing scientific questions. He has encouraged me to approach academic problems with professionalism, consideration, and rigor. Thank you for your supervision and support at every stage of my Ph.D. studies.

I would also like to express my sincere appreciation to Professor Zhiqiang (John) Zhai for his valuable time, advices, and expertise in co-supervising my Ph.D research studies. His constructive guidance and suggestions play an essential role in shaping this research. Big thanks to Professor Shelly Miller for her insightful comments and esteemed advice in the cooperation of our research projects.

I am grateful to the members of my dissertation committee, Professor Fariborz Haghighat, Professor Hua Ge, and Professor Xianming Zhang, for their precious, critical, and insightful comments on my thesis work.

I would like to acknowledge the supports from National Research Council Canada, Dr. Liang (Grace) Zhou, Dr. Justin Berquist, and Dr. Chang Shu. Without their support, the experimental validations of the developed model in this research would be impossible. Thanks for the suggestions and discussions during this research.

Great thanks to all the group members in Professor Leon's lab. I appreciate the help and supports from my colleagues and friends, Jiwei Zou, Maher Albettar, Bingyan Jia, Dongxue Zhan, Dr. Danlin Hou, Dr. Senwen Yang and Saki, Dr. Lili Ji, Eslam Mohamed, Ibrahim Reda, Jing Li, Zahra Salehi, Shengwei Fu, etc. Special thanks go to Maher for his kindly instructing me about establishing Niagara IoT framework. I am lucky to meet and work with all of you.

Table of Contents

List of Figures

List of Tables

Nomenclature

A_L Effective air leakage area [m²]

B Breathing rate [m³/s]

C Number of infection cases

C_{avg} Average quanta concentration [quanta/m³]

C_D Flow discharge coefficient

C_i Contaminant concentration in the infectious zone [quanta/m³]

C_j Contaminant concentration in neighbor zones [quanta/m³]

C_s Contaminant concentration of the supply air [quanta/m³]

C_{rec} Contaminant concentration of the recirculation air [quanta/m³]

C_{oa} Contaminant concentration of the outdoor air [quanta/m³]

C_r CO_2 concentration in the room [ppm]

C_{out} CO_2 concentration of outdoor air or ventilation flows [ppm]

ΔC_r Change in C_r over the time step Δt

E Total volumetric CO_2 generation rate in the room [L/s]

F_m Percentage of mask-wearing occupants

G Generation rate of quanta from the infector [quanta/m³]

M_{inh} Inhale removal efficiency of masks [%]

M_{exh} Exhale efficiency of masks [%]

n	Number of inhaled quanta
Q	Volumetric flow rate [m³/s] or ventilation rate [L/s]
Q_e	Equivalent air change rate [1/h]
Q_{OA}	Outdoor air ventilation rate [1/h]
Q_{MERV}	Equivalent air change rate from MERV filters [1/h]
Q_{PAC}	Equivalent air change rate from portable air cleaner [1/h]
Q_{GUV}	Equivalent air change rate from in-duct GUV light [1/h]
$Q_{deposition}$	Quanta deposition rate [1/h]
$Q_{deactivation}$	Viral deactivation rate [1/h]
Q_r	Volumetric flow rate of the return air [m³/s]
Q_{lx}	Volumetric flow rate of the local exhaust air [m³/s]
Q_{ac}	Volumetric flow rate of the air cleaner [m³/s]
Q_{UVr}	Equivalent volumetric flow rate of in-room GUV devices for pathogen inactivation [m³/s]
Q_{dep}	Equivalent volumetric flow rate of aerosol deposition [m³/s]
Q_{dec}	Equivalent volumetric flow rate of viral aerosol decay/inactivation [m³/s]
Q_{exf}	Exfiltration flow rate to neighbor zones [m³/s]
Q_{inf}	Infiltration from zone j [m³/s]
Q_{exf}	Exfiltration from zone j [m³/s]

S	Number of susceptible individuals
t	Time [s]
V	Volume [m³ or L]
Δt	Exposure time [h]
ΔP_r	Reference pressure difference [Pa]
$\Delta P_{j,i}$	Pressure difference between zone j and zone i [Pa]
C_E	Conversion factor from volumetric concentration to ppm [10^6 ppm]
W_t	Wiener process
σ	Incremental variance in the Wiener process [ppm/$\sqrt{dt}$]
Z	Standard normal random variable [mean 0, variance 1]

Contribution of authors

Chapter 3 of this thesis is based on the following published journal paper:

Yan, S., Wang, L. L., Birnkrant, M. J., Zhai, J., & Miller, S. L. (2022). Evaluating SARS-CoV-2 airborne quanta transmission and exposure risk in a mechanically ventilated multizone office building. Building and Environment, 109184

Contributions: Shujie Yan proposed the methodology and designed the analysis, performed the simulations, visualized the results and wrote the paper. Liangzhu (Leon) Wang contributed to the original draft, conceptualization, methodology, formal analysis, review, and editing. Michael J. Birnkrant contributed to the project administration. Zhiqiang (John) Zhai contributed to review and editing. Shelly Miller contributed to review and editing.

Chapter 4 of this thesis is based on the following published journal paper:

Yan S, Wang L, Birnkrant MJ, Zhai Z, Miller SL. Multizone Modeling of Airborne SARS-CoV-2 Quanta Transmission and Infection Mitigation Strategies in Office, Hotel, Retail, and School Buildings. Buildings. 2023; 13(1):102. (Issue Cover)

Contributions: Shujie Yan proposed the methodology and designed the analysis, performed the simulations, visualized the results and wrote the paper. Liangzhu (Leon) Wang contributed to conceptualization, methodology, formal analysis, review, and editing. Michael J. Birnkrant contributed to the project administration. Zhiqiang (John) Zhai contributed to review and editing. Shelly Miller contributed to review and editing.

Chapter 5 of this thesis is based on the following unpublished manuscripts:

Yan, S., Zou, J., Shu, C., Berquist, J., Brochu, V., Veillette, M., Hou, D., Duchaine, C., Zhou,

L., Zhai, Z., & Wang, L. Implementing Bayesian inference on a stochastic CO_2-based grey-box model for assessing indoor air quality in Canadian primary schools. (2024, in submission)

Chapter 1 Introduction

1.1 Introduction

The COVID-19 pandemic has underscored the critical importance of controlling airborne respiratory infections in indoor environments [1-4]. Insufficient ventilation designs and improper operations in crowded public buildings often lead to outbreaks and superspreading events, raising significant concerns about occupants' indoor exposure [5-7]. Consequently, many countries implemented shutdowns of public shared spaces, compelling individuals to "stay at home" [8, 9]. Recently, as many countries have eased restrictions, there has been a shift towards the long-term management of COVID-19 [10, 11]. The challenge now lies in reopening public spaces while simultaneously reducing transmission risks [12, 13].

Engineering mitigation strategies can effectively reduce the airborne transmission of pathogens such as SARS-CoV-2, measles, tuberculosis (TB), chickenpox, and influenza in public spaces [14-16]. Virus-laden aerosols in the air can be diluted with outdoor air, trapped by filters, or disinfected using germicidal ultraviolet light (GUV) [17-19]. It is therefore crucial to determine the adequate amount of outdoor ventilation air needed to control airborne disease transmission in different building types, identify appropriate air treatment options, and implement measures to manage infection risks, especially in the current post-pandemic era [7, 20-22].

Multizone building simulations provide deeper insights into aerosol transmission potential within real buildings and systematically consider the influence of different mitigation strategies across the entire building context [23-25]. Besides accounting for building leakage, multizone simulations enable the evaluation of average and transient contaminant concentrations during occupant exposure, thus helping to assess infection risks. Estimating ventilation air change rates in indoor environments remains a challenging task due to inherent uncertainties in the deterministic approach commonly used, which struggles to account for system uncertainties

[26]. These uncertainties can stem from model limitations, unknown or uncertain parameters, measurement noise, and estimation bias [27, 28]. Efforts have been made to address these uncertainties through stochastic modeling principles for indoor air quality (IAQ) predictions [29-32]. The stochastic grey-box model [33, 34], which combines physical system principles with data from field measurements, has shown promise in managing these uncertainties. However, its potential for estimating ventilation rates using CO_2 measurements in rooms has not been extensively explored. Additionally, critical parameters such as room occupancy and CO_2 generation rates from occupants are often unavailable, resulting in significant uncertainties. It has been suggested that these parameters could be reasonably inferred with Bayesian inference based on measurements data [35, 36]. Thus, integrating the stochastic CO_2-based grey-box model with Bayesian inference has significant potential to improve the precision of ventilation rate predictions.

In summary, this study aims to develop effective strategies in response to the COVID-19 pandemic and to improve indoor air quality (IAQ) in the post-pandemic era. The first part investigates multizone modeling of aerosol transmissions to determine the priorities of different mechanical mitigation strategies. This study also introduces a novel methodology that integrates Bayesian inference with a CO_2-based stochastic grey-box model to enhance the prediction accuracy of indoor ventilation conditions.

1.2 Research objectives

In light of the ongoing challenges posed by the COVID-19 pandemic, it is essential to develop comprehensive strategies for reducing airborne transmission risks in various indoor environments. This research aims to address these challenges by focusing on several key objectives that will contribute to safer indoor air quality and effective infection control measures. The main research objectives of this study are as follows:

- Develop an approach to evaluate aerosol infection risks of SARS-CoV-2 in multizone CONTAM buildings: This objective involves creating a robust methodology to assess

2

how SARS-CoV-2 aerosols spread and pose infection risks within different zones of a building modeled in CONTAM. This approach will help in understanding the dynamics of airborne transmission in complex indoor environments and identify high-risk areas.

- Evaluate the effectiveness of different engineering mitigation measures on reducing infection risks in offices, hotels, retail spaces, and schools: By testing various engineering strategies, such as enhanced ventilation, filtration, and UV disinfection, this research aims to determine which measures are most effective in different types of buildings. This evaluation will provide practical recommendations for mitigating infection risks in diverse public and private spaces.

- Integrate Bayesian inference with a CO_2-based stochastic grey-box model for a better estimation of ventilation rate and confirm its validity: This objective focuses on improving the accuracy of ventilation rate estimates by combining Bayesian inference techniques with a CO_2-based stochastic grey-box model. This integration will allow for more precise and reliable predictions of indoor air quality, accounting for uncertainties and variable conditions.

By addressing these objectives, this study aims to advance our understanding of aerosol transmission in indoor environments and develop effective strategies to mitigate infection risks, thereby contributing to safer and healthier building designs in the post-pandemic era.

1.3 Outline of the thesis

This chapter introduces the background and the main objectives of this study. To achieve the research objectives, this study proposes a novel approach for assessing indoor infectious risks using CONTAM-quanta simulations. This method was subsequently applied to five commercial DOE prototype buildings to identify the necessary air-cleaning efforts for various scenarios. Additionally, a CO_2-based ventilation design approach was developed to assist in long-term control of indoor aerosol transmission, using measurement evidence. The practices were illustrated using the measurements from Canadian primary classrooms. The following

chapters are organized as follows:

Chapter 2 reviews the literature related to multizonal aerosol modeling and CO_2-based ventilation designs. It begins by exploring previous efforts in using CONTAM multizone modeling for assessing indoor air quality. A comprehensive review is conducted on studies related to multizonal aerosol transmission, risk assessments, and various mitigation strategies. To further enhance the CONTAM modeling framework, the chapter examines research that utilizes CO_2 as an indicator of indoor ventilation conditions. Additionally, the review includes studies on Bayesian inference and stochastic CO_2 grey-box models, which show promising potential for predicting ventilation rates through in-situ CO_2 monitoring.

Chapter 3 presents a novel approach for assessing indoor infectious risks using the CONTAM-quanta simulations. This method evaluates the effectiveness of various mitigation strategies, illustrated through a case study of a Large Office building. Key strategies include increased ventilation, MERV filters, portable air cleaners, UV lights, and mask usage. The findings highlight the most effective measures to reduce infection risks in mechanically ventilated buildings.

Chapter 4 systematically evaluates infection risk mitigation strategies for five prototype commercial buildings using the CONTAM-quanta approach. The study analyzes zone-to-zone quanta transmissions and air treatment strategies under different occupancy levels and masking conditions. Key findings indicate that in-duct air treatment alone is insufficient for small spaces, necessitating additional in-room air-cleaning devices. Correlations of infection risk with room volume, exposure durations, and equivalent air exchanges are developed to generalize findings across different building configurations.

Chapter 5 presents a CO_2-based ventilation design and practices for Canadian classrooms. The proposed approach utilizes Bayesian inference within a stochastic CO_2-based grey-box model to realize long-term indoor air quality management. The study confirms the accuracy and

robustness of the model through CO_2 tracer gas experiments and quantifies uncertainties in real-life contexts. The approach is then applied to evaluate ventilation conditions in two primary school classrooms in Montreal, identifying insufficient clean air supply. Recommendations include supplementing air-cleaning devices to meet required clean airflow rates. Various mitigation strategies are assessed for the classrooms for their equivalent clean air supply levels.

Chapter 6 summarizes the main contributions, limitations and future works of this study.

Chapter 2 Literature review

In this section, previous efforts on CONTAM multizone modeling for indoor air quality and CO_2-based ventilation evaluations were explored. A comprehensive review was conducted on multizonal aerosol transmission studies, risk assessments, and mitigation strategies. Studies related to Bayesian inference and stochastic CO_2 grey-box models were also included, given their promising potential to predict ventilation rates using in-situ CO_2 monitoring.

2.1 Multizone CONTAM modeling of aerosol transmissions

2.1.1 Introduction to the multizone modeling and CONTAM program

Efforts to model multizone airflow began as early as the 1970s, and it was during this period that isothermal wind-driven airflows and network airflow models were first introduced [37-43]. In 1989, an element-assembly formulation of multi-zone contaminant dispersal theory was proposed, and the processes of assembly element equations as well as the development of the CONTAM family program were introduced [44, 45]. Then the model was further modified to incorporate ducted air handling system in the 1990s in CONTAM93 and CONTAM96 [46, 47]. Based on the knowledge of fundamental mass conservation and mechanical energy-conservation rules, semi/fully empirical dissipation relations, assumed boundary conditions, and zone-field assumptions, equations were assembled to control the air flows in multizone buildings [48, 49]. Later, realizing the contaminants dispersal was influenced by building thermal and the need for detailed airflows, methods to couple it with building thermal and computational fluid dynamics (CFD) models were also proposed [50, 51]. Figure 2-1 demonstrates the representation of building models in different detailed levels.
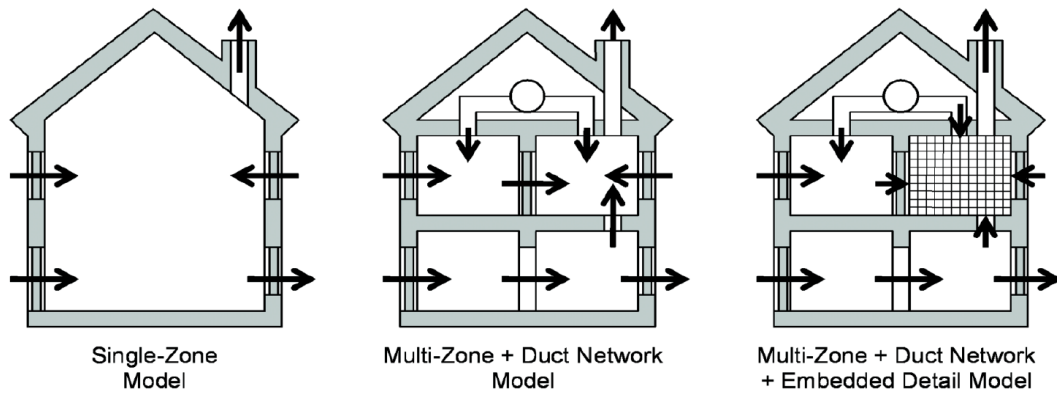
Figure 2-1 The representation of building models with increasing details [37]

Over the years, substantial efforts have been dedicated to assessing the validity of the well-mixed assumptions employed in CONTAM and examining the airflows simulated by it [52, 53]. In 2008, Wang et al. [54] evaluated the well-mixed assumptions made for temperature and contaminants concentration as well as the effects of neglecting air momentum. It was suggested that when the dimensionless temperature gradient is smaller than 0.03 and the Archimedes number for the source zone is larger than 400, the neglection of temperature and contaminants concentration gradient would be acceptable with an estimation error of less than 20%. When windows have large openings accompanied by strong air momentum effects, neglecting air momentum can still be acceptable, provided the distance between the upstream and downstream openings exceeds the maximum jet throw length from the upstream opening. Consequently, the assumptions made to simplify the CONTAM simulations are deemed reasonable and acceptable under most circumstances.

In past decades, empirical validation efforts were devoted to identifying the applicability of CONTAM models [24, 55-58]. Emmerich [24] reviewed the validation efforts on residential-scale CONTAM and COMIS models for the prediction of airflow rates, results suggested that most of the statistical parameters are within or close to the guidelines of ASTM D5157. In 1996, Haghighat and Mergi reported the "good" agreement evidence of airflow predictions for a four-

zone CONTAM model [57]. In their empirical tests, fan pressure tests were conducted with blower doors and the flow coefficient C and flow exponent n were estimated with both active and passive approaches. Verijkazemi et al. [58] compared the CONTAM particulate matter (PM) evaluation results with field measurements in an Iran hospital, and results indicate that the CONTAM can evaluate particle entry into the hospital building effectively under different weather and building operating scenarios.

In 2001, Musser et al. conducted a validation and calibration study on CONTAM, affirming the model's accuracy in simulating pressurized spaces when individual room flow rates were precisely defined based on experimental evidence [59]. The study underscored the significance of accurately refining fan flow rates for spaces like bathrooms and kitchens in buildings, as it directly influences the prediction accuracy. Overall, after decades of rigorous work, CONTAM has been established as a reliable tool for predicting building air flow rates from a macroscopic perspective.

2.1.2 Multizone CONTAM modeling of aerosol transmissions

Multizone building simulations provide a comprehensive understanding of aerosol transmission potential in real buildings, allowing for the systematic evaluation of various mitigation strategies within the entire building context. In addition to accounting for building leakage, multizone simulations enable the assessment of both average and transient contaminant concentrations during occupant exposure, thereby facilitating the evaluation of infection risks.

The multizone modeling was applied to analyze the transmission of virus-laden aerosols between floors through door and window leakages during a SARS outbreak in Hong Kong [60]. The importance of the building leakage and actual building operations was highlighted in a multizone contaminant transport simulation for a hospital building [61]. Emmerich et al. [62] applied the simulation software CONTAM for two infectious agents, a tuberculosis-like particle with a diameter of 0.64 μm and a burst emission, and a squamous cell particle with a

diameter of 10 µm released at a constant generation rate. The study showed the importance of building leakage and the impacts of an actual building system operation. Although their study targeted healthcare facilities, it illustrated the importance of addressing the interactions of weather conditions, mechanical system operations, pressure differentials, and inter-zonal leakages in terms of airborne virus transmission. These interactions cannot be addressed systematically without a multizone building environment modeling approach.

On the other hand, building ventilation renovations are typically conducted at the whole-system scale, making it crucial to consider the interactions between different rooms, buildings, and indoor and outdoor environments [63]. Investigating multizone buildings for specific building types is particularly important as public buildings reopen [64, 65]. Evaluating building-wide protection, rather than just room-level protection, under realistic weather conditions, air leakages, and occupancies, is essential [66, 67]. This approach helps identify gaps in renovation strategies, enhance mitigation effectiveness and efficiency, and develop tailored solutions that address the variable needs of the post-pandemic era, considering specific buildings, climates, and schedules. A few recent multizone simulation studies show the importance of pressure controls and leakages in a hospital building [68, 69] and HVAC filtrations on energy costs in an office building [70, 71]. Besides, López-García et al. combined a zonal ventilation model with a multicompartment SIS Markovian model for evaluating the infection of patients within a hospital ward [72]. However, the inter-zonal airflows have not been studied in depth in a detailed airflow network by the previous studies [61, 73], and the airborne zonal infection transmission in commercial buildings was rarely investigated.

Conducting multizone analysis of airborne disease transmission in buildings with a more physically realistic setting offers numerous benefits for occupant health, safety, productivity, and energy-efficient operation, especially during emergencies such as pandemics. Recently, many countries and governments have recognized the importance of building ventilation and introduced initiatives to retrofit existing buildings for reopening and future epidemics [63, 74].

However, investing government funds to achieve these health, safety, and energy-efficiency goals must consider the complexities and multifactorial interactions within buildings [75]. Additionally, public guidelines provided during the pandemic may be insufficient. Therefore, a physically realistic analysis tailored to different building types and climates is essential.

2.2 Risk assessments and mitigation strategies

Risk assessment is an effective method for evaluating the efficacy of ventilation strategies in controlling infection risks. Since the outbreak of the COVID-19 pandemic, extensive efforts have been made to quantify the risk of SARS-CoV-2 transmission[76-81]. The airborne quanta emission rate was evaluated under various conditions of viral load, respiratory activity, and physical activity levels, providing crucial input for classic Wells-Riley risk assessment models [82-86]. Dai and Zhao [87] examined the impact of air change rates on infection risks in different environments, including buses, classrooms, aircraft cabins, and offices. Shen et al. [88] investigated the effectiveness of various mitigation strategies in indoor settings such as long-term care facilities, schools, meat plants, buses, and taxis. Additionally, a simulation study compared the effectiveness of displacement and mixed-mode ventilation in reducing long-range airborne exposure to SARS-CoV-2 in a small office [89].These studies, based on the assumption of uniform aerosol distribution within a room, considered changes in ventilation rate, exposure time, quanta generation rate, and room volume for different indoor environments. However, their evaluations were limited to single-zone scenarios and did not account for buildings with multiple floors and rooms where zone-to-zone transmission could occur.

Jimenez et al. [90] developed a publicly available spreadsheet known as the "COVID-19 Aerosol Transmission Estimator". The tool provides information on key input parameters based on recent COVID-19 studies. It enables the evaluation of infection risks and mitigation strategies based on specific information for various scenarios. In response to the COVID-19 pandemic, the ASHRAE Epidemic Task Force has issued guidelines for commercial buildings and schools emphasizing the need for a holistic framework to reduce exposure to SARS-CoV-2 [91, 92]. These guidelines include general recommendations for specific spaces such as lobbies, elevators, and conference rooms. However, the mechanical systems, configurations,

and operations of different indoor spaces can vary significantly, necessitating case-by-case assessments.

Mitigation strategies that have been proposed for buildings include ventilation, filtration, GUV, and personal protective equipment. While many studies have concentrated on healthcare facilities [93, 94] and single-zone building scenarios, there is a scarcity of research on multizone commercial buildings [95, 96]. ASHRAE and REHVA have issued their guidelines in the COVID-19 pandemic context [97, 98]. General recommendations have been provided for HVAC operations, outdoor air settings, and filtration [99]. However, these guidelines often lack the performance-based information needed to inform mitigation strategies tailored to specific building types. The most effective mitigation strategy can vary significantly depending on the building type, configuration, occupancy schedule, HVAC system, and operational settings [100, 101].

It was demonstrated by Peng et al. [90] that employing multiple layers of protection—such as reducing occupancy and exposure time, wearing masks, increasing ventilation rates, and using HEPA filtration and GUV disinfection—can significantly lower COVID-19 infection risk. Sun and Zhai [102] introduced indices for social distancing and ventilation effectiveness to the Wells-Riley model, suggesting that reducing occupancy density by half can reduce the probability of infection by 20 - 40% within the first 30 minutes of an event. Zhang [103] estimated that integrating various mitigation strategies, including source control, ventilation, and air cleaning, can reduce infection risk in schools and offices by a factor ranging from 9 to 500.

Most investigations mentioned above have paid attention to evaluate infection exposure risks in single-zone scenarios only. Recently, empirical evidence of zonal aerosol transmission has been reported in an Eastern Canadian hospital [104]. Additionally, Taewon et al. [105] suggested the possibility of SARS-CoV-2 transmission between different floors of an apartment building, with five out of nineteen cases reporting no direct contact with other

residents. In Spain, it was reported that bathrooms in older buildings with communal ducts may have allowed for aerosol exchanges [106]. Therefore, multizone aerosol transmission patterns must be considered when developing detailed mitigation strategies for specific building types or zones, especially during the reopening stage of commercial buildings [107].

2.3 Ventilation rate estimation via indoor CO_2 monitoring

Among the mitigation strategies, outdoor ventilation is crucial for reducing the probability of infection, particularly in naturally ventilated buildings. Characterizing ventilation rates in buildings has long been an effective way to understand the amount of fresh air delivered to occupants. This practice gained significant attention during the COVID-19 pandemic, with the widespread installation of CO_2 sensors to monitor indoor ventilation conditions. Proper and accurate interpretation of CO_2 readings is essential for assessing indoor air quality and developing effective mitigation strategies. This section reviews previous efforts to measure indoor ventilation rates using CO_2 monitoring, the application of Bayesian approaches in the built environment, and stochastic modeling of indoor air quality.

2.3.1 Ventilation rate measurement approaches

It has been indicated that typically the predominant way to measure the ventilation rate of a building is using the tracer gas approach [108-112]. Only under specific conditions, such as in an exceptionally well-sealed building where all air inflows and outflows occur exclusively through ducts, can the ventilation rate be determined directly from duct airflow measurements [108, 113]. The tracer-gas technique usually releases a designated amount of tracer gas (a single release, constant release, or controlled release) and then observes its decay with time. Due to its simplicity and less dosing volume of tracer, various studies used the concentration decay method to evaluate ventilation performance and thereby estimate indoor air change rate [114, 115].

Selecting tracer gas is important in this method. The desirable properties of tracer gases have been indicated to be detectability, nonactivity, and a relatively low concentration in the air [109,

116-118]. Over the years, a variety of tracer gases have been used in tracer gas measurements such as carbon dioxide (CO_2), sulfur hexafluoride (SF_6), nitrous oxide (N_2O), hydrogen (H_2), and helium (He), etc [119]. A comparison table is listed in Table 2-1 [120, 121]. In terms of the ventilation rate measurement, Edouard et al. [122] compared the CO_2- and SF_6- based tracer gas approaches and found similar results in terms of the ventilation rates prediction. The results predicted by CO_2 mass balance approach were 10% - 12% lower than those for SF_6. Among the tracer gases listed above, CO_2 is one of the commonly used tracer gases as it appears to be safe, and environmentally friendly, and its concentration can be easily measured with inexpensive sensors [60, 123-125].

Table 2-1 Comparisons between different tracer gases

	Inflammability	Molecular	Measurability	Global warming potential (GWP)
CO_2	Non-flammable	44	CO_2 sensor / gas chromatography	1
SF_6	Non-flammable	146	gas chromatography	23500
N_2O	Non-flammable but support combustion	44	gas chromatography	298
H_2	Flammable	2	gas chromatography	Insignificant
He	Non-flammable	4	gas chromatography	0

There are three most commonly used approaches for evaluating ventilation conditions using tracer gas: concentration decay, concentration injection, and constant concentration [109]. When applying these techniques to measure the air change rate, certain assumptions are typically made [109]. For instance, a common assumption is that of a well-mixed environment, where the tracer gas concentration in the observed room is represented by a single value. Simultaneously, it was also assumed that the air change rate remains constant, requiring stable ventilation conditions in the measured chamber throughout the assessment period. The

accuracy of different calculation approaches is usually evaluated in a single-zone chamber, which could provide a well-controlled environment to measure the tracer gas concentrations under different mechanical ventilation conditions. Cui *et al*. [60] investigated the use of CO_2 concentration decay approach for determining the ventilation rates in a test chamber. In their study, they tested the ventilation conditions in a range of 7.8 ACH to 40.6 ACH. The study suggests minor discrepancies between in-situ CO_2 sensors at different places. Besides, the multi-point decay method tends to be more accurate than the two-point decay method. Overall, it has been suggested that CO_2 could serve as an ideal tracer gas for determining indoor ventilation rates.

2.3.2 Bayesian inference in built environment

In built environment studies, Bayesian inference is a powerful tool that can be used to quantify the uncertainty in estimated model parameters [126-129]. This approach considers the inferred parameters with prior information, then it uses the likelihood function (based on the measurement data) to update prior distribution following Bayes theorem [130, 131]. The updated results are the posterior distributions, which are the new beliefs of the interested variables. In recent years, with the advancement in computational capabilities and the development of Markov Chain Monte Carlo (MCMC) algorithms such as Metropolis-Hastings, Gibbs sampling, and Hamiltonian Monte Carlo [132-134], an increasing number of studies in the built environment field have begun to utilize this approach to infer parameters in established models [135-140]. Zhong et al. [141] developed a logistic regression model for predicting occupants' usage of air-conditioning, and Bayesian inference was used to establish the relationship between field measurements and model outputs, the unknown model parameters, model bias, and measurement errors were inferred. Zhao et al.[142] attempted to improve the fault diagnosis of sensors installed in HVAC systems. The distance function for sensor calibration was established, and the posterior distributions of an offsetting constant and unknown parameters were inferred accordingly. In 2020, Wang et al. [143] inferred the neutral temperature based on an assumed linear relationship between the thermal sensation and

temperature. The unavoidable regression error ε_i was also inferred assuming that it follows a Gaussian distribution with a variance of σ^2. A review of Bayesian inference on building energy models was conducted by Hou et al. [144] for clarifying current research progress and instructing implementation of this approach. Besides, Lim et al. [145, 146] analyzed the influence of meta-model accuracy and energy data on the Bayesian calibration results for building energy simulation models.

In the field of indoor air quality, Wang et al. [147, 148] applied Bayesian approaches to a source-detector relationship derived from CFD simulations of airflow in indoor spaces and underground utility tunnels to estimate source parameters such as leakage rate and location. Septier et al. [149] proposed a Bayesian inference procedure on inverse dispersion modeling to tackle the challenging source term estimation (STE) problem, using a Gaussian assumption for source emission rates due to its practical performance. Hou et al. [150] utilized Bayesian inference on indoor CO_2 concentration models to assess ventilation conditions in primary schools. Their study identified outdoor ventilation rate, CO_2 generation rate, and occupancy level as the most sensitive variables affecting indoor CO_2 levels. Rahman et al. [151] developed a Bayesian inference approach to estimate occupancy distribution in a mechanically ventilated multi-room office. Using CO_2 concentration data simulated by the CONTAM program, their study considered scenarios with and without 5% random noise to account for uncertainty. They found a significant increase in RMSE for occupancy estimation as sensor measurement uncertainty increased. The study suggested that Bayesian inference could be more effective in solving inverse problems if it can handle realistic data with noise.

To summarize, Bayesian inference has been widely accepted as a powerful approach for inferring unknown parameters and quantifying uncertainties. In order to obtain a reasonable estimation for the interested parameters, firstly the interpreted model, or to be more specific, the input-output relationship needs to be clearly defined [152]. Previous studies also suggested that the fluctuations of measurement data may also play a significant role in the estimation

accuracy [153]. In the meanwhile, prior knowledge of inferred parameters would also influence the predicted outcomes. Uniform distributions and Gaussian distributions are the most frequently used assumptions with acceptable performance in real practice [154, 155]. For the practices in indoor air quality models, previous researchers have applied it to estimate the source information, occupancy, and ventilation rate. It was indicated that the Bayesian inference would have a better performance when the real-life measurement noise could be considered.

2.3.3 Stochastic grey-box modeling for the indoor air quality (IAQ)

Over the years, the stochastic nature of indoor air quality (IAQ) modelling has been gradually realized [156-158]. Stochastic grey-box models, which are capable of capturing the uncertainties occurring within the system [159], have been identified as highly effective for modeling IAQ systems. Stochastic models are mathematical representations used to describe systems or processes that exhibit random behavior or inherent randomness [160, 161]. Compared with deterministic models, stochastic models will allow for some randomness in some of the coefficients in the model, therefore putting uncertainties into consideration [162]. To be more specific, parameters will be taken as random variables, and the stochastic models will generate different outcomes with the same given inputs. The solution will involve randomness and will be in the form of an approximated probability density function (PDF). This distinguishes the stochastic models from the traditional deterministic models that we are familiar with.

In mathematics, statistics, and computational modeling, a grey-box model [163] integrates partial theoretical structures with empirical data to complete the model. Unlike white-box (physically based) models, which rely entirely on theoretical knowledge, and black-box (data-driven) models, which rely solely on data, grey-box models combine both physical knowledge and data-driven insights [164-166]. The parameters of a grey-box model are estimated using parameter estimation algorithms and measured data from the system [167, 168]. These models

often incorporate stochastic components to account for uncertainties and variability, such as measurement errors and system fluctuations. The choice of parameter estimation algorithm is crucial in developing a grey-box model. Common algorithms include maximum likelihood estimation (MLE), genetic algorithms (GA), nonlinear least squares, and simplex search [160].

For modeling indoor air quality (IAQ), a deterministic mass-balance equation for contaminants is often expressed as an ordinary differential equation (ODE). By allowing randomness in some coefficients, this equation transforms into a stochastic differential equation (SDE), which more accurately reflects real-life scenarios. Researchers have significantly advanced the predictive and inferential capabilities of SDE models for IAQ. In 1988, Haghihat et al. [169] introduced a predictive stochastic model for indoor air quality, incorporating inputs as random variables within the SDE framework. This model effectively captured the variability in predictions of contaminant concentrations. The moment equations for mean, variance, and skewness were derived using stochastic Itô calculus. The inclusion of a 'white noise' term not only accounted for system randomness but also ensured a unique and satisfactory solution. Importantly, the solution to the SDE model is an Itô stochastic process with both the Markov and strong Markov properties [170]. This characteristic implies that future predictions depend solely on the current state, making the model highly effective for forecasting.

Marcel et al. [171] proposed a predictive control approach to model CO_2 concentrations using a grey-box model, where stochastic differential equations were established based on tracer-gas mass balance. The study indicated that the model's parameterization was suitable and applicable, and its predictions were more accurate than those from traditional deterministic approaches. Following this, an inferential study estimated the ventilation air change rate using the stochastic grey-box model [172]. This study employed a maximum likelihood method for parameter estimation, demonstrating the robustness of the approach. Niels et al. [168] further developed an estimation scheme for the stochastic grey-box model, utilizing an extended Kalman filter, which incorporated both maximum likelihood and maximum a posteriori

estimation. The performance of grey-box modeling programs CTSM and MoCaVa was evaluated and compared. Despite the substantial potential and benefits of using Bayesian inference for parameter estimation in stochastic grey-box models, limited studies have investigated this approach to date.

In summary, traditional ventilation evaluation methods rely on deterministic approaches that fail to account for real-life uncertainties. The accuracy of these methods depends on how closely real situations match idealized assumptions, the precision and comprehensiveness of input data, the thoroughness of model development, and the absence of disturbances during measurements. Since idealized conditions are rare in reality, it is crucial to quantify uncertainties in the interpretation process. Bayesian inference and stochastic grey-box modeling has been suggested to be powerful tools to face this issue, and thus help in interpreting indoor ventilation conditions via CO_2 measurements.

Chapter 3 Developing a CONTAM-quanta Approach for Evaluating Multizonal Airborne Transmission

Abstract

The world has faced tremendous challenges during the COVID-19 pandemic since 2020, and effective clean air strategies that mitigate infectious risks indoors have become much more essential. Not much information is available for reducing this risk in the whole-building multizone context. In this study, a novel approach based on the Wells-Riley model applied to a multizone building was proposed to simulate exposure to infectious doses in terms of "*quanta*". This modeling approach quantifies the relative benefits of different risk mitigation strategies so that their effectiveness could be compared. A case study for the US Department of Energy Large Office prototype building was conducted to illustrate the approach. The infectious risk propagation from the infection source throughout the building was evaluated. Different mitigation strategies were implemented, including increasing outdoor air ventilation rates and adding air-cleaning devices such as MERV filters and portable air cleaners (PACs) with HEPA filters in-room/in-duct germicidal ultraviolet (UV) lights, layering with wearing masks. Results showed that to keep the risk of the infection propagating low the best strategy without universal masking was the operation of a very large industrial-sized air cleaner; whereas with masking all strategies were acceptable. This study contributes to a better understanding of the airborne transmission risks in multizone, mechanically ventilated buildings and the how to reduce infection risk from a public health perspective of different mitigation strategies.

3.1 Introduction

The COVID-19 pandemic has caused more than 276.1 million people to be infected (including more than 5.3 million deaths) worldwide as of December 2021 [173]. Recently, its new variants are more contagious and caused more severe symptoms among younger people [174-176], driving another surge of cases worldwide. While vaccinations have been underway in many countries, there are still many regions and areas in the world that have made little progress in controlling the pandemic, such as India and Brazil [177, 178]. It is likely that COVID-19 may linger longer than expected, turning into an "endemic" pathogen [179]. Therefore, we must be prepared for the possibility that COVID-19 is here to stay and also that other pandemics may occur in the future.

An important aspect of the COVID-19 pandemic is that the infection is transmitted by inhalation of airborne particles, or an aerosol, containing the SARS-CoV-2 virus. These particles are released by an infected person from their respiratory tract as they are breathing, talking, singing, *etc*. Although the size of the SARS-CoV-2 virus varies from 0.06 to 0.14 μm [180], the virus-containing aerosol consists of particles made of virus in a respiratory fluid, which is a complex mixture of various organic and inorganic constituents (water, salts, lipids, proteins, bacteria, other viruses) suspended in air; thus their size greatly exceeds the diameter of the naked virus itself. So far, multiple sizes of airborne virus-laden particles for SARS-CoV-2 have been detected, ranging from ~ 0.25 μm to 5 μm [181-185], which enables them easily transported over long distances.

Close contact with infected individuals, poor ventilation, no air cleaning, and prolonged exposure time indoors are the main reasons for elevated risk of transmission and infection in buildings [186]. Building ventilation is essential to dilute and remove aerosol, especially in highly occupied spaces. Air cleaning can both inactivate and remove aerosol through germicidal ultraviolet light and physical filtration [187]. Short-range and long-range transmissions occur indoors, with the difference being that at short range, the airborne particle

concentration is much higher. Long-range transmission occurs when the aerosol travels long distances and accumulates indoors. Both the Federation of European Heating, Ventilation and Air Conditioning Association (REHVA) [188] and the American Society of Heating, Refrigerating, and Air Conditioning Engineers (ASHRAE) [189, 190] recognized that building ventilation plays an important role to limit the risk of transmission . In the guidance of re-opening buildings, ASHRAE [191] (as of September 2021) suggests at least the minimum amounts of outdoor air for ventilation needs to be adopted, combined with recirculation filters higher than MERV13. Or alternatively, the combined effect of outdoor air, filtration and air-cleaning devices can achieve this level (minimum ventilation + MERV13). In addition, flushing rooms before and after occupancy, installing in-room germicidal ultraviolet lights (GUV), and equipping by-passing heat recovery sections were also recommended [192]. In comparison, REHVA as of April 2021 recommends applying the principle As Low as Reasonably Achievable pollutant concentration to set the required ventilation rate and setting the demand-control ventilation setpoint to 550 ppm CO_2 (absolute value) as an indicator of good ventilation. They also recommended using as much outdoor air as reasonably possible and open windows much more than normal if thermal discomfort is not a concern; the recirculation dampers are required to be HEPA filters or at least have a particulate matter efficiency of 80% for an optical diameter between 0.3 μm and 1.0 μm based on ISO 16890 [193]) (termed ePM1) as compared to the equivalent level of 50% of a MERV 13; germicidal UV lights may be used in return air ducts or in rooms if they can be correctly sized, installed, and maintained; and by-passing heat recovery section and avoiding potential leaks. Many Canadian guidelines follow ASHRAE, for example, the Insititut national de santé publique Quebéc (INSPQ) recommends as of Jan 2022 applying adequate ventilation to occupied buildings, especially if there are infected individuals inside the building [194].

These are general building guidelines, whereas specific building type and use recommendations are often unavailable because buildings and their systems are variable and need to be assessed on a case-by-case basis. To evaluate transmission risk and develop

building/space specific mitigation strategies, many studies have been conducted. Jimenez et al. developed a publicly available spreadsheet known as the "COVID-19 Aerosol Transmission Estimator" (COVID-19 Estimator hereafter). The tool provides information on key input parameters based on recent COVID-19 studies and makes it possible to evaluate infection risks and mitigation strategies and has been detailed in a paper by Peng et al. [195]. Existing tools, e.g., Jimenez et al.'s estimator, have been used to evaluate mitigation measures that reduce airborne transmission risk in specific cases, e.g., an indoor choir practice, classrooms, subways, supermarkets, and sports stadiums. Dai and Zhao [87] calculated the required ventilation rate to lower infection risk under 1% for different exposure times using the Wells-Riley model. They modeled typical scenarios and concluded that the minimum required ventilation rate can be reduced by a quarter by wearing a mask, which can be achieved by the normal ventilation mode in most buildings. Lelieveld et al. [196] estimated the infection risk in several indoor environments, concluding that wearing a mask and actively ventilating rooms reduces risk by 5-10 times and is comparable to high-efficiency particulate filtering.

A recent study by Peng et al. [195] showed that multiple layers of protection, such as occupancy and exposure-time reduction, mask wearing, increased ventilation rates, and air cleaning through HEPA filtration and UVGI disinfection, are important to reduce the COVID-19 infectious risk to low levels. This is particularly true during the current situation of new variants such as Omicron. Zhang [197] estimated that by integrating different mitigation strategies for schools and offices, including source control, ventilation, and air cleaning strategies, infection risk could be reduced by a factor of 9 to 500. Sun and Zhai [198] modified the Wells-Riley model by introducing two indices for social distancing and ventilation effectiveness and showed that half occupancy density could reduce the infection risk by 20-40% in the first 30 minutes of an event. In a later study, as an application of Jimenez's approach, an archetype library of twenty-nine building types was developed based on standards and references and publicly available data and made available through an interactive website. The urban archetype buildings allow decision-makers and managers to compare various mitigation strategies and

generalize conclusions when urban-scale data are not readily available. As a demonstration, the impacts of six mitigation measures on infection risks in various building types were evaluated. Additionally, Shen et al. [199] evaluated the effectiveness of multiple control strategies in mitigating the infection risk in different scenarios and building types, including elevated outdoor airflow rates, high-efficiency filters, advanced air distribution strategies, standalone air cleaning technologies, personal ventilation, and face masks.

Many of these works have focused on evaluating risks in single zones only. Empirical evidence has been reported for aerosol zonal transmission in an Eastern Canadian hospital [200]. Taewon et al. [201] have also suggested the possibility of SARS-CoV-2 transmission between different floors of an apartment building. In their epidemiology investigation, five of nineteen reported cases claimed no direct contact with other residents in the building. In Spain, it was reported that bathrooms of older buildings with communal ducts may have allowed aerosol exchanges [202].

One multizone simulation study by Emmerich et al. [203] applied the simulation software, CONTAM, for two infectious agents, a tuberculosis-like particle with a diameter of 0.64 μm and a burst emission, and a squamous cell particle with a diameter of 10 μm released at a constant generation rate. The study showed the importance of building leakage and the impacts of an actual building system operation. Although their study targeted healthcare facilities, it illustrated the importance of addressing the interactions of weather conditions, mechanical system operations, pressure differentials, and inter-zonal leakages in terms of airborne virus transmission. These interactions cannot be addressed systematically without a multizone building environment modeling approach. Another multizone contaminant transport simulation was also performed in a hospital building to evaluate existing air-cleaning strategies; the importance of building leakages was highlighted [204]. Prateek et al. simulated the indoor dispersion of airborne SARS-CoV-2 aerosols in a medium office CONTAM model and found that the unventilated stairwells are vulnerable to airborne viruses [205]. Shen et al. [199] pointed out that their study represented the most typical configurations for a building/space

type, whereas a specific building could be more complicated, and the transmission risk depends on specific configurations [197]. On the other hand, a building ventilation renovation is often performed at the whole-system scale, so different rooms/buildings with rooms and indoor and outdoor interactions are essential. Indeed, a study on multizone buildings for specific building types is important with the reopening of public buildings. Building-wide protection instead of room-level protection will need to be evaluated with realistic weather conditions, air leakages, and occupancies. This will help identify loopholes in the renovation strategies, improve mitigation effectiveness and efficiencies, and develop building- and climate-specific, schedule-specified solutions to meet the variable, post-covid era needs. A few recent multizone simulation studies based on Modelica [206, 207] show the importance of pressure controls and leakages in a hospital building [206] and HVAC filtrations on energy costs in an office building [207]. In addition, López-García et al. linked a zonal ventilation model with a multicompartment SIS Markovian model for evaluating the infection of patients within a hospital ward [208]. However, the inter-zonal airflows model have not been studied in depth in a detailed airflow network by the previous studies [204] and the airborne zonal infection transmission in commercial buildings were rarely investigated.

Conducting multizone analysis of airborne disease transmission in buildings with a more physically-realistic setting has many benefits from an occupant's health, safety, and productivity perspective and for energy-efficient operation during regular or emergent operations such as a pandemic. Many countries and governments have recently realized the importance of building ventilation and released new initiatives encouraging retrofits of existing buildings for reopening and future epidemics and pandemics. However, investing governmental funds to achieve healthy, safe, and energy-efficient goals needs to be addressed, considering the complexities of buildings and their multi-factorial interactions. Furthermore, the general public guidelines provided in the early and current stages of the pandemic may not be adequate. Thus a physically-realistic analysis tailored for different building types and climates should be conducted. This paper adopts a multizone simulation tool, CONTAM, to

model SARS-CoV-2 transmissions in a US DOE prototype building, which represents a generic yet realistic building of a specific category in the US, and further estimates exposure risks based on the Wells-Riley model by considering the dynamic interactions of many influential parameters, including weather, occupancy, system operation, and temperature variation. The goal is to evaluate the multizone risks of airborne transmission of viruses and compare mitigation strategies in the context of a whole building compared to a single space. The final simulation input project and output files of the US DOE prototype buildings are also shared with this submission for future readers to apply the same approach to other building types.

3.2 Methodology

3.2.1 Multizone contaminant transport model

This study develops and demonstrates a new modeling approach for SARS-CoV-2 transmission risk in multizone mechanically ventilated spaces based on CONTAM. The US National Institute of Standard and Technology's multizone airflow and indoor air quality model CONTAM [209] implements simulations using DOE prototype commercial building models based on EnergyPlus [210]. CONTAM can analyze the complex and dynamic interactions of ambient conditions, building system operations, and occupancy behaviors in a more physically-realistic setting. Although EnergyPlus has an internal "airflow network" model, which is based on an earlier version of AIRNET [211] and COMIS [212], it has many limitations and is not designed for multizone analysis of pollutant transmission but instead for estimation of ventilation-related energy loads. It is also not included in the well-known EnergyPlus models of prototype buildings to reduce simulation costs.

Using this approach, we evaluate the potential for SARS-CoV-2 airborne aerosol transmission and exposure risk in mechanically ventilated multizone spaces and specifically address:

- the risks of room-room and floor-floor spreading,

- building mechanical system operations, including schedules and flow rates,

- leakages, pressure differentials, and room temperature schedules, and occupancy schedules.

If room-room spreading is significant, we also use the model to identify potentially vulnerable neighbor zones other than the source zone. If room-room spreading is relatively low, we investigate the impacts of single-zone mitigation strategies performed in the context of actual building operation in a multizone environment. Compared to existing SARS-CoV-2 models and tools, such as the single-zone model, FaTIMA [213], and multizone models based on Modelica [206, 207], the proposed approach models whole-building multizone exposure risks [82]. Some recent multizone studies include risk models, such as Pease et al. [204], which, however, did not solve the airflow network. In comparison, the proposed approach covers both detailed multizone airflow and risk estimations for the DOE prototype buildings.

3.2.2 Airborne Transmission Under Various Mitigation Approaches

In the context of the multizone simulation of airborne transmission, the concentration of virus-containing aerosol is estimated based on a mass conservation equation, Eq. 3-1 [213]. The time-change rate of the concentration in zone i $C_i(t)$ with volume V is a function of the generation $G(t)$ from an infector located in zone i; external sources $C_s(t)$ from the supply of a mechanical ventilation system or $C_j(t)$ from the infiltration of a neighboring zone; the losses Q_r for the return to the mechanical system, Q_{lx} from the local exhaust such as an exhaust fan, Q_{ac} from an air cleaner, Q_{UVr} from an in-room GUV device, Q_{dep} from the particle deposition, Q_{dec} from the virus infectivity decay process, and Q_{exf} from the exfiltration to neighboring zones. The loss rates are expressed as a volumetric flow rates [m^3/s]. Note that Q_{UVr}, Q_{dep}, Q_{dec} are not actually flow rates, but are expressed as equivalent flow rates, as if it was a loss due to ventilation. A ductwork filter, such as a MERV-rated filter (i.e., η_{MERV}) and a duct UVGI device (i.e., η_{UVd}) contribute to lowering the supply concentration level $C_s(t)$ of the mechanical ventilation system (Eq.3-2).

The impacts of mask-wearing are evaluated in terms of the mask efficiency M_{exh} for the exhalation of the infector in, and M_{inh} for the inhalation of the susceptible in the exposure equation Eq. 3-1 For a given exposure time duration from t_1 to t_2, Eq. 3-1 estimates the susceptible's exposure particle counts (n) at a breathing rate B and a probability or a percentage of mask-wearing F_m, given the airborne particle concentration in the space $C_i(t)$ as calculated by Eq. 3-1.

The exposure particle counts are then used as the input for the estimation of infection risk.

$$V\frac{dC_i}{dt} = (1 - M_{exh})G(t) + Q_sC_s(t) + \sum_{j=1}^{n} Q_{\text{inf,j}}C_j(t) \tag{3-1}$$

$$-\left(Q_r + Q_{lx} + \eta_{ac}Q_{ac} + Q_{UVr} + \sum_{k=1}^{s} Q_{\text{dep,k}} + Q_{dec} + \sum_{j=1}^{n} Q_{\text{exf,j}} \right)C_i(t)$$

$$Q_sC_s(t) = [(1 - \eta_{MERV})Q_{rec}C_{rec}(t) + Q_{oa}C_{oa}(t)](1 - \eta_{UVd}) \tag{3-2}$$

The outdoor air concentration, C_{oa}, is usually zero in this context so

$$Q_sC_s(t) = (1 - \eta_{MERV})Q_{rec}C_{rec}(t)(1 - \eta_{UVd}) \tag{3-3}$$

$$\mu = B(1 - M_{inh} \times F_m)\int_{t_1}^{t_2} C_i(t)dt \tag{3-4}$$

C = active virus concentration in the air [#/m³] with the following subscripts: **o**utdoor **a**ir through HVAC system, infectious zone i where the infectious person is located, neighbor zone j, **s**upply, **rec**irculation of HVAC system;

M_{exh} = mask exhale efficiency

Q = volumetric flow rate [m³/s] with subscripts: **s**upply, **r**eturn, **l**ocal e**x**haust, **a**ir **c**leaner, **UV** light in in-room (equivalent), **dep**osition to interior surfaces (equivalent), virus infectivity **dec**ay (equivalent), **inf**iltration from neighbor zone including the ambient, **exf**iltration to neighbor zones including the ambient, **rec**irculation of HVAC system;

η = filtration efficiency with subscripts: **a**ir **c**leaner, **MERV** filter, and **GUV** light in HVAC **d**uct;

G = virus generation rate [#/s];

s = number of interior surfaces;

n = number of neighboring zones;

V = zone volume [m³]; and

t = time [s].

To compare the relative significance of each term, Eq. 3-1 and Eq.3-2 are non-dimensionalized by $G(t)$:

$$\frac{V}{G(t)}\frac{dC_i}{dt} = 1 - M_{exh} + (1 - \eta_{MERV})Q_{rec}C_{rec}(t)(1 - \eta_{UVd}) + \frac{1}{G(t)}\sum_{j=1}^{n} Q_{\text{inf},j}C_j(t) - \qquad \text{3-5}$$

$$\frac{1}{G(t)}\left[\eta_{ac}Q_{ac} + Q_{UVr} + \sum_{k=1}^{s} Q_{\text{dep,k}} + Q_{dec} + \sum_{j=1}^{n} Q_{\text{exf,j}} + Q_{lx} + Q_r\right]C_i(t)$$

Note when $C_{rec} = C_i$

$$\frac{V}{G(t)}\frac{dC_i}{dt} = 1 - M_{exh} + \frac{1}{G(t)}\sum_{j=1}^{n} Q_{\text{inf},j}C_j(t) - \frac{1}{G(t)}\left[\eta_{ac}Q_{ac} + Q_{UVr} + \sum_{k=1}^{s} Q_{\text{dep,k}} + \qquad \text{3-6}\right.$$

$$\left. Q_{dec} + \sum_{j=1}^{n} Q_{\text{exf,j}} + Q_{lx} + Q_{\underset{oa}{exh}} + \eta_{MERV}Q_{rec} + (1 - \eta_{MERV})\eta_{UVd}Q_{rec}\right]C_i(t)$$

In reality, it is often that $C_{rec} < C_i$ because of the mixing in the ductwork and the diluting of the aerosol transport process among different zones. When virus aerosol reaches the MERV filter, the actual concentration could be much lower than that in the source zone. Thus, the efficacy of the centralized duct-level mitigations, e.g., the MERV filter or the in-duct GUV, may decrease with the size of the mechanical system because of the long dilution process during aerosol transport. Thus, localized virus aerosol mitigation strategies are preferred compared to the strategies applied in the ductwork, and larger mechanical systems should have more localized solutions inside rooms. Because $C_{rec} < C_i$ in reality, Eq.3-6 may overestimate the efficacy of MERV filters and GUV in the ducts.

The above dimensionless equations reveal how different mitigation strategies affect airborne transmission. Of interest is how significant each term is when compared to each other and to the mask efficiency. For an exposure time of Δt, the mask efficiency M is proportional to other building component removal processes generally according to:

$$M \sim \frac{QC}{G}$$

3-7

Table 3-1 details these equivalent removal efficiencies used in a building to reduce the aerosol concentration and thus exposure.

Table 3-1 Estimated equivalent removal efficiencies for different mitigation strategies

Strategy	Masks	Outdoor Air	PAC	MERV Filter	In-Room GUV	In-Duct GUV
Removal efficiency (%)	M	$\dfrac{Q_{oa}C}{G}$	$\dfrac{\eta_{ac}Q_{ac}C}{G}$	$\dfrac{\eta_{MERV}Q_{rec}C}{G}$	$\dfrac{Q_{UVr}C}{G}$	$\dfrac{(1-\eta_{MERV})\eta_{UVd}Q_{rec}C}{G}$

The air mass balance equation is given in Eq. 3-8 [209]:

$$Q_s + \sum_{j=1}^{n} Q_{\text{inf,j}} = \sum_{j=1}^{n} Q_{\text{exf,j}} + Q_{lx} + Q_r$$

3-8

The infiltration, exfiltration, and internal-zonal airflow are modeled by a power law. An example of infiltration from Zone j to Zone i is as shown in Eq. 3-9 [213].

$$Q_{\text{inf,j}} = \frac{C_D A_L}{1000} \sqrt{\frac{2}{\rho}} (\Delta P_r)^{0.5-n} \Delta P_{j,i}^n$$

3-9

C_D = flow discharge coefficient; A_L = leakage area, m^2; ρ = air density, kg/m^3; ΔP_r= reference pressure difference, Pa; $\Delta P_{j,i}$=pressure difference between zone j and zone i, Pa; and n = flow exponent.

In a CONTAM simulation, the wall leakage is often divided into three portions vertically to represent the leakages at the top edge, middle section, and bottom edge of a wall. The pressure difference includes three components: thermal buoyancy, wind pressure (if applicable), and zone pressure differences due to HVAC operations. The thermal buoyancy component is a function of the zone temperature difference as defined by users (or from an energy simulation

29

software, such as EnergyPlus [210]). The wind pressure component depends on the local wind pressure coefficient and is a function of local terrain features, building orientation, and reference wind velocity from the weather conditions. In this study, the well-mixed assumption of air was made without considering turbulent mixing of airflows in zones. However, in the real world, occupants' activities and heat sources may all interrupt airflow patterns in the room, exerting an influence on zonal infiltrations. This could be investigated in future studies using the CFD capabilities of CONTAM [214, 215].

3.2.3 Airborne Infectious Risk Estimation

This study developed an approach, which is named "CONTAM-*quanta*", to enable the CONTAM model to estimate airborne virus transmission in terms of quanta and calculate the probability of infection for SARS-CoV-2. The concept of quanta for airborne transmission, a hypothetical infectious dose unit, was first proposed by Wells in 1955 [216]. A *quantum* was defined as the inhaled dose needed to infect a person. The number of infected occupants bears a Poisson relation to the number of quanta they breathe, which means 63% of occupants will be infected when each occupant breathes one quantum on average. This relationship is widely known as the Wells-Riley equation [82], which is expressed as follows:

$$P = \frac{C}{S} = 1 - e^{-n_q} \qquad \text{3-10}$$

where P = the probability of infection, also known as the individual exposure risk [186] , C = the number of infection cases, S = the number of susceptible.

The number of quanta inhaled n_q (quanta) is expressed by

$$n_q = B(1 - M_{inh} \times F_m)C_{q,avg}\Delta t \qquad \text{3-11}$$

Where $C_{q,avg}$ = the time-average quanta concentration quanta/m^3).

Modeling is often challenged by the uncertainties in the input parameters. Although this thesis reports the quanta concentrations in different zones of a building, we recommend the risk estimation and the comparison of different risk mitigation strategies be conducted on a relative basis. The proposed CONTAM-*quanta* approach was verified by comparing the predicted

numerical results to those from the literature. The details can be found in Appendix 1.

A few studies have investigated the quanta emission rate of SARS-CoV-2 [87, 199]. Buonanno et al. [186] proposed an approach that provided a range of estimates for different infection scenarios. Here are some assumptions used in this evaluation approach: Firstly, the air in the room was assumed to be well-mixed. In addition, this study assumed a generation rate for loud speaking of 65 quanta per hour and one infector in the source zone. Detailed assumptions for the investigated scenario are described in the next section. We also assumed a quanta deposition rate of 0.3 h^{-1} estimated by Thatcher et al. [217] for particles from 0.55 to 1.54 μm in diameter, and a quanta deactivation rate for SARS-CoV-2 of 0.63 h^{-1} [218]. The removal efficiency of air cleaning using filtration that mechanically removes particles from an air stream depends on the size of the particles being cleaned. This study used efficiencies for particle sizes between 1 μm and 3 μm [219]. Minimum efficiency values were adopted for conservative estimation. The MERV filter efficiency in the CONTAM simulation was then determined using [220]. For example, for the MERV8 filter, its quanta removal efficiency was 20%. The HEPA filter efficiency in the PAC was 99% [221]. It is also possible to use CONTAM with removal/deposition rates as a function of particle size. The maximum building occupancy was based on the corresponding EnergyPlus prototype building [222, 223]. The total number of occupants was divided into infectors and susceptibles. Infectors were individuals who could generate "quanta" in the building, and the number of susceptibles was equal to total occupancy allowed in the building minus the number of infectors.

To determine the acceptable level for individual exposure risk from a public health perspective in which outbreaks need to be minimized, the basic reproduction number R_0 was used. The basic reproduction number is defined as the expected secondary infections (C) caused by a typical infector (I) among a completely susceptible population ($R_0 = C/I$) [224]. Wells' study of airborne spread of measles in an elementary school in 1978 also used this approach. When $R_0 > 1$, the virus may spread in the population [82], so the target exposure risk level was set to $R_0 < 1$. This metric has also been applied in other studies [87, 88, 224], including a study tracing

airborne SARS-CoV-2 transmission in public buses and subway trains [225]. Note that because of the uncertainties of the model, $R_0 > 1$ does not imply there will be a 100% chance of infection. From the probability point of view, it should be interpreted on a relative basis; for example, a lower R_0 means less chance of the community virus transmission or vice versa.

3.3 Case Study – US DOE Large Office Prototype Building

3.3.1 Simulation Model and Inputs

The US DOE prototype commercial building models were created to assess building energy efficiency measures and the development of energy standards and codes. Sixteen prototype building types were developed to represent 70% of the commercial building stock [222]. The corresponding CONTAM models of these DOE prototype building models were later created for building ventilation and IAQ analysis [226]. Building parameters such as ventilation, occupancy, and building envelope airtightness were defined following the *ASHRAE Standard 90.1-2013 [227]* and *ASHRAE Standard 62.1-2013 [223]*. The airflow paths and possible mitigation strategies are illustrated in Figure 3-1. This study chose the Large Office prototype building model to demonstrate the CONTAM-*quanta* approach (Figure 3-2).
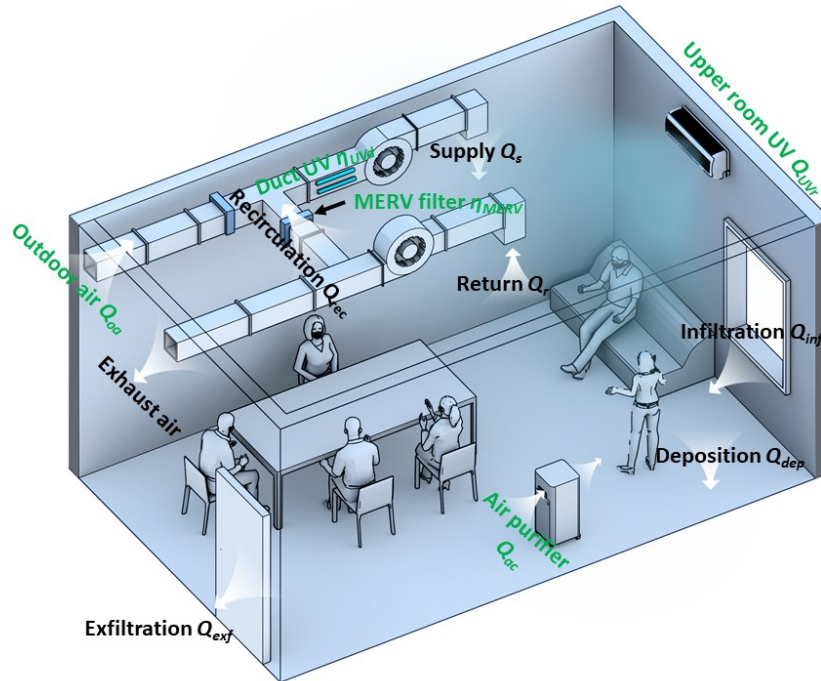
Figure 3-1. Schematic of airborne transmission routes

The building has 12 floors, a footprint of 3563 m², one basement, and a flat roof. Except the basement, each floor has a central core zone (2324 m²) with one staircase, elevator, and restroom located in the middle of the zone, a data center, and the perimeter zones in four directions. The height from floor to ceiling is 2.74 m and the floor-to-floor height is 4.0 m because of the additional height of the plenum on each floor. Each floor is connected to the top and bottom floors with the staircases and elevators and floor/ceiling leakages, and to the ceiling plenum through one return grill of each zone. Internal wall leakages between every two zones are defined as the three leakage paths at the top, middle and bottom locations. Large internal leakage paths are important and include the leakage path between each perimeter zone and the core zone (as shown by the colored circles in Figure 3-2 (a)), which is 50% of the wall area; the leakage paths between the restroom (transfer grille), staircase, elevator and the core zone (as shown by the arrows in Figure 3-2 (b)); and a leakage path representing the return air grill from the core zone to the plenum.

The HVAC system includes four individual variable-air-volume (VAV) systems serving the

basement, the 1st floor, the 2nd–11th floors, and the 12th floor as shown in Figure 3-2 (a) with different supply, return and outdoor air (OA) rates.
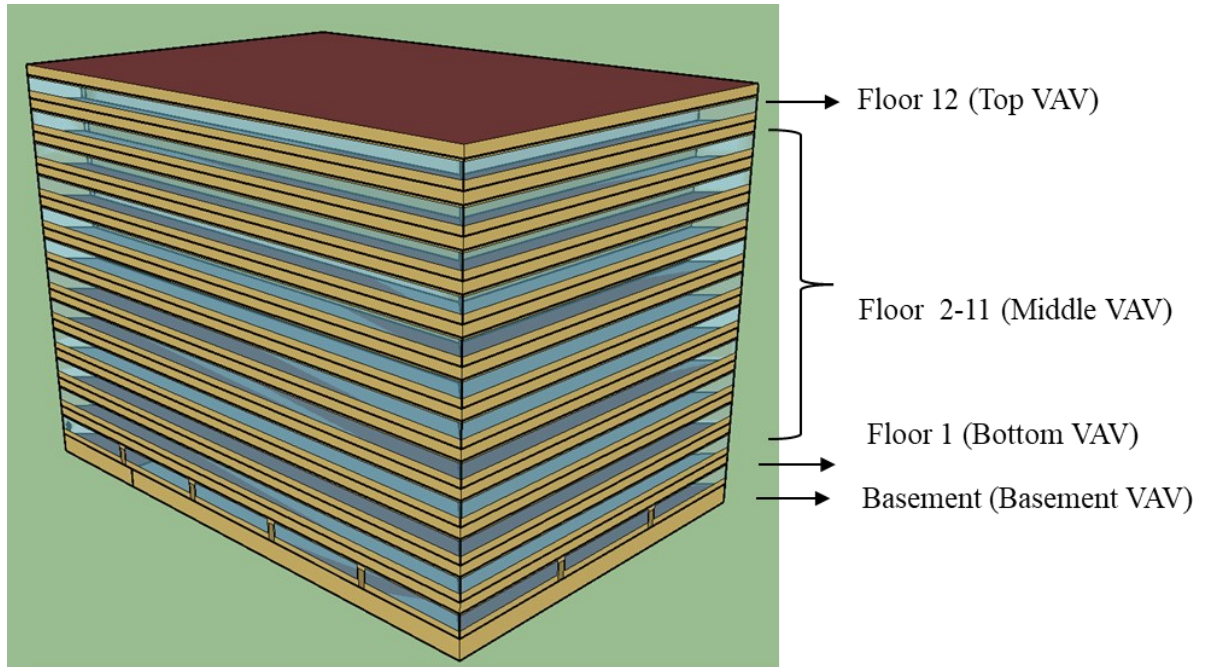
VAV System	Basement	Floor 1	Floor 2-11	Floor 12
Supply/Return (m³/s)	4.63/4.17	11.65/10.49	9.44/8.49	10.33/9.30
Baseline OA (%)	26	14	17	16

(a)
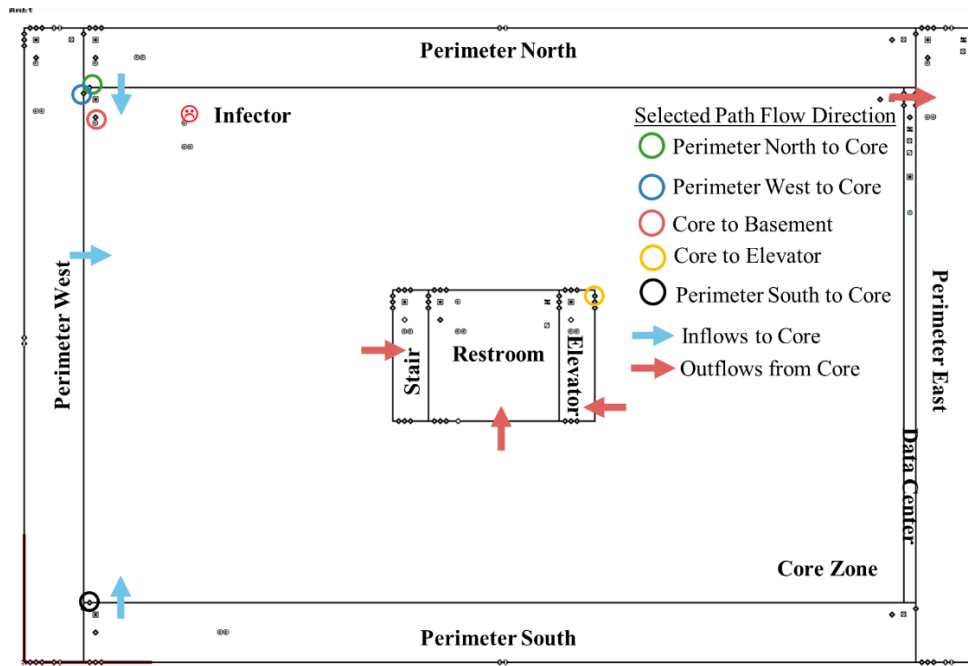
(b)
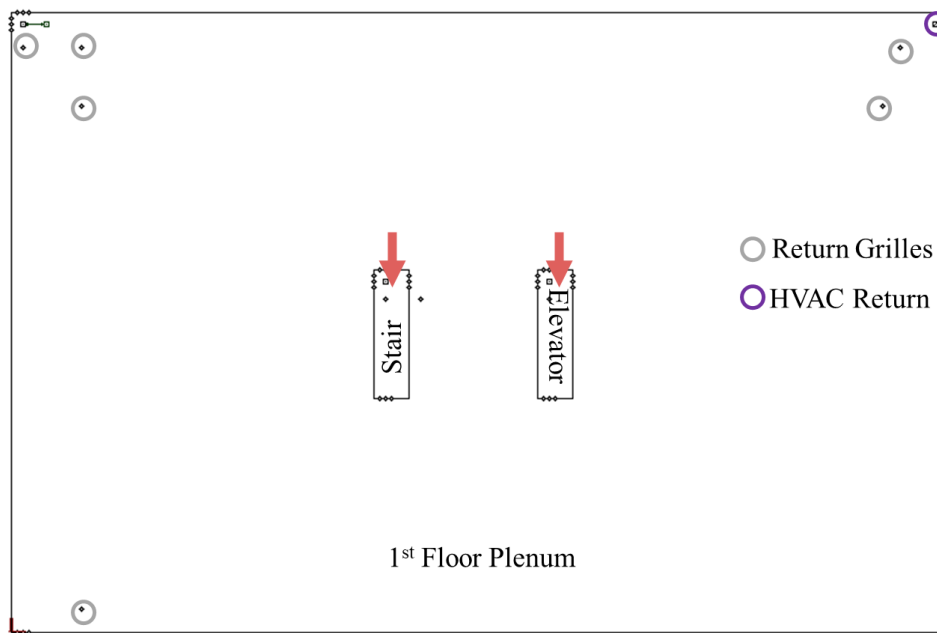
(c)

Figure 3-2. (a) Drawing of the DOE large office prototype building with ventilation air flow rates and outdoor air percentage; (b) CONTAM model schematic of the 1st-floor; and (c) drawing of the 1st-floor plenum with the return grille and HVAC return [228].

The simulations were conducted for one weekday, a Typical Meteorological Year version 3 (TMY3) weather winter design day (December 21st), in Chicago, with the hourly weather in Figure 3-3. Each floor was assumed to have 134 occupants in each core zone. One infected person was assumed to be in the 1st floor core during working hours (8:00–17:00) without leaving the space. The assumption that the infected person did not leave the building was probably the worst-case scenario with the highest exposure risk. The core zone was selected because typically most of the office staff stay here during working hours. The first floor was chosen as vertical transmission risks exist in the elevator shaft and stairs (Figure 3-7). Vertical transmission evidence for the SARS-CoV-2 has been previously reported [201]. The VAV system started at 6:00 and turned off at 22:00. The CONTAM model was created to match the operation and occupancy schedules of the EnergyPlus model. The maximum design flow rates determined by the EnergyPlus simulation were used as inputs for the HVAC supply rates in the CONTAM model [229].
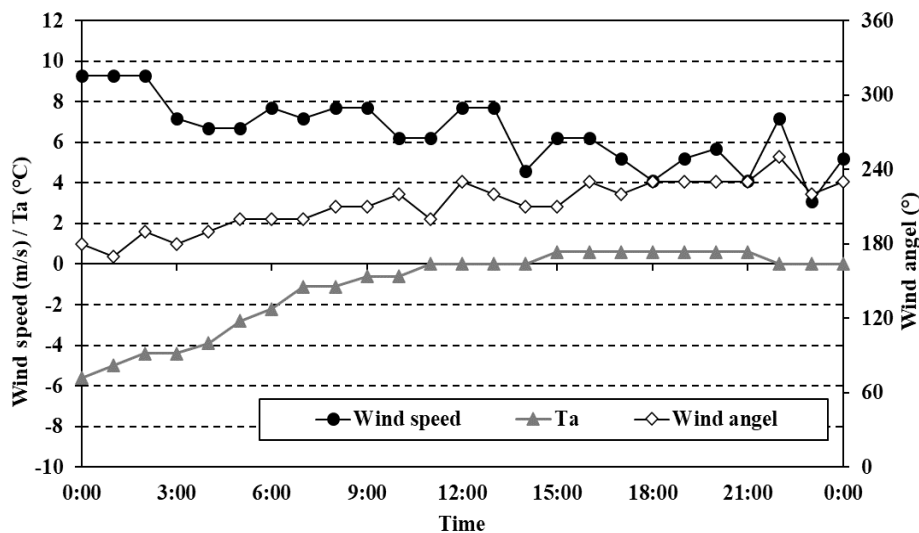
Figure 3-3. Weather parameters for Chicago (December 21st)[222].

Table 3-2 Input parameters for the CONTAM-*quanta* simulation of the DOE Large Office prototype building 1st-floor core zone

Inputs			Parameters	References
Zone geometry	Volume (m^3)/ Area (m^2)	Core	6376 / 2324	[229]
		Perimeter West (Perimeter East)	608 / 222	
		Perimeter North (Perimeter South)	803 / 293	
		Restroom	277/101	
		Stairs (Elevator)	75.7/27.6	
		Data Center	98.6/36.0	
Zone occupancy	Infector		1	-
	Susceptibles		133	[229]
Initial quanta concentration	Concentration (quanta/m^3)		0	-
Quanta generation	Quanta generation rate (quanta/h)		65	[186]
	Breathing rate (m^3/h)		0.72	[230]
	Generation duration		8:00 -17:00 (9h)	-
Deposition and deactivation	Surface deposition rate		0.3 h^{-1}	[217, 231]
	Particle deactivation rate		0.63 h^{-1}	[218]
Germicidal ultraviolet light	in-room GUV removal rate		4 h^{-1}	[232]
	in-duct GUV removal efficiency		87%	[233]
MERV removal	MERV8 removal efficiency		20%	[220]
	MERV11 removal efficiency		65%	[220]
	MERV13 removal efficiency		85%	[220]
PAC airflow rates	PAC1 (CADR)		0.46 m^3/s	
	PAC2 – 18SF (CADR)		1 m^3/s	From manufacturer
	PAC3 – 23SF (CADR)		1.45m^3/s	
	PAC4 – FN1AAF006000 (CADR)		17 m^3/s	
	HEPA removal efficiency		99%	[221]
Mask	Mask wearing percentage		0 or 100%	-
	Exhale removal efficiency		50%	[234]
	Inhale removal efficiency		30%	

Table 3-2 summarizes the key simulation parameters used in this study. The effectiveness of different strategies on mitigating virus aerosol exposure risks was investigated, including increasing outdoor air ventilation rates, equipping the building with air-cleaning devices such as MERV filters, PACs with HEPA filters, and in-room/in-duct GUV, and layering with personal mask-wearing. The baseline OA rate from the DOE prototype building model (see the table in Figure 3-2 (a)) with a MERV8 filter was defined as the baseline (BL) case "MERV8 + BL"; whereas the total supply and return flow rates of the VAV systems were kept the same for all strategies.

3.3.2 Simulation results

3.3.2.1 Room-to-room quanta transmissions and exposure risks

The multizone analysis starts with understanding how the airflow patterns on the same floor for the baseline case (MERV8+BL), (i.e., inter-zonal airflows between the core zone and the neighbor zones) impact room-to-room quanta transmission. The ambient environmental conditions and the operation of HVAC systems impact the zonal airflows. Figure 3-4 (a) illustrates the transient airflows for the five paths (Figure 3-2) on the 1st floor with the positive values for the inflows to the core zone. The airflow of the Perimeter South zone varies the most, whereas other flows are more stable throughout the day. The inter-zonal outflows tend to be relatively more steady than the inflows, which were more subject to the ambient conditions because they were connected to the perimeter zones. Figure 3-4 (b) shows the nine-hour average inter-zonal total airflow rates between two zones of the 1st floor: the average of the summation of all airflow paths between the two zones with the airflow directions indicated by the arrows (Figure 3-4 (b)). Although the HVAC system pressurizes the building during the winter (the return is 90% of the supply as shown by Figure 3-2 (a)), three zones (Perimeter North, Perimeter West, and Perimeter South) all have the inflows to the Core Zone as a result of the dominating wind direction of the day of 180° ~ 240° (Southwest winds) and 4 ~ 8 m/s. The outflows from the Core Zone to the Restroom, Elevator, and Stair were significantly higher than other paths due to the combined impacts of the pressurization of the HVAC system and

the stack effects in these spaces. The Restroom is even more underpressurized due to an exhaust fan operating from 6:00 to 22:00 at 0.15 m^3/s. Another potential transmission route is the return grilles at the ceiling of the 1st floor to the plenum (Figure 3-2 (c)). Because all return airflows go through the plenume return grilles back to the VAV systems, the leakages in the plenum also potentially contribute to airborne transmision to the stairs and the elevators as indicated by the airflow directions in Figure 3-2 (c). This would result in potential floor-floor transmissions through these vertical spaces.
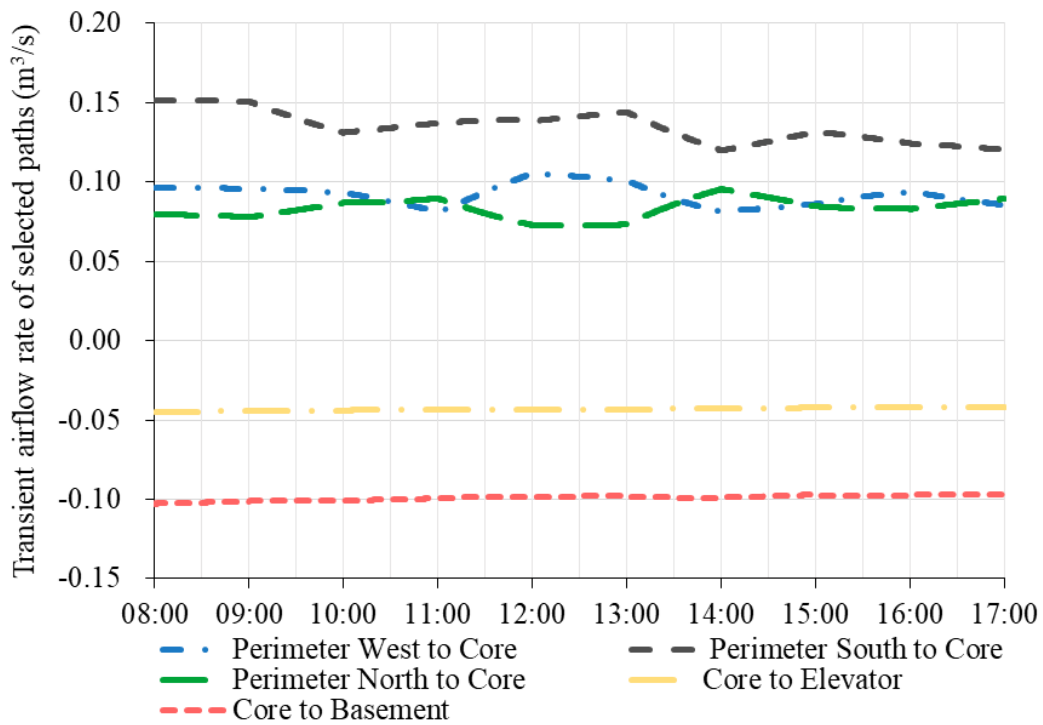
(a)
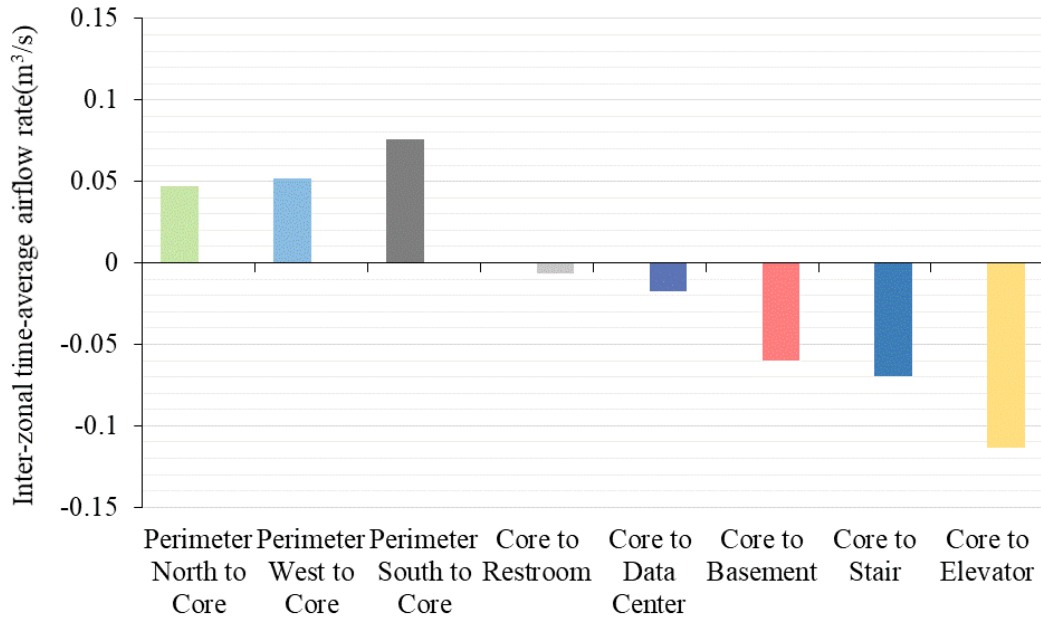
(b)

Figure 3-4. (a) Transient airflow rates for selected paths (positive values indicate airflows into the Core Zone, negative values indicate airflows out of the Core Zone); (b) average internal-zonal airflow rates. The zone locations can be found in Figure 3-2.

Figure 3-5 (a) reports the simulated transient quanta concentrations in all zones of the 1st floor when the infector was located in the 1st-floor Core Zone (Figure 3-2 (b)). For the baseline case (MERV8+BL OA), during the initial two hours (8:00 – 10:00), the quanta concentration accumulated in the zones rapidly; it reached steady state after 10:00. The average quanta concentration in the Core zone was more than twice the levels of other zones except for the Restroom, which has the 2nd highest quanta level. Figure 3-5 (b) shows the accumulated individual exposure risk for an occupant in different zones on the 1st floor over the working hours. At the end of the nine working hours, the infection risk is less than 2% in the Core Zone, 1.6% in the Restroom, about 1% in the Elevator, Stair and Datacenter, and less than 0.7% in all other ones of the 1st floor.

(a)

(b)

(c)
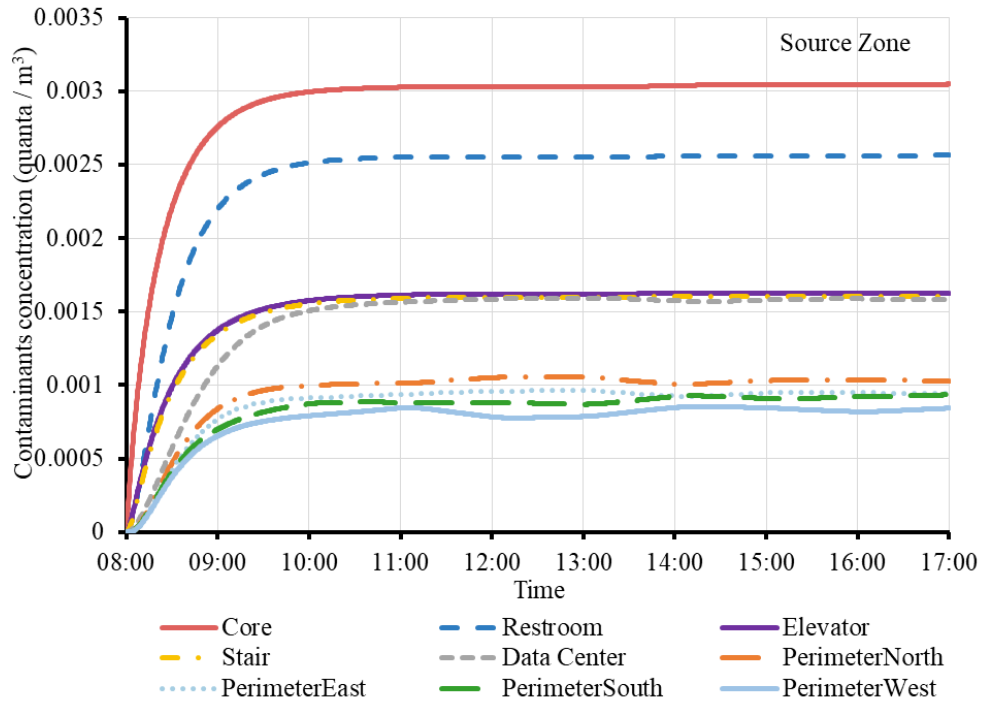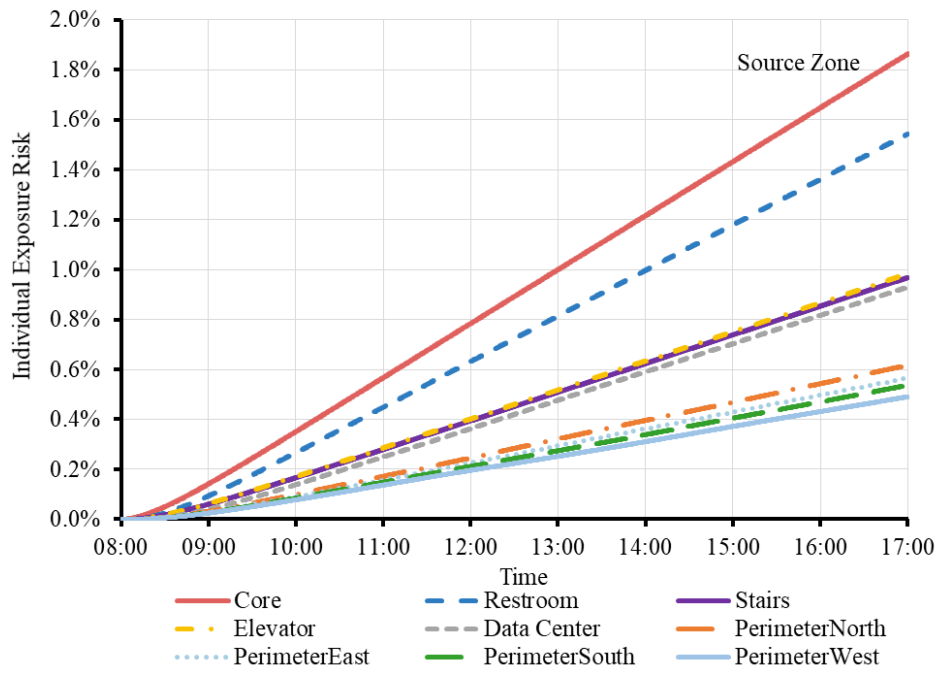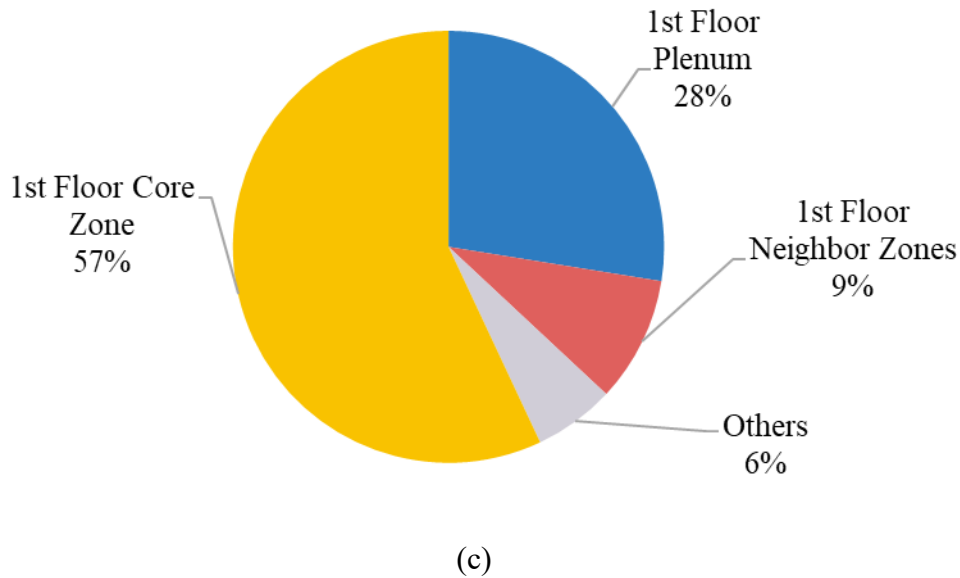
Figure 3-5. (a) Airborne quanta concentrations as a function of time in the zones on the 1st floor; (b) transient exposure risks for an occupant in the zones of the 1st floor; and (c) airborne quanta distribution on the 1st floor.

Figure 3-5 (c) explains the fate of all the airborne quanta at the end of working hours on the 1st floor. More than half of the airborne quanta stays in the source zone (Core). Because all air returns to the VAV system through the plenum, this explains the non-zero concentration levels in the Perimeter North, West and South despite only inflows from these zones to the Core Zone. In other words, these quanta concentrations mostly come from the return air from the Core Zone through the VAV system. This shows that a poorly-balanced pressure distribution could create potential inter-zonal transmission risks. Thus, it is preferred to avoid spaces with intensively negative pressures, preventing the possible transmission risk. In summary, the room-room transmission routes in the 1st floor were: Core→Restroom through the restroom return grill; Core→Staircase and Core→Elevator through leakage paths; Core→Data Center through internal partition path; and Core→Perimeter Zones through the plenum returns.

3.3.2.2 Floor-Floor quanta transmissions and exposure risks

The HVAC pressurization and stack effect in the staircase and elevator shafts could contribute to floor-floor transmission, but the 1st floor ventilation does not because it has its own individual VAV system. Here, for the baseline case (MERV8+BL OA), we report the relative exposure risks of all zones in the building compared to the risk in the 1st-floor Core Zone when the infected person is in the 1st-floor Core Zone (i.e., $P_{floor-zone}/P_{1st-Core}$) in Figure 3-6. At the 1st floor, the 1st-floor Core Zone has the highest exposure risk, followed by the Restroom, Elevator and Stair. On the higher floors, the elevator and stair are the most infective zones. Noteably, at the 7th floor, the Core and Restroom zones' risks start to increase and the the 12th floor risk gets a suprising rebound.
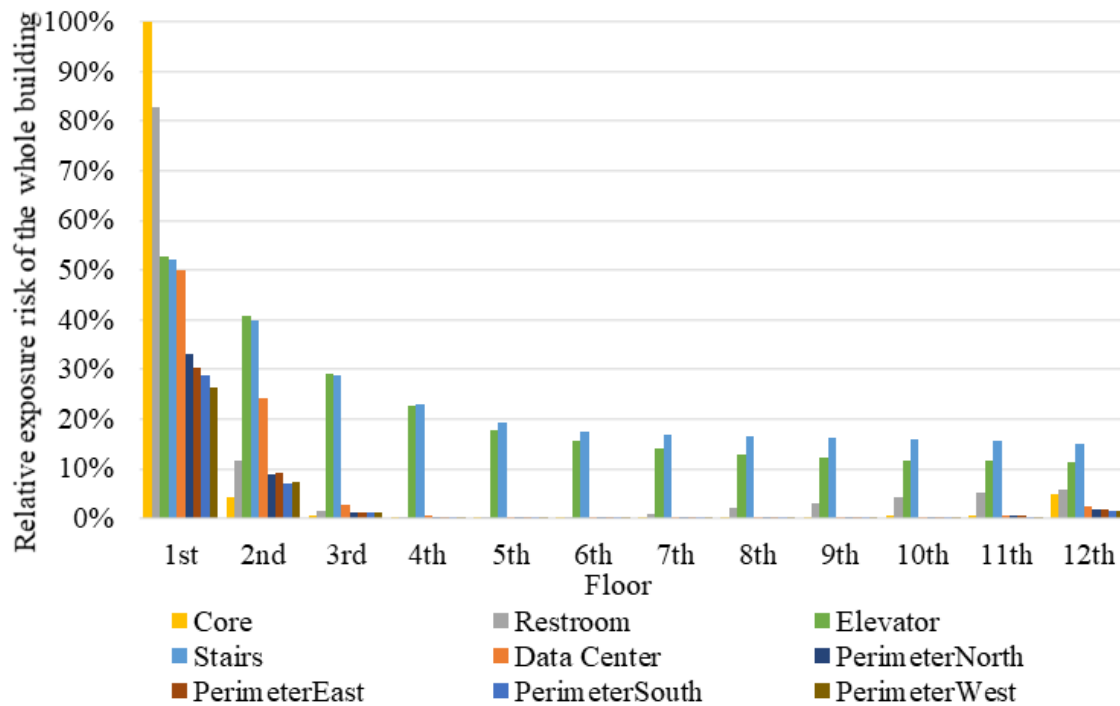
Figure 3-6. Relative risks of all floors and zones compared to the 1st-floor zones ($P_{floor}/P_{1st-Core}$ x 100%).
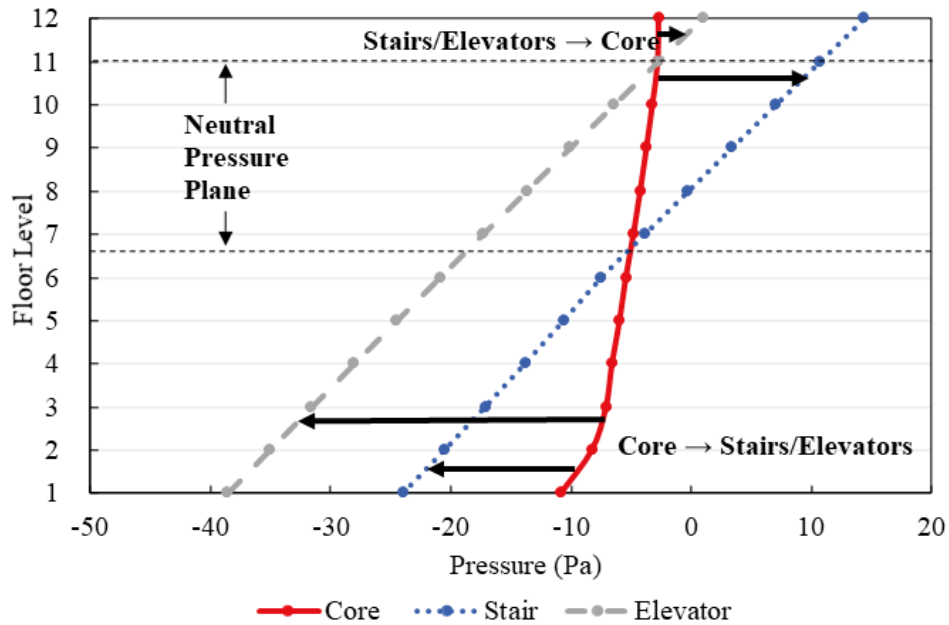
Figure 3-7. Average pressure profiles of the Core Zones, Stairs and Elevators.

The above observations may be explained by the pressure profiles in the stairs and elevators as shown by Figure 3-7. Higher risks of the elevators than that of stairs at the lower floors (<the 4th floor) can be explained by their higher inflows to the elevators (Figure 3-4 (b)) and the stronger stack effect than the stairs (Figure 3-7). However, the elevator risks continuously decrease with the height because the stronger stack effect tends to drive more non-polluted air from the neighbor zones into the elevators, thus helping to dilute the space. This continues until the 7th floor, where the airflow from the stairs starts to enter the Core zones carrying the airborne quanta because the neutral pressure plane (NPP) of the stairs is established above the 6th floor. This explains why the restrooms above the 6th floor have non-zero risks. The elevator NPP forms on the 11th floor, above which the airborne quanta of both the stairs and elevators start to infiltrate to the 12th floor. As a result, the Core Zone and Restroom of the 12th floor have higher risks than lower floors. These results show that the Floor-Floor transmission is possible as a result of the dynamics of pressure distributions in a whole building, and higher floors could become vulnerable due to the combined impacts of the stack effects and pressurization of the

44

HVAC systems. To compare the multizone to the single-zone analysis further, Appendix 2 discusses the difference between the CONTAM-quanta approach and other single-zone models (i.e., COVID19 Estimator, REHVA calculator, FaTIMA), and multizone models (i.e., CONTAM without the *quanta* approach).

3.3.2.3 Mitigations of exposure risk

The previous analysis shows that the most vulnerable space is where the infective source is located in 1st-floor Core Zone, which is also the most populated. Therefore, the following risk mitigation analysis is focused on this zone. The results of predicted exposure risks for the occupants' nine-hour exposures in the 1st-floor Core Zone are demonstrated in Figure 3-8 (a). The acceptable risk level ($R_0 = 1$) was calculated to be 0.75% for this zone. For the baseline case, the exposure risk was estimated to be 1.83% without mask-wearing. By increasing the OA rate to 1.3BL, 2BL or 100% fresh air, the exposure risk would drop to 1.79%, 1.66%, and 1.12%, respectively. The upgrade of the MERV8 filter to a MERV11 or MERV13 reduces the risk to 1.30% and 1.22%. Adding germicidal GUV, the in-duct GUV would decrease the baseline exposure risk to 1.19%, while the room GUV could lower the risk to 0.89%. In addition, adding PACs would also contribute to effective mitigation. The use of PACs (with recirculating airflow rates of 0.46m^3/s, 1 m^3/s, 1.45m^3/s) would reduce the exposure risks to 1.73%, 1.60% and 1.51%, respectively. The largest PAC (17m^3/s) would help limit the risk to 0.51%, achieving the acceptable level (0.75%). In comparison, wearing masks is the most effective and can keep $R_0 < 1$ for all evaluated mitigation strategies.

It should be noted that the risk estimation was conducted mainly for comparing different mitigation strategies. For each of the mitigation strategies, the relative risk reduction compared to the baseline is shown in Figure 3-8 (b). Upgrading the MERV filters from MERV8 to MERV11 and MERV13 tend to be more effective than adding small capacity PACs (0.46 to 1.45 m^3/s). The use of MERV13 and in-duct germicidal UV with the Baseline OA provides similar performance to that of 100% OA. When the 100% OA strategy (the yellow dotted line)

is adopted, the most relative reduction compared to baseline that can be achieved is 40%; to reduce the risk even further, in-zone strategies need to be adopted also such as operating PACs or in-room germicidal UV light.
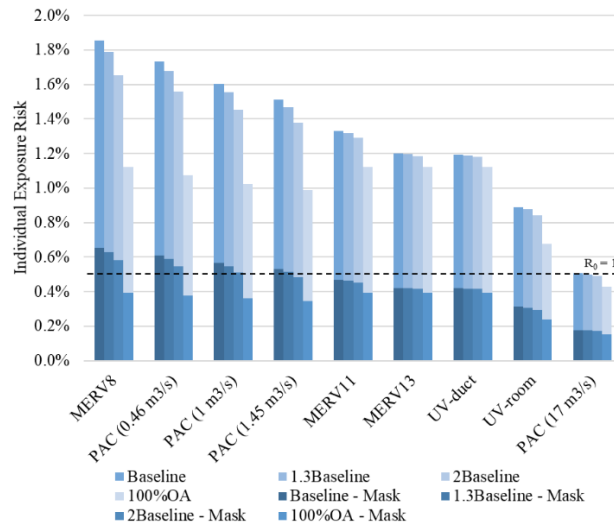
(a)
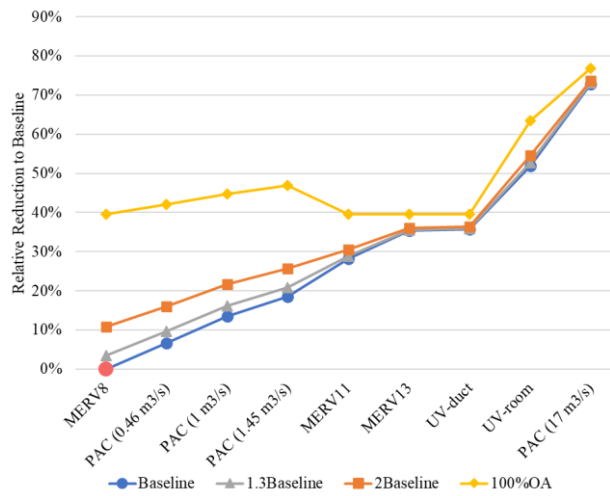
(b)

Figure 3-8. a) Individual exposure risks under different combined mitigation strategies; b) relative risk reduction compared to the baseline case (the baseline case is denoted by the red dot). Each line is for a different OA rate. As mitigation strategies are adopted the relative risk reduction increases.

3.4 Discussion

For the evaluated mitigation strategies, Figure 3-8 shows that doubling outdoor air ventilation did not effectively reduce exposure risks unless 100% OA was applied. When the outdoor air percentage was adopted as 100%, the exposure risk was reduced to 1.12%, 40% down from the baseline case. However, operating the HVAC system with 100% fresh air raises concerns over energy cost and thermal comfort indoors. It is relatively difficult to implement high OA ventilation rates in many existing systems. In reality, some existing buildings implemented a "Pandemic Mode" operation by only increasing OA rates 1.3-2 times the baseline ventilation rates. In the current study, the analysis shows that the relative reduction in risk achieved by increasing OA flow rates by 1.3 or 2 were minimal when compared to other strategies.

Other active mitigation strategies should be implemented to reduce the risk level further, for example, small retrofits that include upgrading MERV filters, and/or adding PACs or germicidal UV lights into the building zones. In this study, three types of MERV filters were investigated: MERV8, MERV11, and MERV13. Results suggest that upgrading from MERV8 to MERV11 reduced substantially individual exposure risks. For the baseline outdoor air ventilation scenarios, exposure risks fell by 29% for MERV11 and 36% for MERV13. Thus, upgrading MERV filters is effective, though a trade-off between risk mitigation and economic cost needs to be considered due to the elevated pressure drops with higher MERV filters. In the Large Office building of this study, a MERV11 upgrade combined with other measures, e.g., PAC and germicidal UV, was effective at achieving the desired risk reduction.

Adding PACs or in-room GUV increased the total equivalent air change rate to the Core Zone without interfering with the existing HVAC system operation. The portable air cleaners evaluated in this study covered a large range of capacity, from 0.5 to 42.5 m^3/s, which were based on the information provided by the industrial collaborator. As illustrated in Table 3-2, these PACs were equipped with filters with a *single-pass efficiency* of 99%. Among the investigated products, it was found that large capacity PACs (>17m^3/s) effectively lowered

exposure risks below $R_0 < 1$. Thus, the capacity of the PAC should fit the room size; for large volume areas, large capacity PACs or multiple small capacity PACs can be considered. Similar observations also apply to the GUV devices: in-room GUV in general performed better than the in-duct GUV devices in the current study.
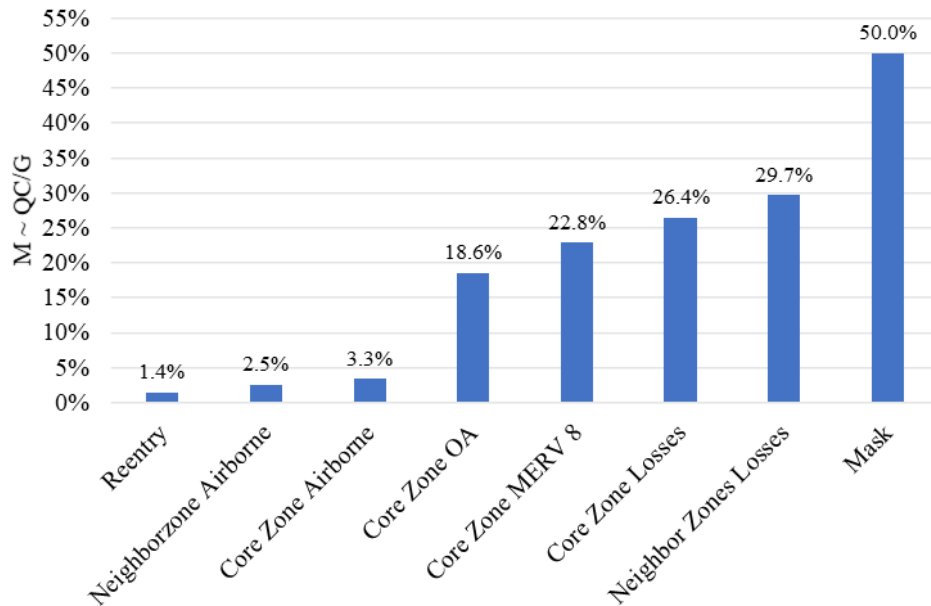
Figure 3-9. Comparison of sources and losses of virus aerosol in the Large Office building core zone to mask efficiency (M ~ QC/G).

Multizone modeling also enables an in-depth analysis of the sources of viral aerosol in the core zone because of inter-zonal airflows and losses in the core due to mitigation measures. The parameter $\frac{QC}{G}$ (Eq. 3-7) is compared to the efficacy of masking (M in Eq.3-7) to better understand whole building mitigation strategies compared to individual strategies and to sources. The comparison is reasonable because mask-wearing is commonly recognized as one of the most effective strategies and thus can be used as a baseline for evaluating the risk mitigation efficacy, it however relies on the individual to wear a mask compared to the building strategy that relies on building systems design and operation. This is achieved by summing the

airflows, Q, and time-dependent zone concentrations, C, for all components as illustrated by Eq.3-6. Figure 3-9 shows that the "Reentry" (Aerosols re-enter the Core Zone from neighboring zones) was 1.4%. This means that, 1.4% of all generated quanta re-entered the Core Zone. Much of generated airborne quanta stayed in the Core Zone (3.3%), and 2.5% remained in all the neighboring zones. The baseline OA rates would flush 18.6% of all generated, and for MERV8 filter, it would filtrate 22.8%. The "Core Zone Losses" and "Neighbor Zone Losses", which include the virus' natural decay, deposition, and exfiltration in the Core Zone and all neighbor zones, contribute to a loss of 26.4% and 29.7% of all generated quanta, respectively. As a comparison, if mask-wearing was enforced, the most effective reduction would be 50%, which is the typical efficiency value for a mask [235]. Therefore, Figure 3-9 shows that mask-wearing would be more effective than the combined effects of the baseline OA and MERV 8 in this case study. In addition, it also suggested that although there may be inter-zonal spreading in the building, the losses in the neighbor zones would also be high.

For all evaluations in this study, the air within the zones was assumed to be well-mixed. However, this assumption may simplify the real exposures in buildings. There could be additional turbulent mixing that happens within and between internal zones in the building due to heat sources, movement of occupants, flows created by doors opening, etc. Differential exposure risks for individuals at different locations in the zone could be considered in future studies by utilizing the CFD capabilities of CONTAM [50, 215].

Office environments are often crowded, poorly ventilated places where staff share the space for prolonged working hours. It has been reported that work environments are one of the most common venues for SARS-CoV-2 transmission [236]. An epidemiological investigation of a superspreading event in an open-plan office in Switzerland found that one index person in the office directly infected 67–83% of the team members [237]. In another study conducted in England, the attack rate was reported to be 55% in a public-facing office [238]. Though the events, office configurations and room ventilation conditions varied, these evaluations suggest

that, in real working situations, the transmission risks could be high. Infected cases reported by these studies not only worked at their desks, but also attended meetings in conference rooms during working hours.

Prateek et al. used steady-state simulations showing that stairwells can potentially experience higher aerosol concentrations than other conditioned zones of an office building [95]. In our study, exposure risks in stairs and elevator shafts of the Large Office building were also found to be higher than that for perimeter zones and the data center (Figure 3-5 (a)). This suggests that virus-laden aerosol could transmit to stair and elevator shafts, where mitigations such as PACs and GUV lights should be considered. Zhang evaluated the effect of integrated IAQ strategies (source control, ventilation, and air cleaning) on reducing infection risks in open-plan offices [197]. In this evaluation, a risk reduction factor (RRF) was estimated for each of the strategies such as doubling the ventilation, adding semi-open partitions *etc*. Compared with the RRF, this study provides a more precise quantification of cleaning performance for mitigation strategies and enables a reasonable comparison. In another assessment of laboratory and office environments of SARS-CoV-2 transmission, the typical office room (two air exchanges per hour) was suggested to be at least vacant for 2.5 h [239]. However, the assessment of pre-flush strategies was not included in this study, and it can be investigated in the future.

Though the approach proposed by this study could serve as an effective way for designing mitigation strategies in buildings, uncertainties cannot be avoided in risk assessments. The classic Wells-Riley model has been used to evaluate airborne exposure risks since the 1970s [82], helping the public understand airborne infection risks. However, the accurate estimation of the "quanta" generation rate remains unclear, although great efforts have been made to understand the quanta generation rate for SARS-CoV-2 under different conditions. Uncertainties in estimated input parameters can also contribute to the variation in risk estimation, such as breathing rates, filter efficiency, GUV inactivation efficiency, mask

inhale/exhale efficiency, and other key parameters. Therefore, uncertainties and the stochastic nature of the input parameters could be included in future studies, such as was done in the Skagit Valley Chorale Outbreak study [240].

3.5 Conclusions

Under the health threats posed by the SARS-CoV-2 virus and, in particular, its highly infectious new variants, aerosol transmission indoors must be addressed. Engineering control strategies can improve the indoor air quality in a building. To assess what strategy is most effective, a modeling approach was derived in this study that could be applied to many different building types and an analysis was undertaken to comprehensively compared mitigation strategies for a DOE prototype office building. The modeling approach described by this study allows for an evaluation of the whole building as a multizone structure, and the effectiveness of ventilation and air-cleaning components in the building could be effectively evaluated and compared. The Large Office scenario simulated in this study served as a good example for implementing mitigation strategies. For the baseline case, the zone-to-zone and floor-to-floor spread were possible though the risk was significantly lower in all zones compared to the source zone. The use of a duct-treatment strategy could approach the effectiveness of 100% outdoor air, and adding room cleaning devices such as portable air cleaners and in-room germicidal UV light could further enhance the air cleaning. More building types could be analyzed in future studies.

This study demonstrates how the multi-zone analysis of a DOE prototype building could be conducted and explained the detailed analysis steps of addressing airflows, pressure profiles, airborne quanta levels, and associated transmission risks. The combined effects of the HVAC system operation (e.g., winter pressurization), stack effect, and the ambient weather conditions could play a significant role in the potential whole building transmission, even to a space far away from the infected space. The single-zone or box-type models cannot achieve this level of understanding because they address the airborne quanta transmission assuming that the whole building is a single zone.

The purpose of this risk analysis was not to predict the absolute level of risk in infection in a building, but rather to compare the relative reduction of risks among different mitigation strategies. The current study focuses on one building type. Building-specific studies are important and should be conducted considering the complexities of different building uses and occupancies. Similar studies can be conducted for other DOE multizone prototype building types, such as hotels, schools, retail stores and hospitals, and with different climate zones. For achieving this purpose, the current study also shares all the input files with detailed settings of the Large Office prototype building with the community to facilitate future studies.

Chapter 4 Multizone CONTAM-quanta Modeling of SARS-CoV-2 Airborne Transmission and Infection Mitigation Strategies in Office, Hotel, Retail, and School Buildings

Abstract

Airborne transmission of SARS-CoV-2 mostly occurs indoors, and effective mitigation strategies for specific building types are needed. Most guidance provided during the pandemic focused on general strategies that may not be applicable for all buildings. A systematic evaluation of infection risk mitigation strategies for different public and commercial buildings would facilitate their reopening process as well as post-pandemic operation. This study aims at evaluating engineering mitigation strategies for five selected US Department of Energy prototype commercial buildings (i.e., Medium Office, Large Office, Small Hotel, Stand-Alone Retail, and Secondary School). The evaluation applied the multizone airflow and contaminant simulation software, CONTAM, with a newly developed CONTAM-quanta approach for infection risk assessment. The zone-to-zone quanta transmission and quanta fate were analyzed. The effectiveness of mechanical ventilation, and in-duct and in-room air treatment mitigation strategies were evaluated and compared. The efficacy of mitigation strategies was evaluated for full, 75%, 50% and 25% of design occupancy of these buildings under no-mask and mask-wearing conditions. Results suggested that for small spaces, in-duct air treatment would be insufficient for mitigating infection risks and additional in-room treatment devices would be needed. To avoid assessing mitigation strategies by simulating every building configuration, correlations of individual infection risk as a function of building mitigation parameters were developed upon extensive parametric studies.

4.1 Introduction

The COVID-19 pandemic has highlighted the importance of airborne respiratory infection control in indoor environments [241]. Insufficient ventilation designs and improper operations in crowded public buildings often lead to outbreaks and superspreading events, which raised significant concerns about occupants' indoor exposure. Shutdowns were implemented for public shared places in many countries, and individuals around the world were forced to "stay at home." Vaccines are more available, and many countries are under substantial socio-economic pressures, which leads to a return to pre-pandemic life and reopening more public spaces. Recently, many countries have passed the peak of the wave of the new SARS-CoV-2 variants [242], which promotes the easing of restrictions and the turning of policies to the long-term management of COVID-19. In the U.S., many states have lifted capacity restrictions on indoor activities, including for restaurants, schools, and offices [243]. Meanwhile, large indoor gatherings have begun to be permitted. Capacity limits in Canada have also been lifted in all indoor public settings [244]. Similar actions and policies were also implemented in England and European countries [245]. The reopening of public spaces while at the same time reducing risk of transmission poses challenges [246]. Engineering mitigation strategies could serve as an efficient way of reducing the airborne transmission of pathogens of viruses such as SARS-CoV-2, measles, tuberculosis (TB), chickenpox, influenza etc. in public spaces [247]. The virus-laden aerosols in the air could be diluted via outdoor air, trapped by filters, or disinfected by germicidal ultraviolet light (GUV). Great attention should thus be paid to understand how much outdoor ventilation air is sufficient to control airborne disease transmission indifferent types of buildings, what air treatment options should be implemented, and how to control infection risks with adequate measures, especially in the current post-pandemic era.

Risk assessment is an effective way of identifying the effectiveness of ventilation strategies on controlling the infection risks. Since the outbreak of the COVID-19 pandemic, extensive efforts have been made to quantify the risk of SARS-CoV-2 transmission. The airborne quanta

emission rate was evaluated for different conditions of viral load, respiratory, and activity levels [186], providing valuable input information of the classic Wells-Riley risk assessment models [82]. Indicators of infection risk were proposed to control the airborne transmission of disease indoors [90]. Dai and Zhao [87] evaluated the influence of air change rate on infection risks of a bus, classroom, aircraft cabin, and office. Shen et al. [88] investigated the effectiveness of different mitigation strategies in indoor areas such as long-term care facilities, schools, meat plants, buses, taxis, etc. Additionally, risks of SARS-CoV-2 infection were evaluated in classrooms under different speaking, class duration, and voice modulation scenarios [248]. A simulation study was conducted to compare the risk reduction effectiveness of long-range airborne exposure of SARS-CoV-2 between displacement and mixed-mode ventilation in a small office [89, 249]. Based on the assumption that aerosols are uniformly distributed in the room, these studies considered the changes in ventilation rate, exposure time, quanta generation rate, and volume for different indoor environments; their evaluations, however, only focus on single-zone scenarios without considering buildings with multiple floors and rooms that zone-to-zone transmission could happen.

Mitigation strategies that have been proposed for buildings include ventilation, filtration, germicidal ultraviolet light GUV, and personal protective equipment (PPE). Many studies have focused on health-care facilities [93] and/or single-zone building situations, whereas relevant investigations for multizone commercial buildings are limited [204, 205, 250, 251]. ASHRAE and REHVA have issued their guidelines in the COVID-19 pandemic context [252, 253]. General recommendations have been made for heating, ventilating, and air-conditioning (HVAC) operations, outdoor air settings, and filters [99]. However, these recommendations may not provide performance-based information to inform mitigation strategies in a specific building type. The most effective mitigation strategy may vary significantly for different types of buildings, configurations, occupancy schedules, HVAC systems, and operation settings. Multizone aerosol transmission patterns should be considered when proposing detailed mitigation strategies for a specific type of building and/or specific zones in a building,

especially during the reopening stage of commercial buildings.

Multizone building simulations enable a deeper insight into aerosol transmission potential in real buildings, and the influence of different mitigation strategies could be considered systematically within a whole building context. In addition to considering the building leakage, multizone simulations would also enable the evaluation of average and transient contaminant concentrations during occupants' exposure, and therefore help evaluate dynamic infection risks. Multizone evaluations of airflow and contaminant dispersion were proposed as early as the 1980s [43, 254]. Based on the concept of an airflow network, a building is comprised of an assembly of interconnected flow elements in a comprehensive process of mass transport both inside and outside of a building and thus driving the dispersal of contaminants throughout the building. In 2004, this theory was used to analyze the virus-laden aerosol transmission between floors through door and window leakages of a SARS outbreak in Hong Kong [255]. Later in 2013, a multizone contaminant transport simulation was performed in a hospital building to evaluate existing air-cleaning strategies; the importance of the building leakage and actual building operations was highlighted [61].

The objective of this study was to investigate how engineering mitigation strategies, layered with wearing masks, impact potential long-range SARS-CoV-2 aerosol transmission risks in typical commercial buildings. The multizone airflow and contaminant simulation software, CONTAM, developed by the US National Institute of Standards and Technology, was used for the modeling and analysis [256]. Aerosol dispersion was simulated, and infection transmission risk was assessed for five prototype commercial buildings (Medium Office, Large Office, Stand Alone Retail, Small Hotel, and Secondary School). These building models were developed with detailed building plans, typical HVAC schedules, and reasonable maximum occupancy for each room [226]. This study applied a novel approach – CONTAM-quanta [257] to assess the multizone SARS-CoV-2 infection risks based on the Wells-Riley model [82, 258] for estimating infection risks. A correlation was developed based on multiple CONTAM whole-

building simulations of the DOE prototype buildings to better understand the fundamental factors governing the relation between the airborne transmission of SARS-CoV-2 risk and mitigation measures in multizone buildings.

4.2 Methodologies

4.2.1 The CONTAM-quanta approach for evaluating infection risks

In this study, the concentration of SARS-CoV-2 aerosol was modeled in the CONTAM program as "quanta", where the "quanta" is defined as a contaminant species. This approach combines the CONTAM multizonal modeling program with the classic Wells-Riley model for infection risks predictions. This modeling method is detailed in our previous study [259] using a Large Office scenario, and named the CONTAM-quanta approach. The concept of "quanta" and Wells-Riley model will be introduced later in this section. The "quanta" concentration in different zones can be calculated, evaluating the combined effects of quanta generation and removal within the zone. The acceptable infection risk was determined using the contagious potential defined as C/I, which is the ratio of new infection cases C to the number of infectors I. An outbreak within the building could happen when C/I exceeds unity [82]. Thus, to avoid the possibility of community spreading in a building when I =1, C/I <1; in our study we assume one infector, thus we require C < 1. The corresponding acceptable infection risk level is therefore P = C/S <1/S, where S is the number of susceptible people.

The CONTAM models used in this study adopted the occupancy and outdoor air ventilation requirements that are employed in the corresponding EnergyPlus models of five DOE commercial prototype buildings [226]. Details of the methodology was illustrated in the last chapter. Mitigation strategies in multizone spaces are illustrated in Figure 4-1. Briefly using CONTAM, the occupant infection risk is determined by integrating the quanta concentration that the occupants are exposed to during their exposure period, which is expressed as:

$$E = \int_{t_1}^{t_2} C_i(t)dt \qquad \text{4-1}$$

The material balance of the quanta concentration is presented in Eq.4-2:

$$V\frac{dC_i}{dt} = (1 - M_{exh})G(t) + Q_sC_s(t) + \sum_{j=1}^{n} Q_{inf,j}C_j(t) - \left(Q_r + Q_{lx} + \eta_{ac}Q_{ac} + Q_{UVr} + \right. \qquad \text{4-2}$$

$$\left. \sum_{k=1}^{s} Q_{dep,k} + Q_{dec} + \sum_{j=1}^{n} Q_{exf,j}\right)C_i(t)$$

The infiltration via the air leakage in CONTAM was calculated based on weather conditions and system induced pressures, using a power-law relationship:

$$Q_{inf,j} = \frac{C_DA_L}{1000}\sqrt{\frac{2}{\rho}}(\Delta P_r)^{0.5-n}\Delta P_{j,i}^{n} \qquad \text{4-3}$$

E is the occupant exposure to contaminant C_i. In this application of CONTAM, C_i is the quanta concentration (quanta/m^3), t is the exposure time, C_s is in the quanta concentration in the supply air (quanta/m^3), G is the quanta generation rate from the infector (quanta/h), M_{exh} is the outward protection effectiveness for masks, Q_s, Q_r, Q_{lx}, Q_{ac}, Q_{UVr}, Q_{dep}, Q_{dec}, $Q_{inf,j}$ and $Q_{exf,j}$ are volumetric flow rates (m^3/s) for different airflow or contaminant removal processes (supply, return, local exhaust, air cleaner, in-room GUV, deposition, decay or deactivation of the virus infectivity, infiltration for zone j, and exfiltration for zone j), η_{ac} is the efficiency of the air-cleaner filters, C_D is the flow discharge coefficient, A_L is the effective air leakage area, ΔP_r is the reference pressure difference [Pa], $\Delta P_{j,i}$ is the pressure difference between zone j and zone i [Pa], and n is the flow exponent. Finally, the CONTAM simulates transient conditions as E/Δt, and the Δt is the output timestep as defined by users.
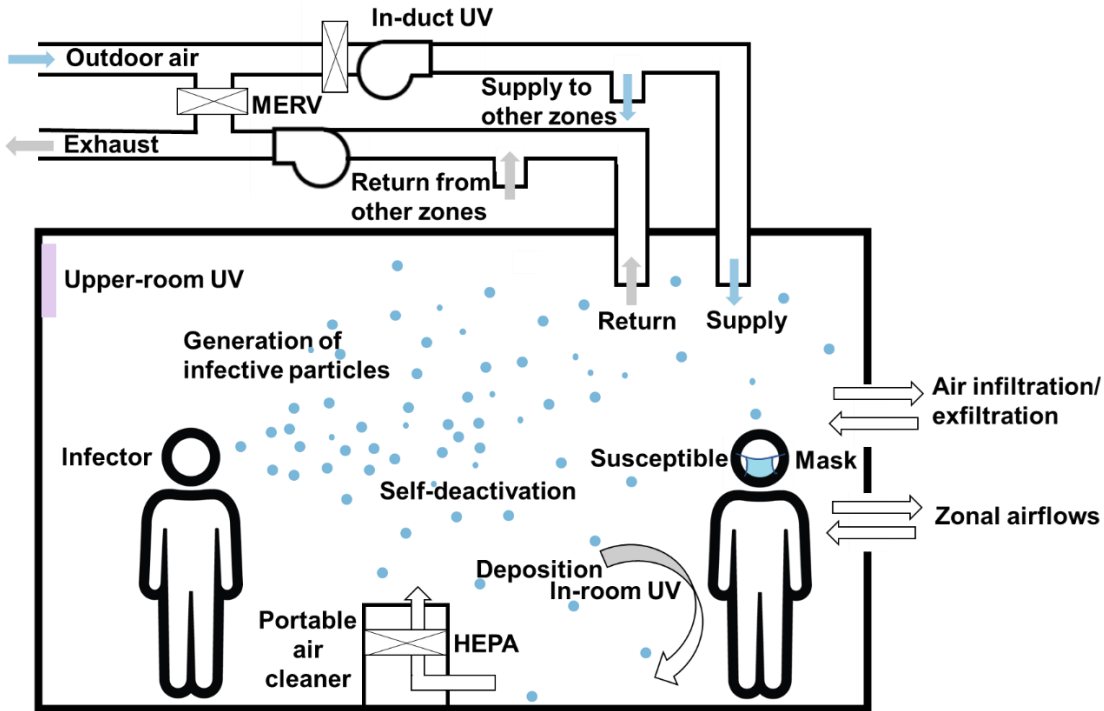
Figure 4-1 Mitigation strategies in multizone spaces for preventing airborne quanta transmission

The concept of a quantum of infection was proposed in 1955 by Wells [260] to determine the number of infectious particles required to infect people, and later in 1978, Riley et al. [82] estimated infectious dose of airborne pathogens using the number of quanta, which would help evaluate the probability of infection (Eq.4-4). This is known as the Wells-Riley equation and has been widely used to evaluate airborne infection risks of indoor spaces [87, 261].

$$P = \frac{C}{S} = 1 - e^{-n} \tag{4-4}$$

P is the probability of infection (or infection risk), C is the number of infection cases, S is the number of susceptible people, and n is the number of quanta inhaled by susceptible people. The inhaled quanta "n" can be expressed as follows:

$$n = C_{avg}B(1 - M_{inh} \times F_m)D \tag{4-5}$$

C_{avg} is the average quanta concentration (quanta/m^3), B is the breathing rate of occupants (m^3/s), M_{inh} is the mask efficiency for inhalation, F_m is the fraction of occupants wearing masks,

and D is the occupant exposure duration.

In this study, we assumed that only one infector caused the transmission, and the infector is removed from the pool of susceptible. The engineering mitigation strategies recommended in this study were all based on this assumption. Only airborne transmissions occur in the evaluated scenarios and infectious particles randomly distributed in the room. At the start of the day, the initial quanta concentration is zero. The fates of airborne quanta include existing the building (via HVAC ventilation and the air leakage), filtration (via filters such as MERV, HEPA etc.), deposition, deactivation and airborne.

4.2.2 Equivalent air change rate

For each investigated strategy, the corresponding total equivalent air change rate (Q_e) was calculated, which is a sum of the air change rates (units are 1/h) from outdoor air ventilation, recirculated ventilation air that passes through MERV filters, portable air cleaners, and inactivation by GUV lights, as well as quanta deposition and deactivation of the airborne virus. This can be expressed as:

$$Q_e = Q_{OA} + Q_{MERV} + Q_{PAC} + Q_{GUV} + Q_{deposition} + Q_{deactivation} \qquad \text{4-6}$$

Where:

Q_{OA} = outdoor air ventilation rate in (m^3/h) divided by the room volume (m^3),

Q_{MERV} = recirculated ventilation airflow rate (m^3/h) × MERV efficiency/Volume (m^3),

Q_{PAC} = CADR(m^3/h)/ Volume (m^3),

Q_{GUVr} = airflow rate passing by the in-duct GUV light (m^3/h)/ Volume (m^3), or clean air delivery rate provided by the upper-room germicidal lamp system $CADR_{UV}$(m^3/h)/ Volume (m^3),

$Q_{deposition}$ = Quanta deposition rate (1/h)

$Q_{deactivation}$ =Viral deactivation rate (1/h)

4.2.3 DOE prototype commercial building models

The floor layouts of CONTAM models of each DOE prototype building are illustrated in Figure

4-2. The Medium Office is a three-story, 1661 m^2 footprint building with four perimeter zones and one core zone on each floor, except the basement. The Large Office building has 12 floors (3563 m^2 footprint), also with four perimeter zones and one core zone on each floor. In the Medium and Large Office, a single large leakage path was modeled, representing the half-height office partitions (fifty percent of the total wall area). The Stand-Alone Retail is a single-floor building with a 2294 m^2 footprint and five zones: core retail, backspace, point of sale, front retail, and restroom. The Small Hotel is a four-story building (1003m^2 footprint) with 19 zones on the first floor and 16 zones on upper floors. The secondary school is a two-story "E"-shaped building (19592 m^2 footprint), with 25 zones on the first floor and 21 zones on the second floor. More detailed descriptions of the buildings can be found in official DOE reports [262]. More information for investigated zones is in Table 4-1.
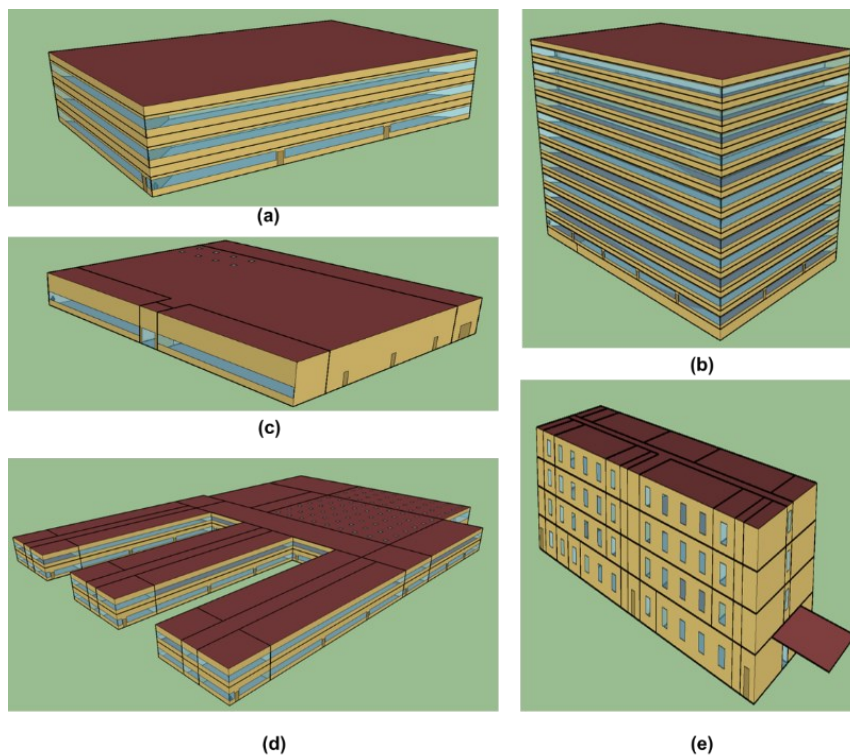
Figure 4-2 DOE prototype models in CONTAM (a) Medium Office (b) Large Office
(c) Stand-Alone Retail (d) Secondary School (e) Small Hotel.

The occupancy and ventilation settings in the CONTAM models were employed from the

EnergyPlus DOE prototype models [263]. Occupants' exposure duration was determined focusing on the most at-risk occupants, namely the employees who spend more time in the buildings. Simulations were performed for December 21st with Chicago Typical Meteorological Year version3 (TMY3) weather (Figure 4-3). It should be noted that weather conditions would not influence system operations such as the outdoor air supply in the current models developed by National Institute of Standard and Technology (NIST). In addition, for the baseline cases in this study, a one-week simulation was performed as comparison for five weekdays in Chicago in December (Dec. 18– Dec. 22).
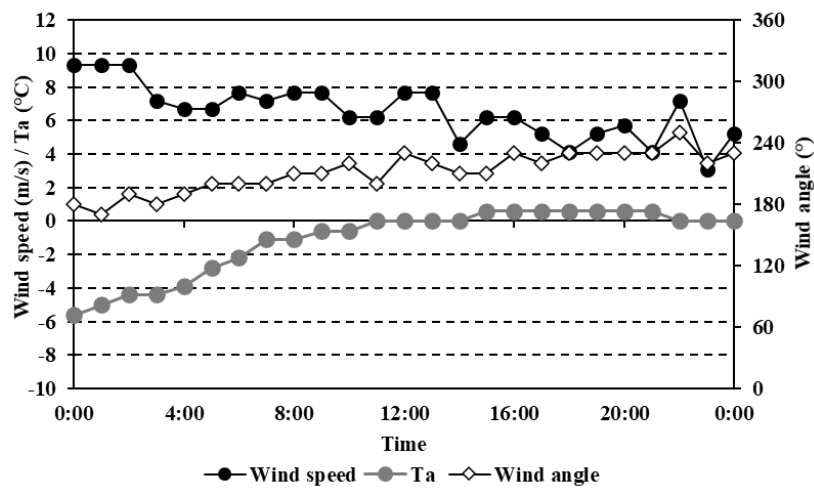
Figure 4-3 Outdoor atmospheric parameters for CONTAM simulations
(Chicago, Dec. 21). Ta is the air temperature

Table 4-1. Infectious Zone Characteristics for Simulated Prototype Buildings

Building Type	Area (m^2)	Volume (m^3)	HVAC system type	Supply airflow rates (m^3/s)	OA ratio (%)	Baseline air change rate (1/h)	Maximum Occupancy	Duration of Exposure Modeled
Medium Office (Core Zone)	822	2255	variable air volume (VAV)	2.95	14.4	0.68	53	8:00-17:00 (9h)
Large Office (Core Zone)	2324	6376	variable air volume (VAV)	8.25	14	0.65	134	8:00-17:00 (9h)

62

Stand-Alone Retail (Core Retail)	1632	9955	constant-volume single-zone system	5.67	33.3	0.68	258	Infector (Staff): 8:00 – 22:00 Susceptible (Customer): 8:00 – 16:00 Susceptible
Small Hotel (Front Lounge)	163	546	packaged terminal air conditioner (PTAC)	0.74	32.1	1.57	53	Infector (Staff): 5:00 – 20:00 Susceptible (Guest): 12:00 – 13:00 (1h)
Small Hotel (Meeting Room)	80	269	packaged terminal air conditioner (PTAC)	0.34	37	1.68	43	Infector: 13:00 – 15:00 Susceptible: 13:00 – 15:00 (2h)
Secondary School (Classroom)	485	1940	variable air volume (VAV)	1.27	73	1.72	180	8:00 – 15:00 (7h)
Secondary School (Corner Classroom)	100	401	variable air volume (VAV)	0.26	73	1.70	37	8:00 – 15:00 (7h)
Secondary School (Auditorium)	1967	7866	constant air volume (CAV)	4.10	70	1.31	1596	15:00 – 19:00 (4h)
Secondary School (Café)	609	2439	constant air volume (CAV)	2.95	70	3.05	67	9:00 – 14:00 (5h)

Table 4-2. SARS-CoV-2 Quanta-Related Modeling Parameters

Input		Parameters	Reference
Initial concentration		0 quanta/m^3	-
Generation rate		65 quanta/h	[186, 264]
Quanta removal	Surface deposition rate	0.3 h^{-1}	[217]
	Quanta deactivation rate	0.63 h^{-1}	[218]
	UVGI (in-room) Q_e	4 h^{-1}	[232]
	Default quanta particle size	1 - 3μm	[265]
	MERV8 removal efficiency	20%	[266]
	MERV11 removal efficiency	65%	[266]
	MERV13 removal efficiency	85%	[266]
	HEPA removal efficiency	99%	[267]
	UVGI (in-duct) removal efficiency	87%	[233]
	PAC1	0.46 m^3/s	
	PAC2	1 m^3/s	
	PAC3	1.45m^3/s	From manufacturer
	PAC4	17 m^3/s	
Mask wearing	Mask wearing percentage	0 / 100%	-
	Outward protection effectiveness	50%	[234]
	Inward protection effectiveness	30%	[234]
	Breathing rate	0.72 m^3/h	[268]

4.2.4 Baseline case of airborne risk mitigation strategies

The baseline model case consisted of a baseline outdoor air setting and a MERV8 filter in the air-handling system. No additional air-cleaning devices were applied. One infector was assumed to stay in the investigated zone (list in Table 4-1) during the entire exposure time.

The mitigation strategies are presented in Figure 4-4. Four different outdoor air (OA) levels were simulated: Baseline OA, 1.3×Baseline OA, 2×Baseline OA, and 100% OA. Three levels of MERV filters were chosen: MERV8, MERV11, and MERV13. The use of PACs with clean air delivery rates at 0.46 m^3/s, 1 m^3/s, 1.45m^3/s, and 17 m^3/s and GUV light in-room and in-duct were investigated. Additional detailed information is listed in Table 4-2.

Outdoor air ventilation	MERV filters	Additional air treatment
Baseline OA	MERV8	PAC (0.46 m³/s)
1.3×Baseline OA	MERV11	PAC (1 m³/s)
2×Baseline OA	MERV13	PAC (1.45 m³/s)
100% OA		PAC (17 m³/s)
		UV (in-room)
		UV (in-duct)
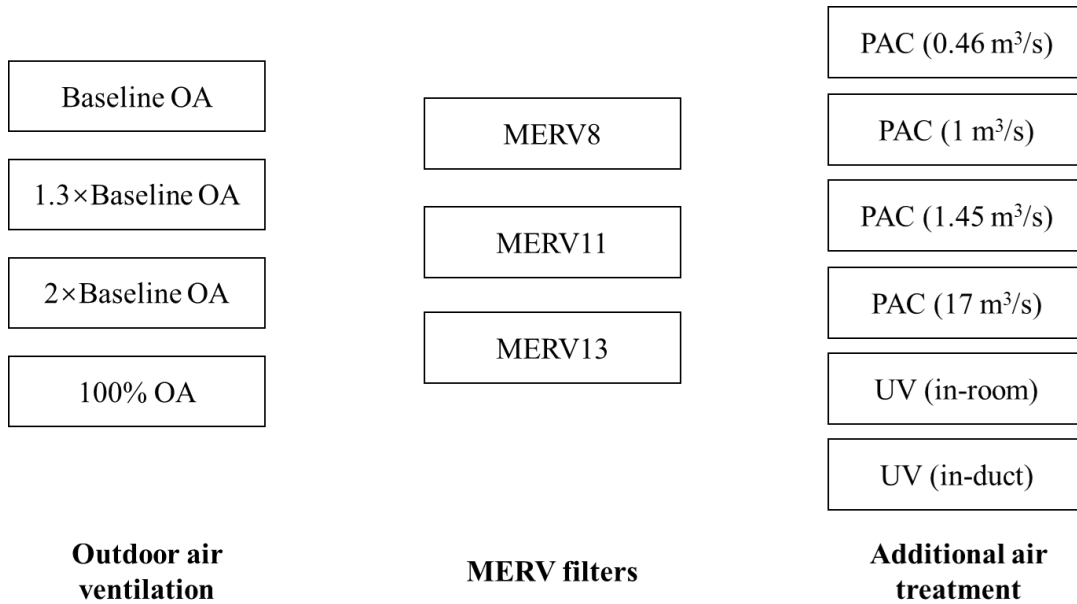
Figure 4-4 Seventy-two combinations of mitigations evaluated in this study

4.3 Simulation Results

4.3.1 Zone to zone transmission
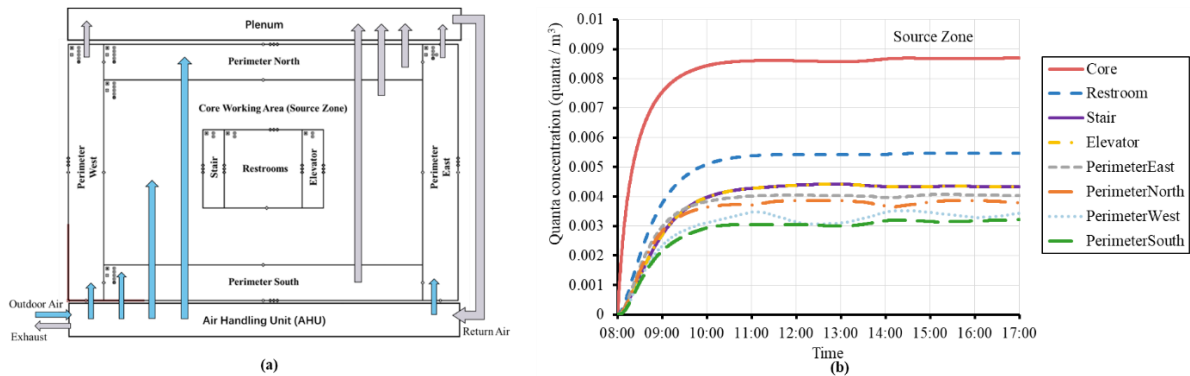
Figure 4-5 Medium Office (a) top-view diagram showing outdoor air flows (blue) and exhaust/return flows (gray) and (b) quanta concentration as a function of time during a workday with the infector in the core zone on the first floor. Contaminant generation source and deposition/deactivation items were added on the top-left of each room (small symbols).
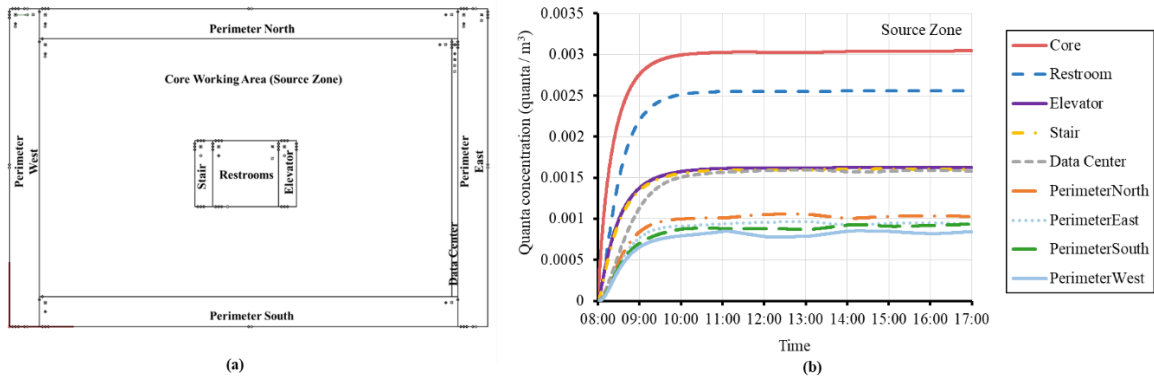
Figure 4-6 Large Office (a) top-view diagram showing outdoor air flows (blue) and exhaust/return flows (gray) and (b) quanta concentration as a function of time during a workday with the infector in the core zone on the first floor. Small icons in each room were contaminant generation source, deposition/deactivation items, and the supply/return of HVAC systems (small symbols).
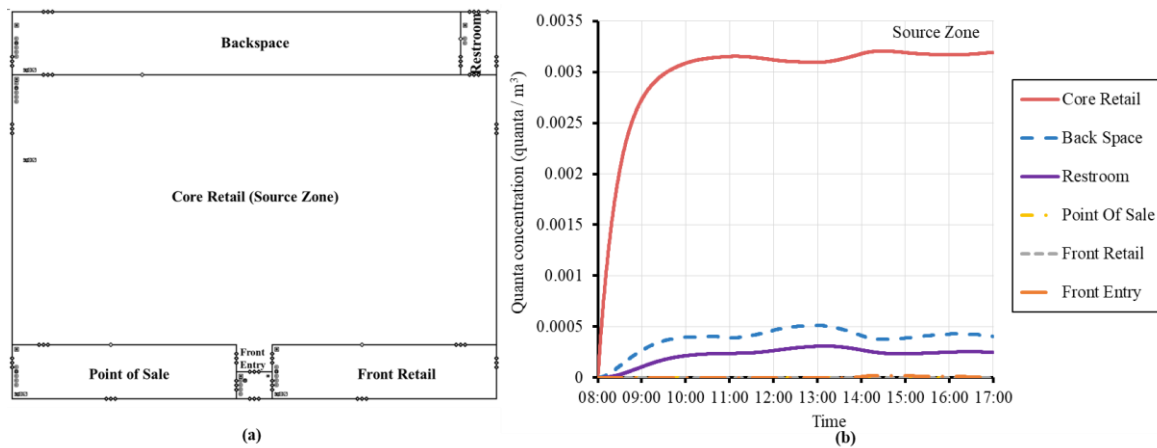
Figure 4-7 Stand-Alone Retail (a) top-view diagram showing outdoor air flows (blue) and exhaust/return flows (gray) and (b) quanta concentration as a function of time during a workday with the infector in the core zone on the first floor. Small icons in each room were contaminant generation source, deposition/deactivation items, and the supply/return of HVAC systems (small symbols).
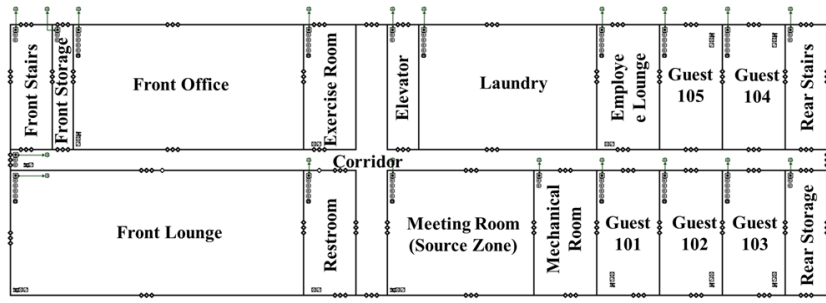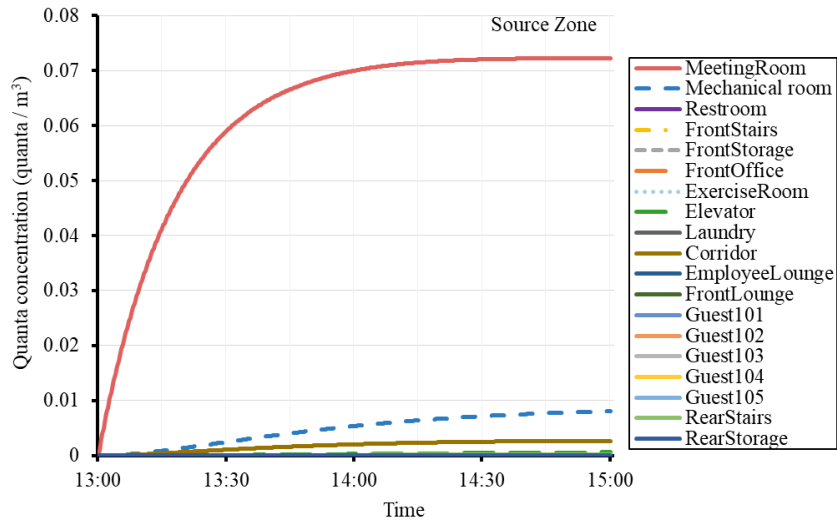
Figure 4-8 Small Hotel (a) top-view diagram showing outdoor air flows (blue) and exhaust/return flows (gray) and (b) quanta concentration as a function of time during a workday with the infector in the core zone on the first floor. Small icons in each room were contaminant generation source, deposition/deactivation items, and the supply/return of HVAC systems (small symbols).
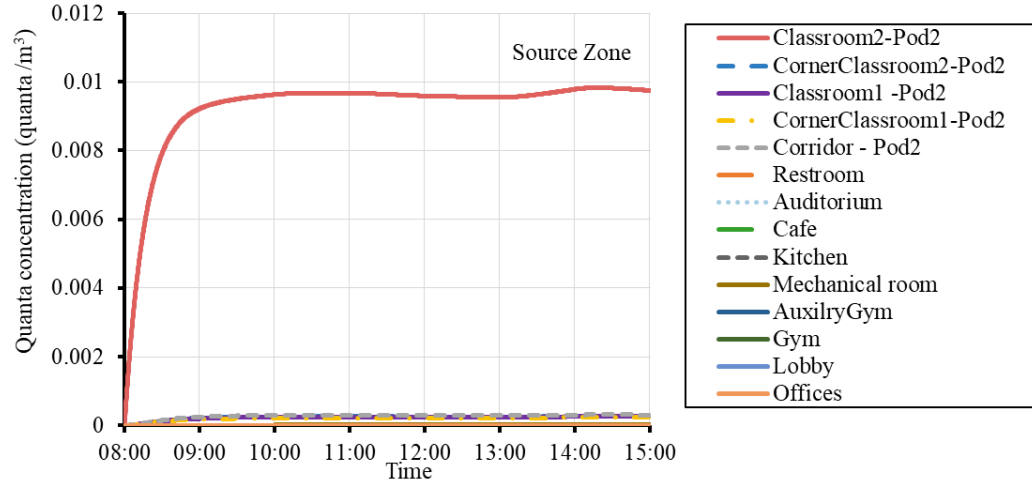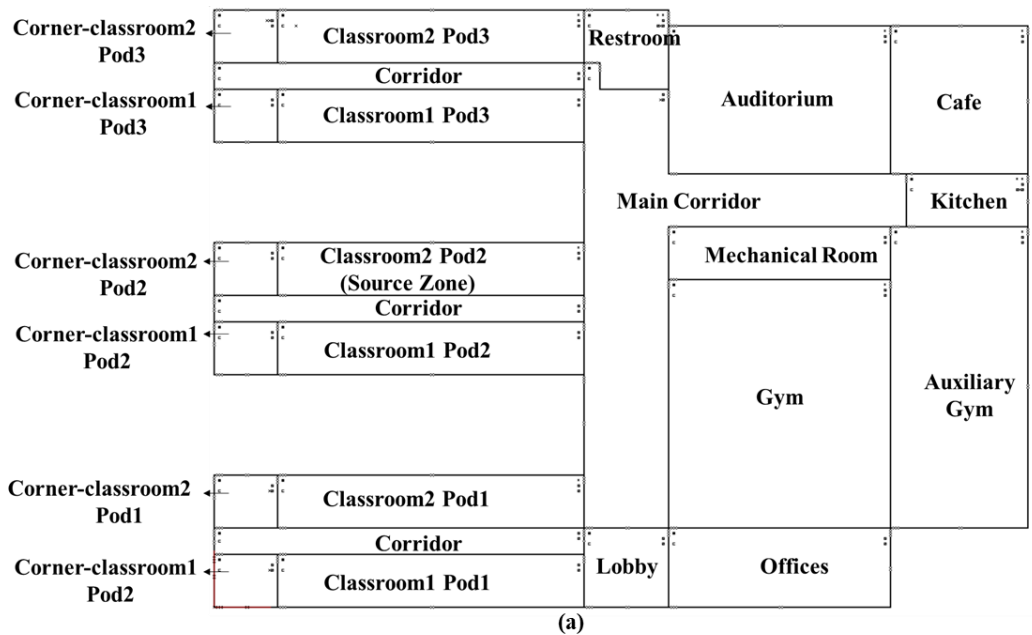
Figure 4-9 Secondary School (a) top-view diagram showing outdoor air flows (blue) and exhaust/return flows (gray) and (b) quanta concentration as a function of time during a workday with the infector in the core zone on the first floor. Small icons in each room were contaminant generation source, deposition/deactivation items, and the supply/return of HVAC systems.

Figure 4-5 - Figure 4-9 illustrate the quanta concentrations in the different zones in the simulated DOE prototype buildings. The zone that contains the index person has the highest infection risk, far higher than the risk in other connected zones. It suggests that while quanta could transfer from the source zone to other zones, the risk that adjacent zones suffer is significantly lower.

In the office buildings, the restroom was the zone with the second-highest infection risk. This is because a return grille was designed on the restroom wall, connecting the restroom and the rest of the whole floor. All air-conditioned areas were pressurized (Core and Perimeter Zones). An exhaust fan was operating in the restroom, leading to the negative pressure inside it. Thus, more quanta could be transmitted to the restroom via air leakage sites and the return grille.

Air leakage may not be the only route for zone-to-zone transmission. In Figure 4-5 and Figure 4-6, neighboring zones in the office buildings tend to be more vulnerable than for the other types of buildings. This is explained by the different designs in the HVAC systems. A central ventilation system (variable-air-volume, VAV) was used in the Medium Office, Large Office, and Secondary School, while the Retail and Small Hotel meeting room used a constant-volume single-zone system and a packaged terminal air conditioner respectively. The central air-handling system for the Medium Office is illustrated in Figure 4-6. Contaminated air in the source zone could re-enter zones through the ducts of the air-handling unit. Though a VAV system was also used in the Secondary School, its risk of zone-to-zone transmission was low, since high outdoor air rates were applied achieving 73% of the total air supplied.

In summary zone-to-zone transmission happened via the air leakage and the HVAC ducts connecting zones. A dramatic ratio increase of OA would effectively limit the zonal transmissions in buildings with central ventilation systems.

4.3.2 Fate of airborne quanta

The impact of system-level mitigation strategies on quanta fates was investigated in this study. Figure 4-10 shows results for the Medium Office and Figure 4-11 is a summary of the fates in different buildings using duct-treatment mitigation strategies. For buildings in which infection risks in multiple zones were investigated (Small Hotel and Secondary School), only one zone was selected to report respectively (meeting room and classroom). Four airborne quanta fates were assessed: exhausted, filtered, deposited, and deactivated; and compared with the quanta that remained airborne. Exhausted sums the number of quanta that exited the building via air

leakage sites and HVAC systems. Filtered added up quanta trapped by filtration (e.g., MERV filters or PACs). Deposited and deactivated includes quanta removed by deposition on to surfaces and deactivation of airborne virus.
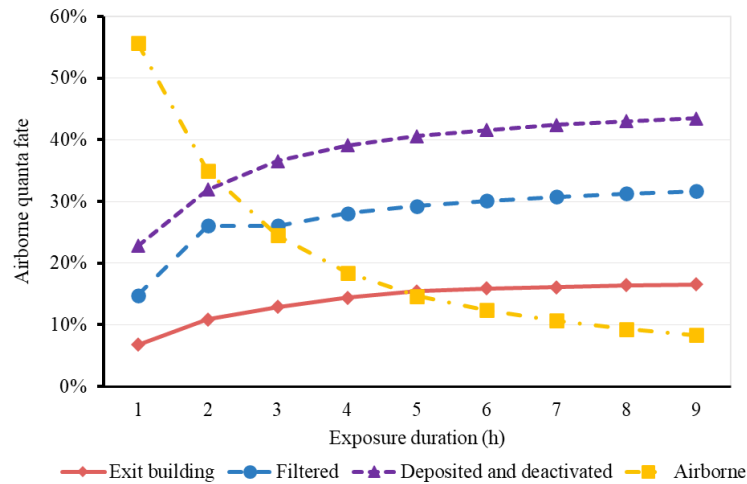
Figure 4-10 The fate of airborne quanta in Medium Office versus exposure duration.

The percentage of airborne quanta in the building decreased with exposure duration while the percentage that was filtered or exited the building through exhaust air gradually increased as the duration extended (Figure 4-10). The longer the exposure, the larger the role that the ventilation system plays in eliminating quanta. For example, during the first hour of exposure, 15% of airborne quanta were captured by the filter of the ventilation system; this number increased to over 30% after eight hours. In addition, settling and deactivation were important removal mechanisms.

The Small Hotel - Meeting Room scenario has the highest percentage of airborne quanta among the five buildings (Figure 4-11); for the baseline case, 20.7% of the generated quanta remained, while for other baseline cases, it was less than 10%. Even with the 100% outdoor air supply scenario, there was still 12.4% of the airborne quanta remaining in the room. This is due to the exposure time (2h) being shorter than other scenarios. During the meeting, to reduce the infection risk, in addition to outdoor air flushing and MERV filtration, room-treatment

70

strategies should be considered, such as PACs and in-room UV light.

For a designated building scenario, the larger the sum of exfiltrated and filtered components, the more prominent role that the duct-treatment strategies play. For example, this sum reached 48.3% for the baseline scenario for the Medium Office case. When the MERV filter was upgraded from MERV8 to MERV13, this sum was 74.3%, like the 100% OA strategy (76.9%). The BL+MERV13 combination was better than the 2×BL+MERV11. Similar phenomena were also found in other building types. As a result, a proper match of outdoor air percentage and MERV filters can effectively improve mitigation effectiveness, and nearly approach the performance of 100% outdoor air.
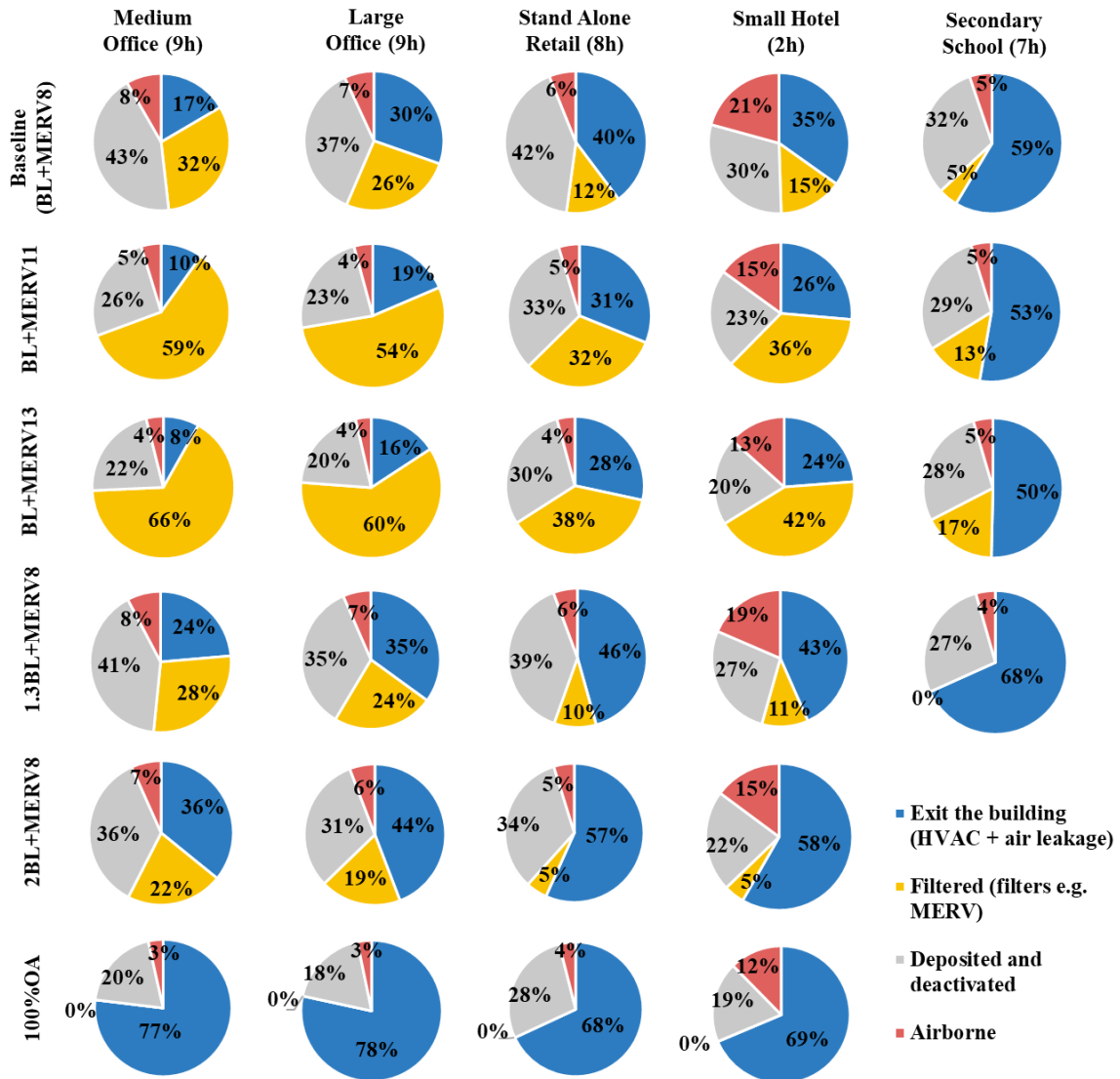
Figure 4-11 Quanta fate of released quanta during susceptible exposure duration.   Infector was in the core zone of all buildings, except for Small Hotel and Secondary School, where they were in the meeting room and classroom respectively. Susceptible duration information is indicated in the column labels (also see Table 4-1).

4.3.3 Risk assessment for baseline cases

The individual infection risk for baseline cases is illustrated in Figure 4-12. The Secondary School (Corner Classroom) and Small Hotel (Meeting Room) had the highest mean infection risks (17.3% and 8.4%) during the five-day simulation period. Compared with other zones, these two areas have smaller volumes (269 m^3 and 401 m^3) and thus quanta concentrations in

these two zones were higher, and therefore their corresponding infection risks were also high (see Eq. 4-1, Eq. 4-2, and Eq.4-3). A confined space tends to have a higher quanta concentration, which is consistent with findings from previous studies [269, 270]. Despite similar baseline supply rates for OA, individual infection risks for the Corner Classroom were about twice as high compared to the Meeting Room. The Corner Classroom had longer exposure (7 h), while occupants stayed in the Meeting Room for only two hours. For confined spaces with longer exposures, infection risks should be addressed with additional mitigation measures, even if the outdoor air ventilation rates are high, such as in the Corner Classroom in the Secondary School.

	Medium Office - Core Zone	Large Office - Core Zone	Stand Alone Retail - Core Retail	Small Hotel - Front Lounge	Small Hotel - Meeting Room	Secondary School - Multiple Classroom	Secondary School - Corner Classroom	Secondary School - Auditorium	Secondary School - Café
Mean (%)	5.16	1.82	1.70	1.76	8.41	4.69	17.29	0.63	2.03
Max (%)	5.29	1.87	1.77	1.83	8.59	4.90	18.82	0.64	2.08
Min (%)	5.06	1.78	1.66	1.66	8.28	4.35	15.85	0.61	1.97
ACR (h-1)	0.7	0.7	0.7	1.6	1.7	1.7	1.7	1.3	3.1
Volume (m3)	2255	6376	9955	546	269	1940	401	7866	2439
Duration (h)	9	9	8	1	2	7	7	4	5

Figure 4-12 Individual infection risk P [%] for baseline cases for evaluated DOE commercial prototype buildings. The height of the column is the mean risk value; error bars are maximum and minimum values.

4.3.4 The effectiveness of risk mitigation strategies

To mitigate infection risks in these buildings, a variety of air-cleaning strategies were tested. Results for the Small Hotel's Front Lounge and Meeting Room are in Figure 4-13. For the Front Lounge, most of the mitigation strategies effectively reduced risks below the contagious potential C/I =1 line (Figure 4-13 (a)), except for the baseline case and 1.3BL+MERV8. By contrast, more mitigation efforts were required for the Meeting Room. As previously mentioned, even the 100% outdoor air was not sufficient. Thus, strategies in the Meeting Room should be supplemented with in-room mitigation. For example, using a portable air-cleaner reduced risks to an acceptable level (Figure 4-13 (b)).

Upgrading MERV filters benefit risk mitigations. For the baseline Hotel case, the upgrade from MERV8 to MERV11 led to a 0.7% decrease for the Front Lounge and a 2% decrease in risks for the Meeting Room. The switch from MERV11 to MERV13 contributed to further risk reductions of 0.2% and 0.6% respectively. This indicates there are diminishing returns for upgrading MERV filters. An enhanced air filtration strategy has been widely suggested during the COVID-19 pandemic; specifically, MERV13 was recommended as the minimum [271]. However, there is a trade-off between improved air-cleaning performance with filter upgrades and added costs and potential operational difficulties in retrofitting existing HVAC systems.

For all evaluated mitigation strategies, individual infection risks for 100% mask-wearing occupants were also calculated and are shown in Figure 4-13 using dark colors. In the Meeting Room, except for the baseline case and 1.3×BL + MERV8, risks for all evaluated cases were mitigated to acceptable levels with masks (C/I = 1). This means that the use of masks could permit a two-hour meeting in a meeting room with basic ventilation settings.
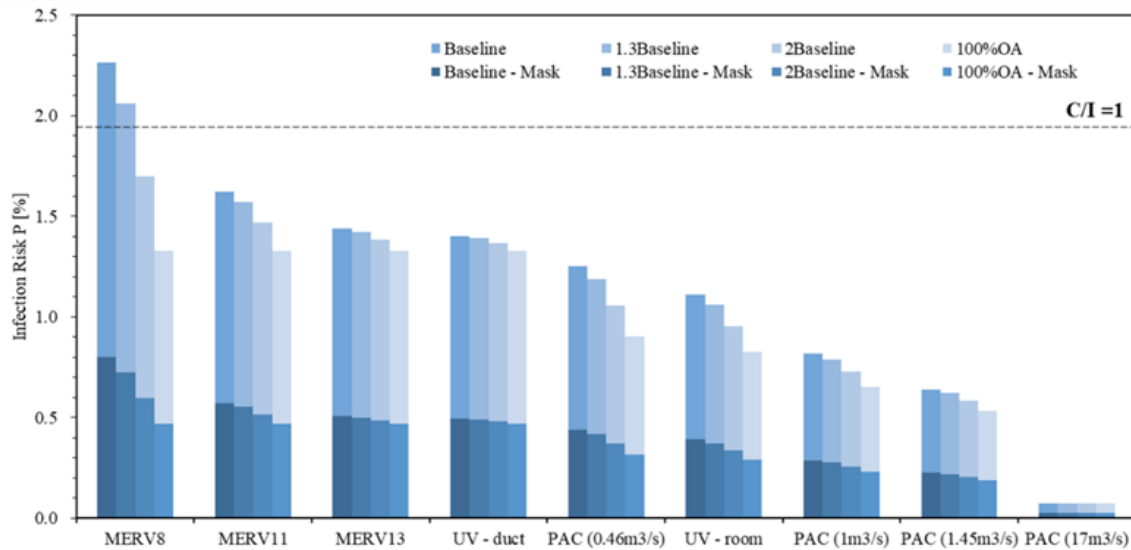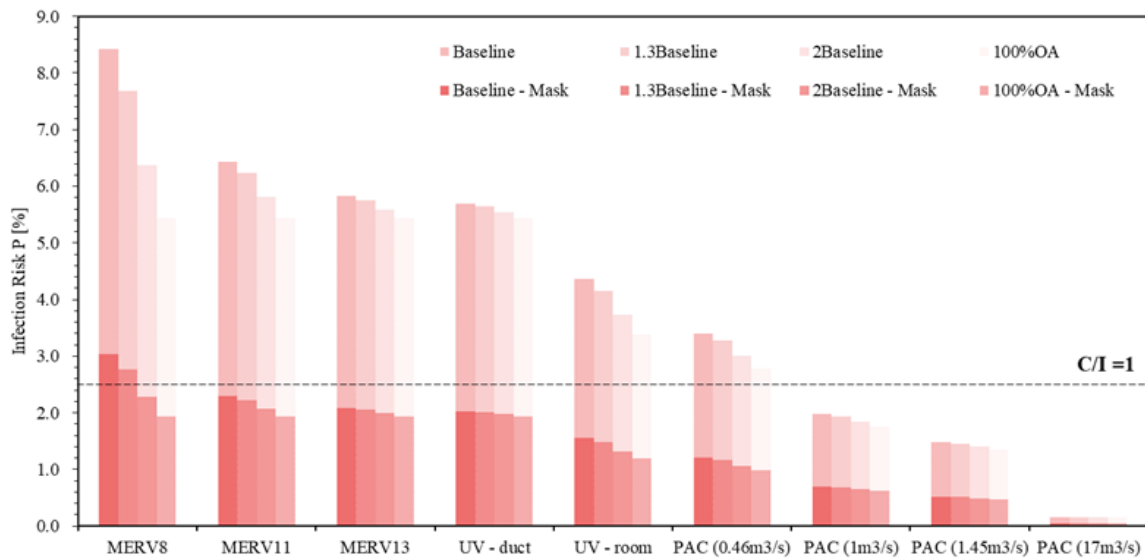
Figure 4-13 Individual Infection risks for Small Hotel: (a) Front Lounge – 1-hour exposure, and (b) Meeting Room – 2-hour exposure. C/I is the contagious potential. The spread could happen when C/I exceeds unity [82].

For all evaluated mitigation strategies, the relative reduction to their baseline risk levels was calculated (Figure 4-14) to compare the effectiveness across strategies. The relative reduction to baseline was calculated as ($P_{baseline} - P_{strategy}$)/$P_{baseline}$. For duct-treatment strategies, the

maximum "relative reduction to baseline" was reached with 100% OA. For the Medium Office, Large Office, Stand-Alone Retail, and Small Hotel, duct air-cleaning devices, such as upgraded MERV filters and in-duct UV lamps, achieved 30% to 40% relative reduction to baseline. For the Secondary School it was in the range of 0% to 20%. Upgrading MERV filters and using in-duct UV should be a high priority in Large Office and Stand-Alone Retail spaces. Note that since high baseline OA rates were designed for the Secondary School, the duct-treatment equipment would be relatively less effective in this application because they only treat return air and OA supply air is quanta free.

For room-treatment mitigations, the PACs performed well in the Small Hotel and Secondary School. The Hotel's front lounge and meeting room were small spaces, resulting in high quanta levels. Moreover, for the zones in the Secondary School, high-design OA supply limited the increasing potential of in-duct air cleaning mitigation performance (see Figure 4-11), thus PACs worked well for supplying extra clean air to these spaces. Notably, in-room UV was very effective at mitigation for all cases; the "relative reduction to baseline" achieved 50% to 70%.
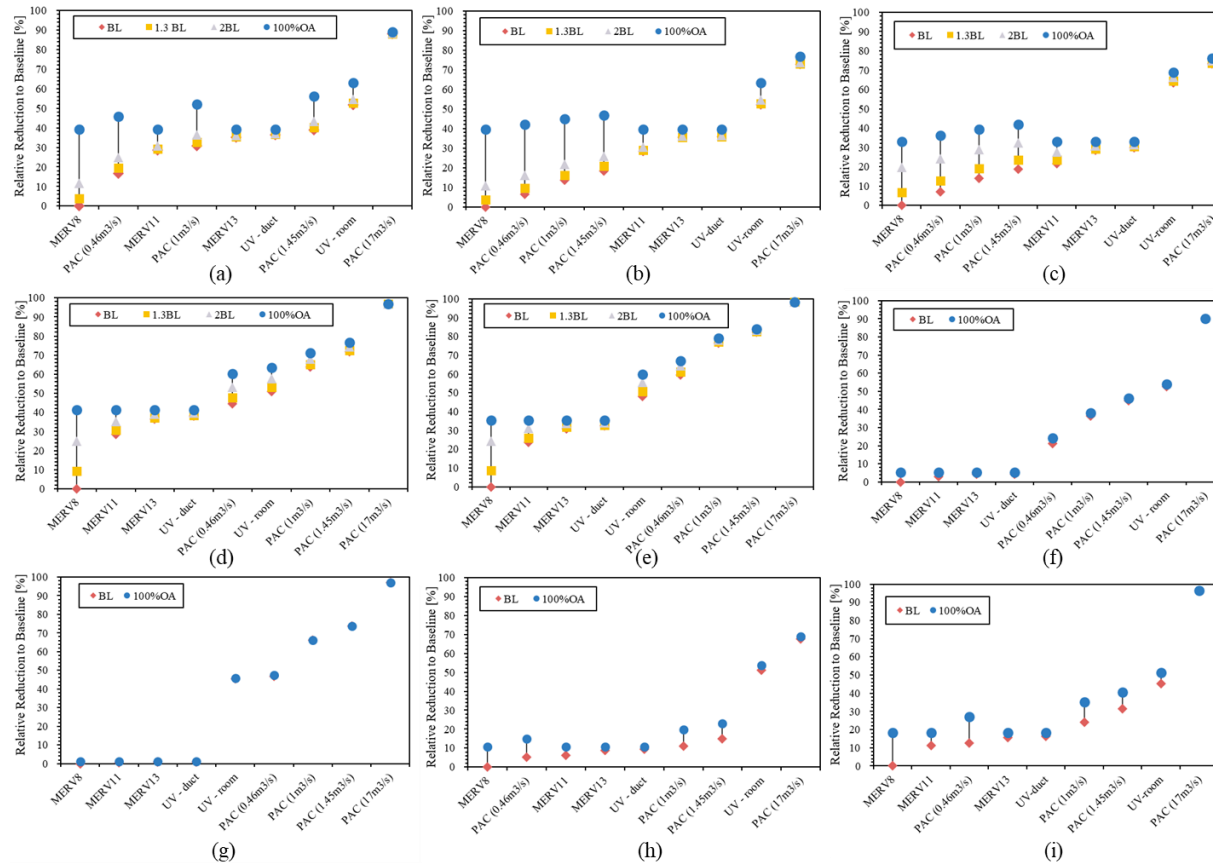
Figure 4-14 Estimated mitigation strategy risk reduction relative to the baseline case (($P_{baseline} - P_{strategy})/P_{baseline}$): a) Medium Office – Core zone, b) Large Office – Core zone, c) Stand Alone Retail – Core Retail, d) Small Hotel – Front Lounge, e) Small Hotel – Meeting Room, f) Secondary School – Classroom, g) Secondary School – Corner Classroom, h) Secondary School – Auditorium, i) Secondary School – café.

4.3.5 Association of infective risks with equivalent air change rate Q_e

Exposure duration (h), room volume (V), and mitigation strategies determined individual infection risks, where the equivalent air change rate (Q_e) represents the summation of mitigation strategies layered together. The Q_e is the overall quanta removal ability of the mitigation measures. The association between h, V, Q_e, and infection risk is presented in Figure 4-15 (a); different mask-wearing situations (50%, 80%, and 100% wearing) were also explored. In the 50% and 80% mask-wearing situations, the infector was assumed to not wear a mask. The association was derived using the multizone modeling results for all building types in this study. Results indicated that 100% mask-wearing would lead to a significant reduction. With the help of Fig.15a, the required Q_e needed to meet a preferred risk can be determined. For example, for a 100-m^3 office with five occupants, an acceptable risk level P =1/5 = 20% and the D / ($Q_e \times V$) with no masking is 0.005 h^2/m^3. Thus, for an eight-hour exposure in this office, the required Q_e is 8/(0.005$\times$100) = 16 h^{-1}. For a 500 m^3 classroom with 25 students, an acceptable risk level P = 1/25 = 4% and the D/($Q_e \times V$) with no masks is 0.001 h^2/m^3. Then for one-hour stay in the classroom, the required Q_e is 2 h^{-1} and it increases to 10 h^{-1} for five-hour exposures (with 100% masking, the mitigation strategies would need to provide 5/ (0.0028$\times$500) = 3.6 h^{-1}). Note that these mitigations are for reducing long-range transmission risk, but mask wearing helps with both long- and short-range transmission. As seen in Figure 4-15 (b), the multizone CONTAM simulation results predict P is lower for a given D/($Q_e \times V$) compared to the single-zone Wells-Riley calculations, since some generated quanta exits to neighbor zones via air leakagesites and the HVAC systems.
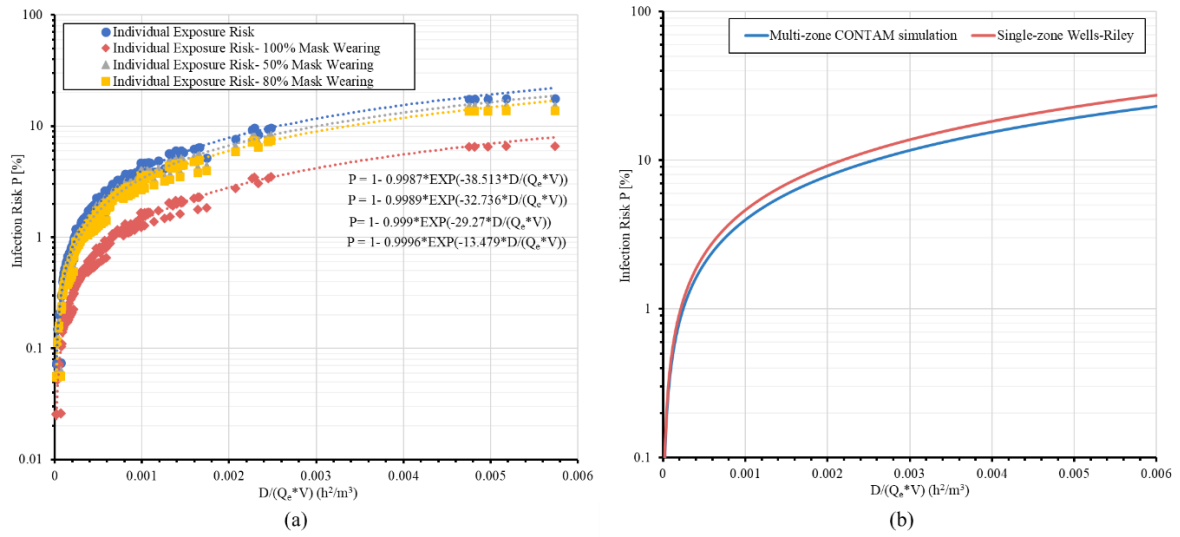
Figure 4-15 The relationship between individual infection risks and $D/(Q_e \times V)$ (Q_e – Equivalent air change rate (per hour); V – Volume; D – Duration). a) Different mask-wearing scenarios b) The comparisons between multizone modeling and single-zone Wells-Riley

For additional scenarios with different quanta generation levels, the relationships were plotted in Figure 4-16. This chart provides a quick check for individual infection risks in a room with known mitigation strategies. With known quanta generation rate, Q_e of the ventilation system plus any mitigation measures, room size, and exposure duration, the infection risk can be estimated. The room design occupancy can help decide the acceptable risk level (see section 4.2.1). Then, for a designated room, we can decide whether current mitigation measures are sufficient for occupants' safety and implement more controls if needed.
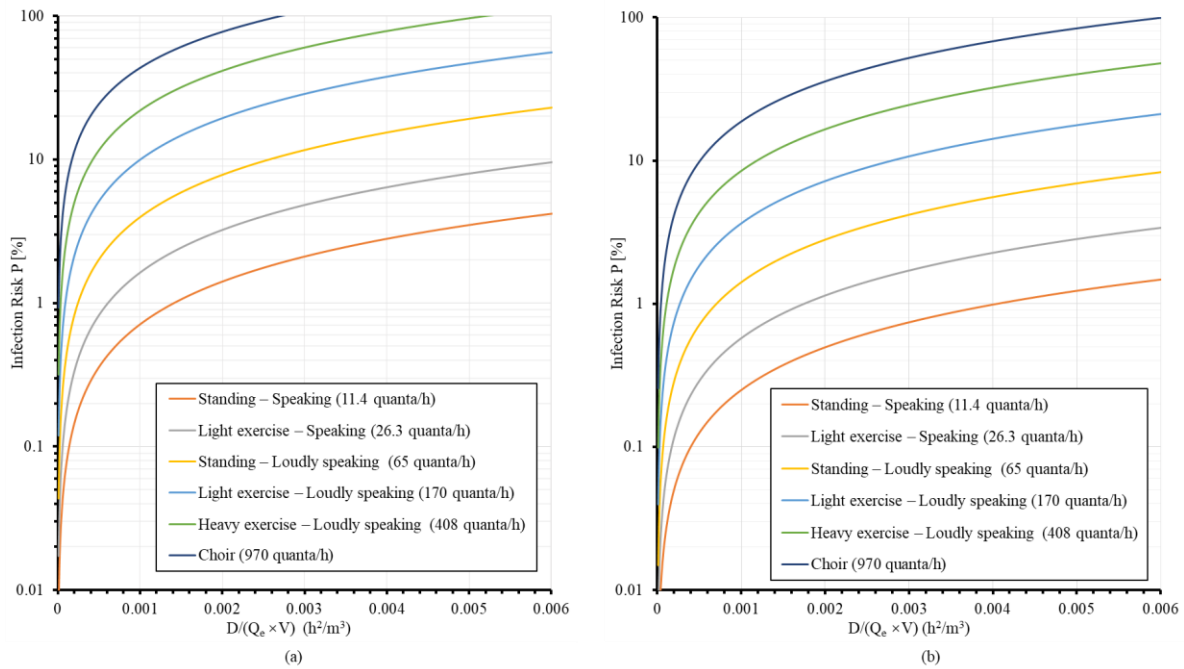
Figure 4-16 The relationship between individual infection risk and $D/(Q_e \times V)$, where Q_e is Equivalent air change rate (per hour); V is Volume (m^3), and D is Duration (h) for (a) No masks; (b) 100% mask-wearing

4.3.6 Mitigation under different occupancies

Minimum equivalent air change rates for different occupancies (100%, 75%, 50% and 25%) for contagious potential C/I = 1 were calculated for no mask-wearing and full mask-wearing scenarios, using $D/(Q_e \times V)$. Results are in Figure 4-17 and Figure 4-18. For example, for the baseline mitigation strategy "BL+MERV8" in the core zone of the Medium Office, 25% occupancy capacity could be allowed for no mask-wearing scenarios while 75% occupancy could be permitted with full mask-wearing. With baseline mitigation, 25% capacity could avoid community transmission for most no-mask wearing scenarios except for the large capacity public spaces: Stand-Alone Retail, Classrooms, and the Auditorium. For these spaces, full mask-wearing is suggested to be combined with 25% occupancy capacity. Moreover, for the auditorium, this was not sufficient, and in-room UV or use of the large capacity PAC (17 m^3/s) must be used to satisfy the mitigation need. To return to the pre-pandemic situation (no mask, full occupancy), office working areas should adopt 100% OA and implement in-room air-cleaning (UV, large capacity PAC). Similar strategies are recommended for Retail and the time spent shopping should be limited.
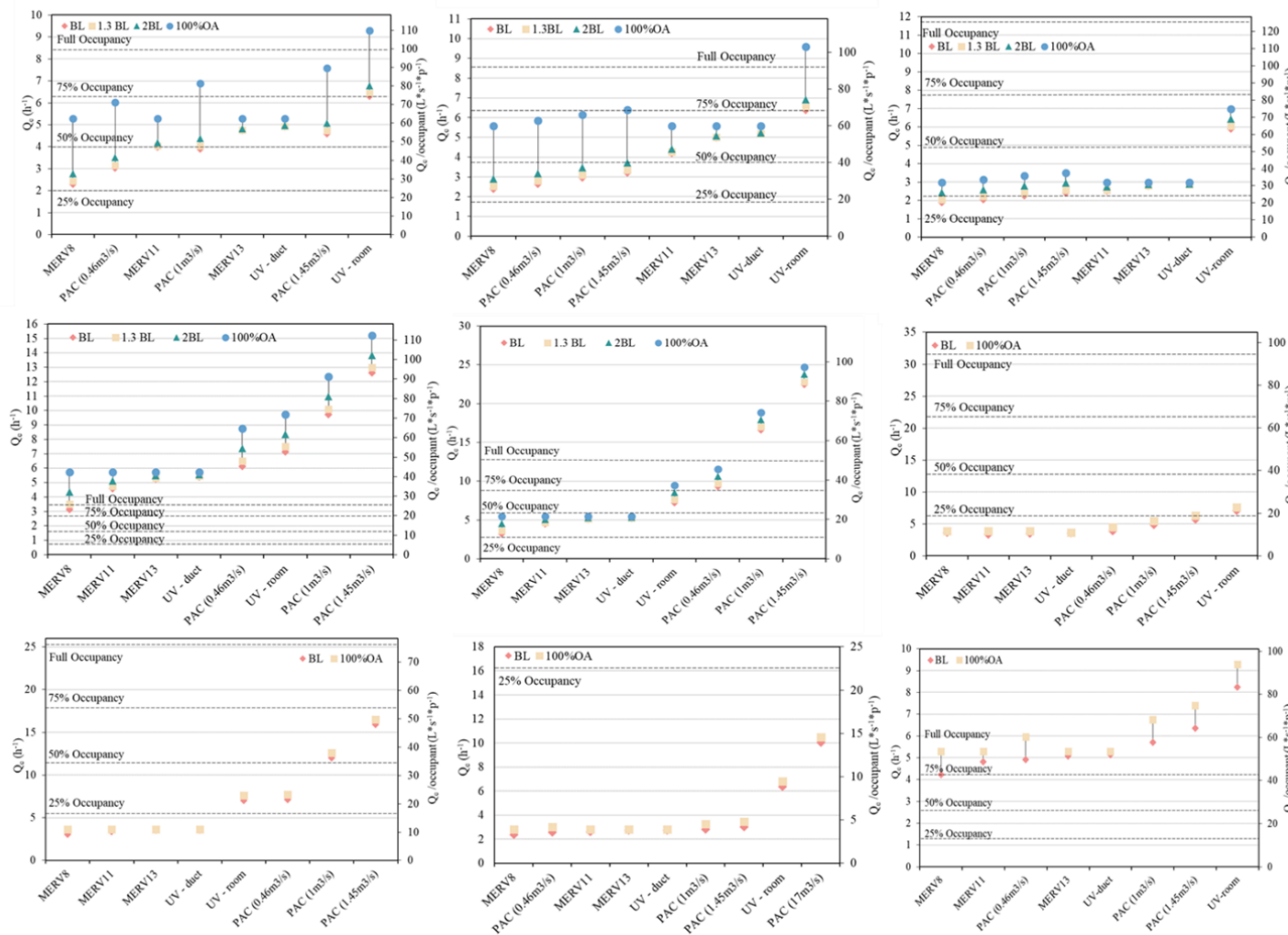
Figure 4-17 Minimum Q_e for different mitigations without mark-wearing: a) Medium Office – Core zone, b) Large Office – Core zone, c) Stand Alone Retail – Core Retail, d) Small Hotel – Front Lounge, e) Small Hotel – Meeting Room, f) Secondary School – Classroom, g) Secondary School – Corner Classroom, h) Secondary School – Auditorium, i) Secondary School – Cafe
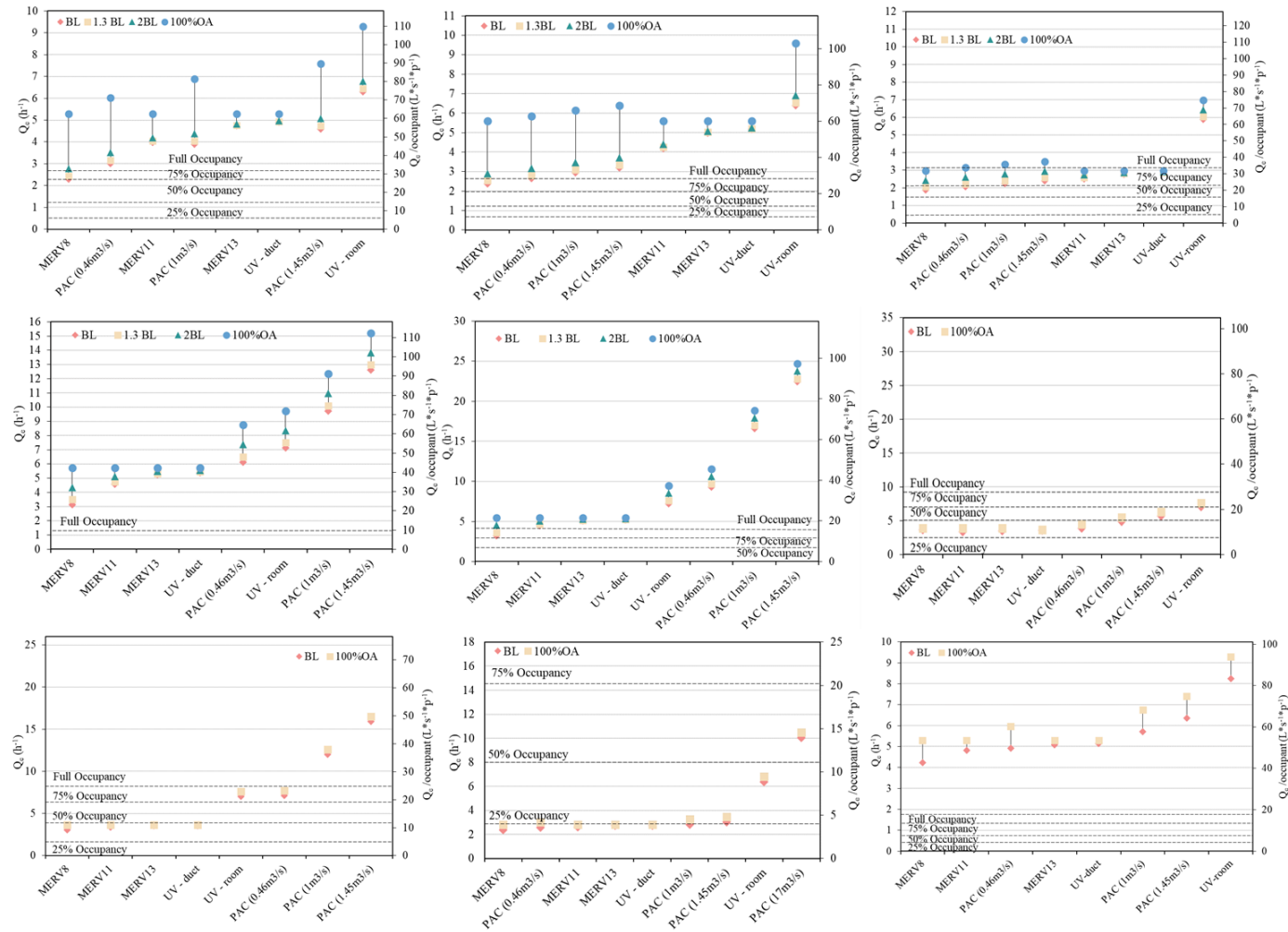
Figure 4-18 Minimum Q_e for different mitigations with mark-wearing: a) Medium Office – Core zone, b) Large Office – Core zone, c) Stand Alone Retail – Core Retail, d) Small Hotel – Front Lounge, e) Small Hotel – Meeting Room, f) Secondary School – Classroom, g) Secondary School – Corner Classroom, h) Secondary School – Auditorium, i) Secondary School

4.4 Discussion

The aim of this study was to identify effective combinations of mitigation strategies for preventing the spread of SARS-CoV-2 in public buildings. The study of layered mitigation strategies modeled long-range transmission of SARS-CoV-2 quanta in five DOE prototype commercial buildings. Results showed that duct-treatment air-cleaning strategies (upgrading MERV filter levels, use of in-duct UV) are relatively more effective in large rooms that can accommodate hundreds of occupants. In contrast, room-treatment strategies (adding PACs, in-room UV) are more effective in smaller spaces. For different rooms, the priority of mitigation strategies would change depending on the room volume, occupants' exposure time, and HVAC system designs. Results from this study can be generalized to other airborne infections such as measles or flu.

For mitigation strategies, the air-cleaning contribution from in-duct air cleaning devices (MERV, UV light) decreases as the OA ratio increases. The overall maximum duct-mitigation performance is in 100% OA supply. An appropriate match of outdoor air and MERV filters can achieve similar risk reduction as 100% OA supply performance. In a study by Stabile et al, twenty-five percent outdoor air and HEPA filters were found to have the same performance level as 100% outdoor air [272].

Thus, to achieve the optimal engineering control for mechanically ventilated buildings, duct mitigation should be designed to achieve the performance level like that of 100% OA. This can be realized by adopting 100% OA or making a proper match of MERV filters and OA supply. Then, according to the expected exposure duration, occupancy capacity, and mask-wearing situation, efforts required for room-mitigation strategies (in-room UV, PACs) could be assessed (see Figure 4-17 and Figure 4-18).

Detailed strategy-design instructions have been investigated in hospitals [273]; note that in commercial public buildings, the current ventilation standard is significantly lower than in hospitals. Previous investigations found that increasing outdoor air supply rates and MERV

filter levels could reduce infection risks, though a "case-by-case" design was suggested [89]. Additional room control measures and personal ventilation were proposed as auxiliary mitigation strategies; however, specific scenarios were not clarified. According to the results from this study, for the same mitigation strategy, the effectiveness could vary dramatically among different types of buildings, for example, for office buildings, the enhancement of duct treatment is more effective than schools, as their baseline OA design rates are significantly lower. The in-depth analysis of different building types and their mitigation measures can be further explored in future studies.

The relationship between infection risks and $D/(Q_e \times V)$ (D - duration, V- room volume and Q_e equivalent air change rate) were established. This enables a quick estimation of Q_e in the engineering design of ventilation. With the known acceptable risk level, the value of $D/(Q_e \times V)$ could be obtained from a given relationship (Figure 4-15 (a)). The Q_e could then be quickly estimated from the given D and V of the scenario, as what have been shown in the section 3.5. The Q_e could then help make ventilation design decisions (MERV filter level, portable air cleaner capacity etc.) in the room. However, each building has its own characteristics, people should analyze their building if they want to understand it. It should be noted that the required Q_e is calculated for the source zone, which is the room contains the infector.   For a multizone building in daily life, the design goal could be adjusted to a more general context. When an infector enters the building, how to make sure that there are no transmission risks inside the building? How to make sure the systematic designs of ventilation strategies could achieve the overall mitigation goal? Limitations do exist in this study for taking a great deal of simulation cases into consideration, these questions could be answered with more detailed analysis in the future.

For future investigations, more real-life scenarios could be evaluated using the CONTAM-*quanta* approach. For example, more infectors could be included to take the local prevalence rate of SARS-CoV-2 into consideration. Occupancy schedules could be applied to evaluate

various ventilation demands during the day. The vaccination rate can also be considered as the immune population is increasing over time. What is more, the stochastic effect could also be considered later as what has been done in the Skagit Valley Chorale super-spreading event investigation [240]. In addition, flow patterns could be manipulated to maximally reduce quanta concentrations in occupants' breathing zone and promote the effectiveness of mitigation strategies. The computational fluid dynamics (CFD) is an effective method for predicting detailed indoor airflows, which has been developed for the CONTAM multizone modeling [50, 274]. Utilizing the CFD capabilities of CONTAM, the pros and cons of different mechanical mitigation strategies would be better understood.

4.5 Conclusion

Effective layered mitigation strategies can reduce individual infection risks when occupying indoor spaces with COVID-19 infectors. The multizone CONTAM modeling used in this study enables a case-to-case design of mitigation approaches, and infection risks and mitigation strategies in five different types of DOE prototype buildings were investigated. The zone-to-zone quanta transmission and quanta fates were also reported. Results indicate that the potential of zone-to-zone transmissions exists, though the threat is relatively lower than that in the source zone. Both air leakage sites and central ventilation systems can induce quanta into neighboring zones. For quanta fates, the sum of the amounts exfiltrated and filtered can display the air-cleaning ability of the ventilation system. A proper match of outdoor air percentage and MERV filters can achieve a similar performance like 100% outside air. Evaluation results also suggest that additional mitigation efforts are needed for confined spaces with long exposure duration. For these spaces, air-cleaning strategies cannot simply depend on duct mitigation; room-treatment strategies (PACs, in-room UV) are also needed. For example, the portable air-cleaner (PAC at 1 m^3/s) is recommended for the Meeting Room scenario. In addition, masks can dramatically reduce infection risks. The use of masks could permit a two-hour meeting in Meeting Room with baseline ventilation settings. Finally, relationships between individual

infection risks and a risk-relevant factor "Exposure duration (D, h)/(Equivalent air change rate $(Q_e, h^{-1}) \times$ Room volume (V, m^3))" was obtained for a quick estimation of risks, which could benefit future air-cleaning design and practice in response to the reopening of commercial buildings during an infectious airborne disease pandemic.

Chapter 5 CO$_2$-Based Ventilation Design for Long-Term Indoor Air Quality Management

Abstract

The COVID-19 pandemic brought global attention to indoor air quality (IAQ), which is intrinsically linked to clean air change rates. Estimating the air change rate in indoor environments, however, remains challenging. It is primarily due to the uncertainties associated with the air change rate estimation, such as pollutant generation rates, dynamics including weather and occupancies, and the limitations of deterministic approaches to accommodate these factors. In this study, Bayesian inference was implemented on a stochastic CO$_2$-based grey-box model to infer modeled parameters and quantify uncertainties. The accuracy and robustness of the ventilation rate and CO$_2$ emission rate estimated by the model were confirmed with CO$_2$ tracer gas experiments conducted in an airtight chamber. Both prior and posterior predictive checks (PPC) were performed to demonstrate the advantage of this approach. In addition, uncertainties in real-life contexts were quantified with an incremental variance σ for the Wiener process. This approach was later applied to evaluate the ventilation conditions within two primary school classrooms in Montreal. The Equivalent Clean Airflow Rate (ECAi) was calculated following ASHRAE 241, and an insufficient clean air supply within both classrooms was identified. A supplement of 0.38 m^3/s clear air delivery rate (CADR) from air-cleaning devices is recommended for a sufficient ECAi. Finally, steady-state CO$_2$ thresholds (C$_{limit}$, C$_{target}$, and C$_{ideal}$) were carried out to indicate when ECAi requirements could be achieved under various mitigation strategies, such as portable air cleaners and in-room ultraviolet light, with CADR values ranging from 0.09 – 0.47 m^3/s.

5.1 Introduction

Since the COVID-19 pandemic started, more than 775.3 million individuals worldwide have been infected, and approximately 7.0 million deaths have been attributed to the disease as of April 7, 2024 [275]. The pandemic has significantly highlighted public concerns about maintaining healthy indoor environments to limit the spread of virus-laden respiratory aerosols [187, 276]. As hygiene and self-protective measures have eased, there are fewer people wearing masks and maintaining social distancing in public spaces. The respiratory diseases, which include not only SARS-CoV-2 but also influenza, respiratory syncytial virus (RSV), etc., would continue to pose health threats [277]. In daily life settings, classrooms in schools are particularly vulnerable [278], where face-to-face interactions are inevitable and frequent. To mitigate health effects from respiratory infections, ensuring sufficient clean air ventilation plays an essential role. Effective ventilation can significantly dilute aerosol concentrations and reduce the quantity of inhaled infectious pathogens. Consequently, assessments of indoor air quality (IAQ) and, more specifically, characterizations of ventilation in schools have become more crucial than ever.

Carbon dioxide (CO_2), which serves as an indicator of indoor ventilation conditions, is recommended for managing the risk of airborne transmission [279]. This is because the indoor CO_2 level could reflect the outdoor ventilation rate per person, provided that information on occupancy and specific space ventilation requirements is available [280]. During occupants' exposures, indoor CO_2 levels will gradually increase until equilibrium is achieved. Poor ventilation conditions will elevate the steady-state CO_2 levels, causing them to exceed the recommended CO_2 metrics. Meanwhile, its concentration can be conveniently measured with portable low-cost sensors installed in classrooms. St-jean et al. [281] found elevated CO_2 levels in 21 day-care centers (DCCs) in Montreal. Andamon et al. [282] reported the elevated CO_2 concentration in 10 classrooms of a secondary school in Victoria, Australia. In response to the COVID-19 pandemic, the province of Quebec, Canada, equipped all kindergarten, elementary,

high school, vocational, and adult education classrooms with CO_2 sensors to monitor indoor air quality and improve ventilation conditions [283]. The widespread installation of CO_2 sensors has facilitated enhanced monitoring of indoor ventilation conditions in classrooms.

In addition, there are several CO_2-based ways to determine ventilation rates from field measurements: steady-state, decay, build-up, and transient mass-balance approach. Andamon et al. [282] used average peak CO_2 concentrations as steady-state values to estimate ventilation rates for investigated classrooms. Kabirikopaei et al. [114] estimated ventilation rates for 220 classrooms in the Midwestern region of the US using three methods (steady-state, decay, and build-up) and found that CO_2 readings can contribute the most uncertainty. Batterman [284] suggested that the transient mass balance method can provide the most accurate results when occupancy is available.

While these traditional approaches have been widely used for indoor ventilation rate evaluations, there are several limitations. Firstly, most of these approaches adopted deterministic CO_2 mass-balance equations, assuming parameters in the model to be constants. In practical settings, however, multiple sources of uncertainties may exist in the room. Secondly, in real-time CO_2 measurements, occupancy data are often unavailable. Inaccurate estimates of occupancy can introduce biases into final evaluation results. Meanwhile, current CO_2 metrics are established only for ventilation standards such as ASHRAE 62.1 [13], and the metrics for managing the long-range transmission of airborne aerosols are yet to be determined.

To capture the uncertainties in the CO_2-based ventilation evaluation process, a grey-box model [163] can be used, which usually integrates a partial theoretical structure with data to complete the model. Compared with white-box (e.g., physically-based) and black-box (e.g., data-driven) models, the grey-box model can be structured with physical knowledge, and the parameters are estimated with the measured data from the system. The stochastic grey-box model often includes stochastic items to account for uncertainties and variability in the system [171]. The randomness of input parameters will allow for the consideration of uncertain components [172]

such as measurement errors, fluctuations in the system, unmodelled parameters, etc.

Haghighat et al. [169] introduced a predictive stochastic model for indoor air quality in 1988, allowing the incorporation of inputs as random variables within the stochastic differential equation (SDE) model. The model can capture variability in predictions of contaminant concentrations. The moment equations for mean, variance, and skewness were given based on stochastic Itô calculus [169]. It was indicated that the 'white noise' term not only described the system randomness but also provided a unique and satisfactory solution. It is worth noting that the solution of the SDE model is an Itô stochastic process with the Markov property and the strong Markov property, which enables future predictions to rely only on the current state [285]. Marcel et al. [172] proposed a predictive control approach to model the CO_2 concentrations using a grey-box model, in which SDE equations were established based on tracer-gas mass balance. The study suggests that the parametrization of the model was suitable and applicable, and the prediction tends to be more accurate than traditional deterministic approaches. Until now, studies that attempted to interpret indoor ventilation conditions using the grey-box model are still rare [171, 172].

Parameter estimation plays a key role in developing a stochastic grey-box model. Contemporary improvements in computational power have substantially enhanced Bayesian inference, making it a robust tool for precise parameter estimations, uncertainty quantification, and effective incorporation of prior knowledge. Many previous efforts have been delivered to apply Bayesian inference to interpret parameters in IAQ models. Wang et al. [147, 148] applied the Bayesian approach to a source-detector relationship established from CFD simulations of flow fields in indoor spaces and underground utility tunnels for estimating source parameters (leakage rate and location). Septier et al. [149] proposed a Bayesian inference procedure on inverse dispersion modeling to solve the challenging source term estimation (STE) problem. The Gaussian assumption was made for the source emission rate for its satisfactory performance in practice, even though the emission rate cannot take negative values. To assess

ventilation conditions with CO_2 meters in primary schools, Hou et al. [150] applied a Bayesian inference approach to indoor CO_2 concentration models. This study identified the outdoor ventilation rate, CO_2 generation rate, and occupancy level as the most sensitive variables to indoor CO_2 levels. Rahman et al. [151] developed an approach to estimate the occupancy distribution in a mechanically ventilated multi-room office using Bayesian inference. The CO_2 concentration, simulated by the CONTAM program, was taken as input for the investigation under the circumstances with and without a 5% random noise considered for uncertainty. The study found a significant increase in the RMSE in estimating occupancy as the sensor measurement uncertainty increases. By applying the moving-average filtering method, the RMSE on estimation was reduced, however it became insensitive to the abrupt occupancy change. It was suggested that the Bayesian inference would be more powerful in solving inverse problems if it could handle realistic data including noises. However, existing literature reveals a noticeable scarcity of interpreting parameters from stochastic models with Bayesian inference.

To summarize, most traditional ventilation evaluation approaches utilize deterministic approaches that cannot accommodate real-life uncertainties. The accuracy of these approaches would rely on how the real situations approach the idealized assumptions, the accuracy and comprehensive collection of inputs, the correct and comprehensive model development, and no disturbances during the measurements, etc. Idealized situations seldom happen in reality, so quantifying uncertainties is essential.

In this study, we employed Bayesian inference on a CO_2-based grey-box SDE model for assessing ventilation conditions for two classrooms in Montreal with CO_2 field measurement data. The methodology and data used in this study will be introduced in Section 5.2. In Section 5.3, the modeling results will be presented and discussed. In Section 5.3.1, a prior sensitivity analysis was conducted on the model. In Section 5.3.2, model validations from an airtight chamber are demonstrated for ventilation rate (Section 5.3.2.1) and CO_2 emission rates (Section

5. 3.2.2). The posterior predictive checks (PPC) and noise-level estimation results are discussed in Sections 5.3.2.3 and 5.3.2.4, respectively. Section 5.3.3 illustrates the case study outcomes, evaluating the ventilation conditions and providing ECAi across three seasons: Spring (March to May), Autumn (September to November), and Winter (December to February). The CO_2 threshold necessary to meet ECAi requirements from ASHRAE 241 was estimated for the classrooms to manage the long-range aerosol exposures. The conclusions of this study are presented in Section 5.4.

5.2 Methodology

The methodology used in this study implemented Bayesian inference on a stochastic CO_2-based grey-box model to interpret parameters and quantify the modeling uncertainties. In Section 5.2.1, the stochastic CO_2-based grey-box SDE model will be introduced, followed by the principles of Bayesian inference to be explained in Section 5.2.2. The validation and PPC process are detailed in Section 5.2.3. The model development process is illustrated in Figure 5-1.

Modeling process	Modeling details	Example
Define the CO_2 grey-box model	Determine the CO_2 stochastic differential equation and modelled parameters	$dC_r = \dfrac{(C_{out} - C_r) \cdot Q + E \cdot C_E}{V} \cdot dt + \sigma \cdot dw$ Observational inputs: C_r
	Obtain the observational CO_2 data	
Apply Bayesian inference	Determine estimated parameters and interested ones to focus on	Estimated parameters: Q, C_{out}, E, σ Interested parameter: Q
	Assume prior distributions for all parameters need to be estimated	$Q \sim U(0,5)$ $C_{out} \sim U(350,550)$ $E \sim U(0, 0.05)$ $\sigma \sim U(\exp(-20), \exp(20))$
	Obtain the joint posterior distribution	$P(Q,C_{out},E,\sigma \mid C_r)$ $= \dfrac{P(C_r \mid Q,C_{out},E,\sigma) \cdot P(Q,C_{out},E,\sigma)}{P(C_r)}$
	Yield the conditional posterior distribution on ventilation rate Q	$P(Q \mid C_r) = \iiint P(Q, C_{out}, E, \sigma \mid C_r) \, dC_{out} \, dE \, d\sigma$
Model Validation	Conduct CO_2 tracer gas experiments in the metabolic chamber	1. Prior predictive check 2. Comparisons between inferred parameters and observations 3. Posterior predictive check

Figure 5-1 The model development process

5.2.1 Stochastic CO_2-based grey-box model

When establishing models for IAQ problems, the deterministic mass-balance equation is often established for the contaminants as an ODE. If the randomness of some coefficients is allowed, it will become an SDE, and it tends to be more realistic to the real-life problems of interest. The establishment of a stochastic CO_2 grey-box model is composed of two components [285]: a drift component, which represents the deterministic description of the system, and a diffusion term, which represents the stochastic or random evolution of the system. The diffusion component captures the variability or uncertainty in the system's behavior attributable to random forces or noise.

The drift components derived from the traditional deterministic CO_2 mass-balance model, or ODE, are represented by Eq.5-1:

$$V \frac{dC_r}{dt} = (C_{out} - C_r) \cdot Q + E \cdot C_E \qquad \text{5-1}$$

Where V is the room volume (L); C_r is the CO_2 concentration in the room (ppm); C_{out} is the CO_2 concentration of outdoor air or the ventilation flows (ppm); Q is the ventilation rate (L/s); E is the total volumetric CO_2 generation rate in the room (L/s); C_E is the conversion factor from volumetric concentration to ppm, which equals to 10^6.

The diffusion component can be considered as a 'white noise' term added to Eq. 5-1 accounting for the uncertainty associated with unknown model inputs and other noises in the system. The stochastic CO_2 grey-box model could, therefore, be expressed as an SDE as shown in Eq.5-2:

$$dC_r = \frac{(C_{out} - C_r) \cdot Q + E \cdot C_E}{V} \cdot dt + \sigma \cdot dW_t \qquad \text{5-2}$$

Where W_t is a Wiener process, which is also known as Brownian motion, is a continuous-time stochastic process that has been widely explored in physics, economics, and applied mathematics [286], and σ is the incremental variance in the Wiener process (ppm/$\sqrt{dt}$).

In this study, the Euler-Maruyama method was used for discretization [287], which provides an approximate solution to the SDE equation over discrete time steps. The Euler-Maruyama approximation is provided through Eq. 5-3:

$$\Delta C_r = ((C_{out} - C_r) \cdot Q + E \cdot C_E)/V \cdot \Delta t + \sigma \cdot \sqrt{\Delta t} \cdot Z \qquad \text{5-3}$$

Where ΔC_r is the change in C_r over the time step Δt; Z is a standard normal random variable (from a normal distribution with mean 0 and variance 1).

In this study, the inclusion of the 'white noise' component assists in quantifying the uncertainty levels in model predictions. Such uncertainties might arise from various sources, including air turbulence, systematic measurement errors, inaccuracies in estimating modeled parameters, effects of unmodeled parameters, variability in the distribution of occupants within a room, and the positioning of sensors. The component also covers factors that are not accounted for in traditional deterministic models, which could lead to discrepancies between the models and the observations. Assumptions made in this study to use this model are: The room is a well-mixed single-zone space; The estimated parameters are assumed to be constant throughout the evaluation duration; The differences of density between indoor and outdoor air are ignored.

5.2.2 Bayesian inference

Bayesian inference is a powerful tool for quantifying uncertainty in estimated model parameters [132, 141-143]. It considers the inferred parameters as random variables with prior information, and then a likelihood function (based on the measurement data) is used to update prior distribution following Bayes theorem [288]. The updated results are the posterior distributions, which are the new beliefs of the interested variables. In recent years, with the advancement in computational capabilities and the development of Markov Chain Monte Carlo (MCMC) algorithms such as Metropolis-Hastings, Gibbs sampling, and Hamiltonian Monte Carlo, an increasing number of studies in the built environment field started to utilize this approach for parameter inferences in established models [132].

In the defined stochastic CO_2 grey-box model, there could be multiple variables required to be estimated. In this study, parameters to be estimated in the model are ventilation rate Q, outdoor CO_2 concentration C_{out}, generation rate E, and incremental variance σ in the Wiener process. By placing prior distributions on all estimated parameters and updating these beliefs, a joint posterior distribution for the entire set of parameters can be obtained. If one parameter is selected as the interested parameter, its marginal posterior distribution will need to be carried out, and the remaining parameters will be regarded as nuisance parameters. With the MCMC algorithms, samples could be drawn from the joint posterior distribution to estimate the conditional posterior distribution of interested parameters. For example, the estimation process for the ventilation rate Q is illustrated as follows:

Step 1: Assume prior distributions for estimated parameters;

Step 2: Obtain the joint posterior distribution of all estimated parameters;

Step 3: Yield the conditional posterior distribution on ventilation rate Q

The prior assumptions are the prior beliefs of the estimated parameters. An example of the prior settings is illustrated in Figure 5-2. The impact of informative priors and non-informative priors (flat priors) on posterior distributions will be evaluated in this study. For example, for the outdoor CO_2 concentrations, a uniform distribution is assumed to be in the range of 350 ppm to 550 ppm [289]. If there is some information about the outdoor CO_2 level available, a normal distribution could then be assumed with a specific mean value and variance level.

Then, the probability of the estimated parameters could be inferred based on the prior distributions estimated for them. The likelihood of the estimated parameters given the measured data Cr (CO_2 indoor concentration) is demonstrated as follows in Bayes's theorem (Eq.5-4):

$$P(Q, C_{out}, E, \sigma \mid Cr) = \frac{P(Cr \mid Q, C_{out}, E, \sigma) \cdot P(Q, C_{out}, E, \sigma)}{P(Cr)} \qquad 5\text{-}4$$

Where $P(Cr \mid Q, C_{out}, E, \sigma)$ is the likelihood probability that measurement data Cr occurs given the prior information, $P(Q, C_{out}, E, \sigma)$ is the joint prior distribution of parameters Q, C_{out}, E, and σ, and $P(Cr)$ is the probability of seeing the measurement results, which is a normalized constant.

After obtaining the joint posterior distribution $P(Q, C_{out}, E, \sigma \mid Cr)$, samples could be drawn from this joint posterior distribution for the nuisance parameters for C_{out}, E, σ to estimate the conditional posterior distribution on ventilation rate Q, which is $P(Q \mid C_{out}, E, \sigma, Cr)$. The process for estimating other parameters follows the same procedure.
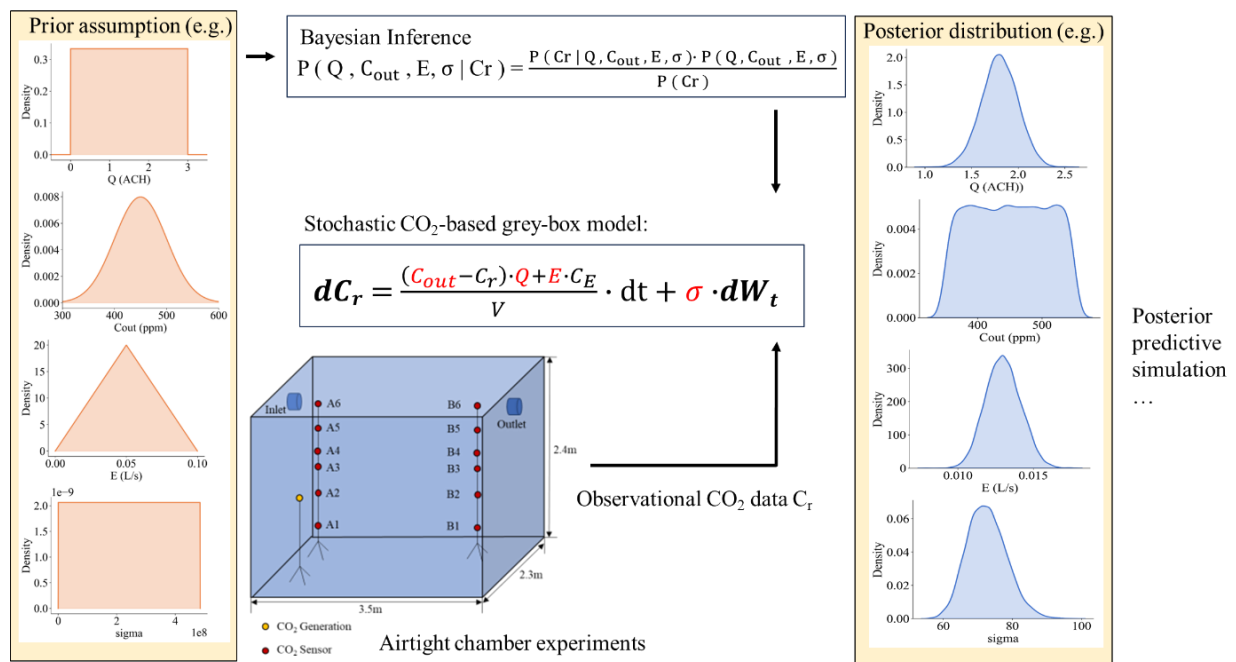
Figure 5-2 The illustration of modeling inputs and outputs

In this study, the likelihood function will be estimated using the Euler-Maruyama

approximation [287]. The Markov chain Monte Carlo (MCMC) method was applied for reconstructing the uncertain parameters. Given the prior distribution and likelihood, the posterior distribution could be obtained. Five thousand draws from the No-U-Turn Sampler (NUTS) algorithm were performed on two chains to sample the parameter intervals using MCMC. The 'burn-in' was set at 500 to help the Markov chain start near the center of equilibrium distribution. The Bayesian stochastic modeling process was established in the Python module PyMC [290].

5.2.3 Validations and PPC evaluations

Experimental validations and PPC evaluations were carried out to assess the performance and validity of the Bayesian inference results on the stochastic CO_2-based grey-box model. Experimental validations are designed to help confirm the model estimation accuracy on ventilation rates and CO_2 emission rates. Meanwhile, the PPC will help evaluate how well the developed model fits the observed data. It is conducted to assess the goodness of fit and adequacy. If the fitness is good, it indicates that the model can generate data in patterns similar to those observed.

5.2.3.1 Experimental validations

CO_2 tracer gas experiments were conducted in an airtight chamber located at the University Institute of Cardiology and Pneumology of Quebec - Université Laval (IUCPQ - ULaval). The dimension of the airtight chamber is 2.3 m (width) × 3.5 m (length) × 2.4 m (height). The inlet and outlet of the mechanical system are at the top of the chamber with a diameter of 5.1 cm (2 in). Two sensor trees were set up in the chamber, and each of the trees is equipped with mounts at six different heights [291]: 0.6 m, 1.1 m, 1.5 m, 1.7 m, 2 m, and 2.3 m. The sensors were established to confirm the uniform distributions of CO_2 inside the chamber. Each of the mounts carries six sets of sensors measuring CO_2 (Vaisala - GMP252), air temperature and relative humidity (Vaisala - HMP110), and air velocity (SWEMA 03+), respectively. Details of the sensor specifications are listed in Table 5-1. The CO_2 was generated through the CO_2 tank outside the chamber (Figure 5-3 (b)), and a mass flow controller was used to control the generation rate.
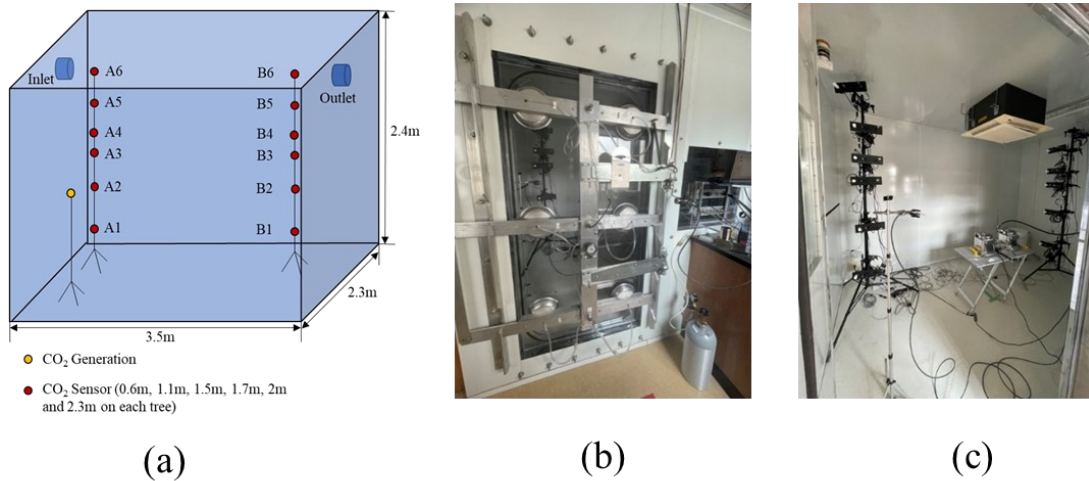
Figure 5-3 Experimental set-ups of the airtight chamber; (a) chamber dimensions and designated measurement locations (red point- CO_2 sensors, yellow point-CO_2 generation location); (b) detailed view of the gas injection and sealing mechanisms; (c) experimental set-ups in the chamber

Table 5-1 Sensor specification details

Reading Type	Sensor Name	Measurement range	Accuracy	Sampling Frequency
CO_2	Vaisala GMP252	0 – 10000 ppm	± 40 ppm	0.05 Hz
Relative Humidity and Temperature	Vaisala HMP110	0–100 % RH -40 – 80 °C	± 1.5 % RH ± 0.2 °C	0.05 Hz
Airspeed	Swema 03+	0.05 – 3 m/s	± 0.03 m/s	100 Hz

The experiments were completed in two sessions: concentration decay and constant injection. In decay measurements, three ventilation conditions (Test 1: Ventilation mode 1- 1.9 ± 0.03 ACH; Test 2: Ventilation mode 2 - 1.51 ± 0.02 ACH; Test 3: Ventilation mode 3 - 0.53 ± 0.01 ACH) were measured. Due to the limited conditions for directly measuring the supply airflows, the referenced ventilation rates for the three different ventilation conditions were calculated from the CO_2 decay approach. A fan was operated during the initial mixture period. The CO_2 injection stops upon the peak and stabilization of CO_2 concentration, and the concentration is recorded throughout the subsequent decay period. During the constant CO_2 injection tests, two distinct CO_2 generation rates, 0.8 L/min, and 1.6 L/min were examined with and without fan operation (Test 4: 0.8 L/min, fan-off; Test 5: 0.8 L/min, fan-on; Test 6: 1.6 L/min, fan-off; Test

7: 1.6 L/min, fan-on). These measurements were conducted under the chamber's Ventilation mode 1. After the CO_2 tracer gas experiments, the measured CO_2 data are used as observational data for the model, as illustrated in Figure 5-2.

5.2.3.2 PPC evaluation

PPC is a useful way of assessing the model and determining if it fits the data directly. Specifically, to check the model's fit, the simulated values were drawn from posterior predictive distributions, and the samples were compared with the observed data. If the proposed model fits, the regenerated simulations from the model should resemble the observations and no major discrepancy would be observed. Traditionally, the previous classical approaches mainly focus on various goodness-of-fit tests, comparing a tested statistic derived from observed data to its distribution under the null hypothesis. Unlike the traditional p-value in frequentist statistics, the Bayesian p-value helps to evaluate how well a Bayesian model describes the observed data. The Bayesian p-value is defined in Eq.5-5

$$\text{Bayesian p-value} \triangleq p\ (T_{sim} \geq T_{obs} \mid Cr) \qquad\qquad 5\text{-}5$$

Where T_{sim} is the simulated statistic, T_{obs} is the statistic for observations, and Cr is the conditions of the observations. A Bayesian p-value close to 0.5 would suggest a good fit, indicating that the observed data appears typical of the data predicted by the model. When values close to 0 or 1, however, would indicate a poor fit, suggesting that observations are impossible under the model. In this study, the target test statistic is the posterior mean value.

5.3 Results and discussion

5.3.1 Prior sensitivity analysis on inferred parameters

A crucial component in the Bayesian modeling and inference process is the prior distribution, which represents our initial assumptions or knowledge about unknown model parameters. In Bayesian analysis, this prior distribution is subsequently combined with the likelihood, which is the probability that observation occurs, given the parameters, to obtain the posterior distribution. The posterior distribution thus reflects an updated belief of the parameters,

incorporating both our prior knowledge and the new evidence. Therefore, the prior assumptions may have a significant impact on the posterior estimates of mean, bias, quantiles, etc. In this section, a prior sensitivity analysis was conducted for the stochastic CO_2 grey-box model to help assess whether the inferred results are influenced by the prior assumption settings.

The prior sensitivity analysis was conducted for ventilation rate Q, outdoor CO_2 concentration level C_{out} and CO_2 emission rate E in the model. In addition, two types of priors are chosen for the investigation: vague proper prior and informative prior. There are two main objectives for this prior sensitivity analysis. The first is to investigate whether different prior assumptions will influence the parameter of interest, for example, ventilation rate Q and CO_2 emission rate E. The second is to investigate whether the prior assumption of nuisance parameters, which are the parameters that are not of direct interest, would play an important role in estimating the interested parameters. The nuisance parameter investigated in this study is the outdoor CO_2 concentration level C_{out}.

The prior sensitivity analysis for one case of this study will be demonstrated here, using the observational data from one constant injection experimental test conducted in the airtight chamber (Test 4). The observational data for this investigated scenario is illustrated in Figure 5-4. The metabolic chamber was set at its Ventilation mode 1 (ACH = 1.9 ± 0.03), and CO_2 tracer gas was constantly injected into the chamber at a rate of 0.8 L /min (0.013 L/s). The information on the investigated priors is listed in Table 5-2.
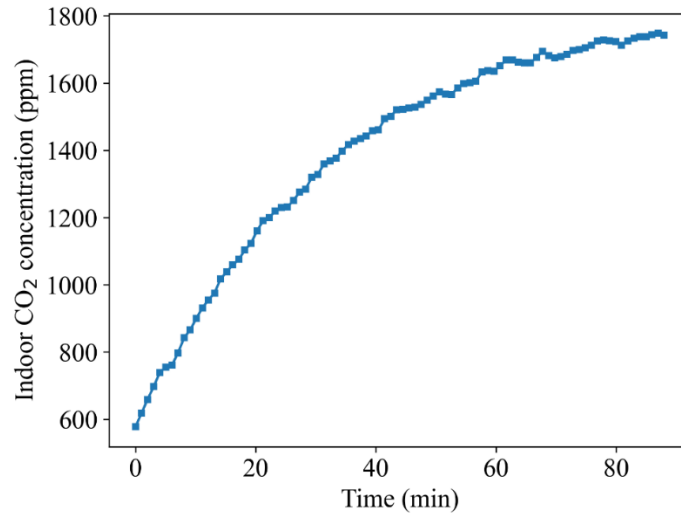
Figure 5-4 The investigated test for prior sensitivity analysis
(Test 4 in the airtight chamber)

Table 5-2 Evaluated priors for inferred parameters

Parameter	Unit	Default Prior	Vague Proper Prior	Informative Prior
Q	ACH	U (0,3)	U (0,10)	N (2, 0.2)
C_{out}	ppm	U (350,550)	U (350,550)	U (396,416) N (400,20)
E	L/s	U (0,0.05)	U (0,0.1)	N (0.013,0.005)

Note. U = Uniform; N = Normal
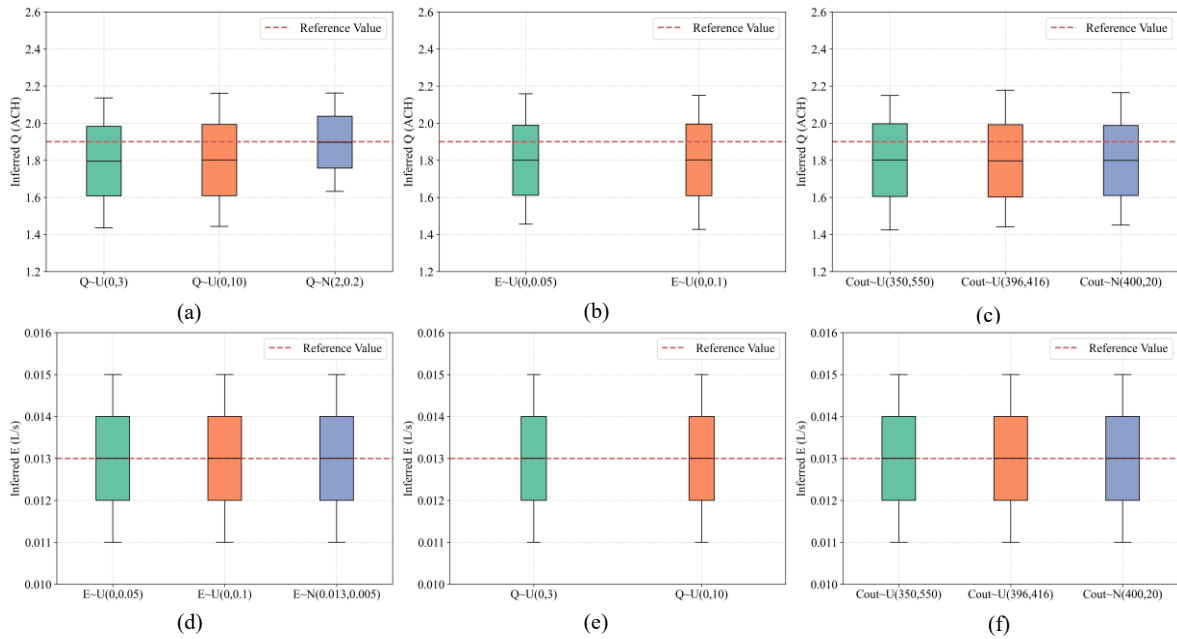
Figure 5-5 Prior sensitivity analysis on estimated parameters; U = Uniform; N = Normal; When investigating a specific prior assumption for a given parameter, default priors will be applied to other parameters; (a) – (c): The influence of prior assumptions of Q, E, and C_{out} on Q; (d) – (f): The influence of prior assumptions of Q, E, and C_{out} on E

As depicted in Figure 5-5, the influence of prior assumptions on parameter inference was investigated within the stochastic CO_2 grey-box model. Specifically, we focus on the ventilation rate (Q) and the CO_2 emission rate (E), aiming at elucidating the model's sensitivity and robustness to varying prior assumptions. The robustness of the model estimations for ventilation rate Q, under varying prior assumptions, is illustrated in Figure 5-5 (a) - (c). It is observed that the adoption of a vague uniform prior (Q ~ U (0,10)) does not introduce significant deviations from the results generated by the default uniform prior (Q ~ U (0,3)). This indicates that a broader assumption range will not influence final evaluations. As a result, both of the two prior assumptions can be considered proper priors in this study. Furthermore, the adoption of an informative prior (Q ~ N (2, 0.2)) could enhance the model's prediction performance on Q (Figure 5-5 (a)), as would be expected. Besides, the changes in prior assumptions regarding the CO_2 emission rate (E) and outdoor CO_2 concentration level (C_{out}) demonstrate negligible impacts on the model's inference performance for Q, as illustrated in

Figure 5-5 (b) and Figure 5-5 (c). It suggests the model's insensitivity to these prior assumptions, thereby reinforcing the robustness of its estimations on the parameter Q.

Similar findings were also observed for the estimations of CO_2 emission rate E, as shown in Figure 5-5 (d). The model achieves good accuracy in estimating E, even under the vague prior (E ~ U (0, 0.1)). This capacity is further demonstrated in Figure 5-5 (e) and Figure 5-5 (f), where the estimation accuracy for E was not affected by the varying priors for Q and C_{out}.

In conclusion, employing Bayesian inference on the stochastic CO_2 grey-box model exhibits good robustness to the variations in prior assumptions for both Q and E. The model could maintain its predictive accuracy across a range of prior assumptions, from vague proper to highly informative prior. This evaluation results prove the rationality of the prior assumptions made for the model.

5.3.2 Model validation

In this section, the accuracy of the inferred parameters (Q and E) was further validated, adopting the verified default prior assumptions listed in Table 5-2. Two types of CO_2 tracer gas tests were used as observational data inputs in this model validation process, distinguished by the CO_2 generation situations: with or without CO_2 release. Detailed information for the validation scenarios is listed in Table 5-3 and Table 5-4. The validation results for the model's estimation performance are presented in the following subsection.

5.3.2.1 Validation of the inferred ventilation rate Q

One of the main purposes of this study is to make reasonable inferences of ventilation rate Q from the indoor CO_2 measurement with the proposed approach. The model estimation performance for Q was compared with the ventilation rate obtained from standard tracer-gas decay tests. For the concentration decay tests, there were three ventilation modes investigated. The comparison results are illustrated in Table 5-3 and Figure 5-6. For the concentration decay test, the difference is less than 5% for the three ventilation modes.

When the CO_2 release was considered in the model (constant injection test), the relative errors for the two release conditions 0.8 L/min (0.013 L/s) and 1.6 L/min (0.026 L/s) were 5.7% and 3.1% under fan-off situations. For the "fan on" scenarios, the differences increase to 12.6% and 11% for the two release conditions. The reasons for this increase in differences are probably due to the fan actively circulating air in the small chamber, leading to a higher actual ventilation rate. It should be noted that there was no obvious difference in the CO_2 measurements observed at the twelve sensors in the two sensor trees, thus the influence of non-uniformity could be ignored. To summarize, the proposed approach in this study can make reasonable ventilation rate estimations for both decay and constant injection scenarios.

Table 5-3 Validations for inferred ventilation rate Q

CO_2 Tracer gas measurements	Test number	Experimental conditions	Estimated Q (ACH)		Experimental Q (ACH)		Relative Error (%)
			mean	sd	mean	sd	
Concentration decay	Test1	Ventilation 1	1.90	0.03	1.91	0.03	0.5%
	Test2	Ventilation 2	1.52	0.02	1.51	0.04	0.6%
	Test3	Ventilation 3	0.51	0.01	0.53	0.03	3.8%
Constant injection	Test4	Ventilation1, CO_2 release =0.013 L/s (0.8 L/min), fan off	1.80	0.20	1.91	0.03	5.7%
	Test5	Ventilation1, CO_2 release =0.013 L/s (0.8 L/min), fan on	2.15	0.26	1.91	0.03	12.6%
	Test6	Ventilation1, CO_2 release =0.026 L/s (1.6 L/min), fan off	1.85	0.31	1.91	0.03	3.1%
	Test7	Ventilation1, CO_2 release =0.026 L/s (1.6 L/min), fan on	2.12	0.06	1.91	0.03	11.0%
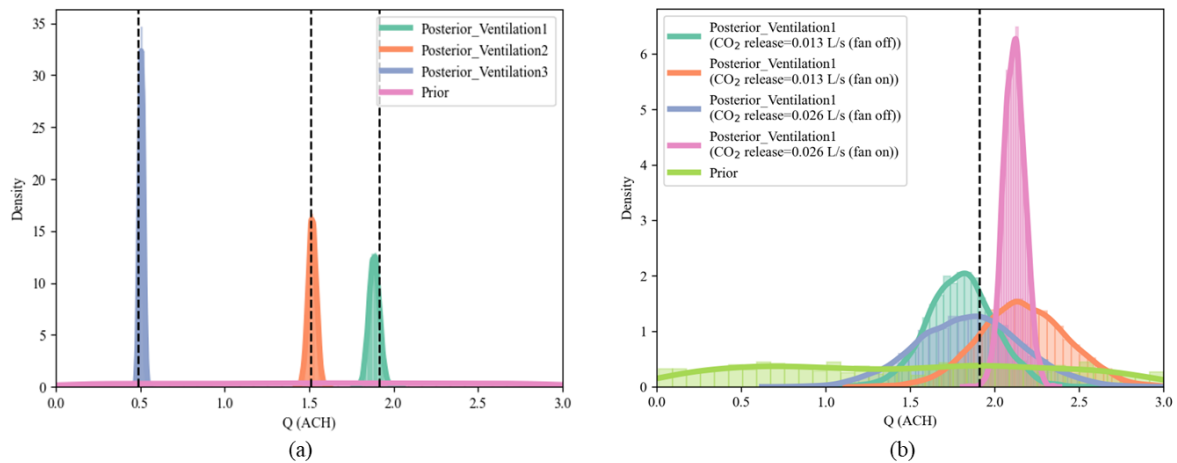
Figure 5-6 Posterior distribution on inferred ventilation rate Q; a) Inferred ventilation rate under three ventilation conditions from CO_2 decay tests; b) Inferred ventilation rate under normal ventilation conditions from CO_2 constant injection tests; The black dashed line indicates the referenced value measured from the airtight chamber

5.3.2.2 Validation of the inferred CO_2 emission rate E

In addition to the ventilation rate Q, the CO_2 emission rate E was another parameter of interest, which can be inferred from the model simultaneously. The interpretation of the CO_2 emission rate in the room can help estimate the occupancy based on the CO_2 emission rate per person under certain ages and physical activity levels. The comparisons between the inferred CO_2 emission rates E and the CO_2 emission readings from the mass flow controller are illustrated in Table 5-4 and Figure 5-7.

From Figure 5-7, it could be found that the inferred CO_2 emission rate E is in good agreement with the measurements obtained from the emission mass flow controller for all tested scenarios. As shown in Table 5-4, in the "fan off" scenario, the estimation errors for the release rates of 0.8 L/min and 1.6 L/min were 2.3 % and 6.4 %, respectively. However, when the fan was turned on, the discrepancies widened, increasing to 12.8 % for 0.8 L/min and 8.6 % for 1.6 L/min. Though the differences increased in the "fan on" conditions when compared with the "fan off" ones, the estimated errors remained in an acceptable range of 5% - 15%.

Table 5-4 Validations for inferred CO_2 emission rates E

Constant injection	Experimental conditions	CO_2 emission rate E (L/s)		CO_2 emission readings from mass flow controller (L/s)		Relative Error (%)
		mean	sd	mean	sd	
Test 4	Ventilation 1, CO_2 release =0.013 L/s (0.8L/min), fan off	0.013	0.001	0.0133	0.0001	2.3 %
Test 5	Ventilation 1, CO_2 release =0.013 L/s (0.8L/min), fan on	0.015	0.001	0.0133	0.0001	12.8 %
Test 6	Ventilation 1, CO_2 release =0.026 L/s (1.6L/min), fan off	0.025	0.003	0.0267	0.0002	6.4 %
Test 7	Ventilation 1, CO_2 release =0.026 L/s (1.6L/min), fan on	0.029	0.001	0.0267	0.0002	8.6 %
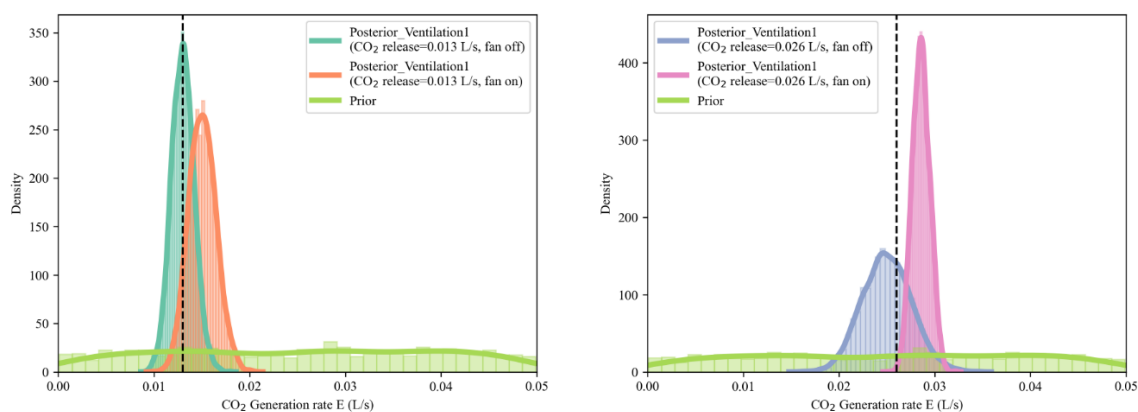
Figure 5-7 Posterior distribution on CO_2 emission rate E; a) Inferred CO_2 generation rate under CO_2 release = 0.013 L/s (0.8 L/min); b) Inferred CO_2 generation rate under CO_2 release = 0.026 L/s (1.6 L/min); The black dashed line indicates the referenced value measured from the airtight chamber

5.3.2.3 PPC evaluation results

The PPC evaluation results for decay and constant injection scenarios are shown in Figure 5-8 and Figure 5-9 as follows. It suggests that the generated data closely align with the observed

data, which further validates the accuracy of the inferred parameters. The Bayesian p-value for the decay and constant injection scenarios fall in the range of 0.37 - 0.40 and 0.63 - 0.66, respectively, all close to 0.50, which suggests a reasonable fit for the model.
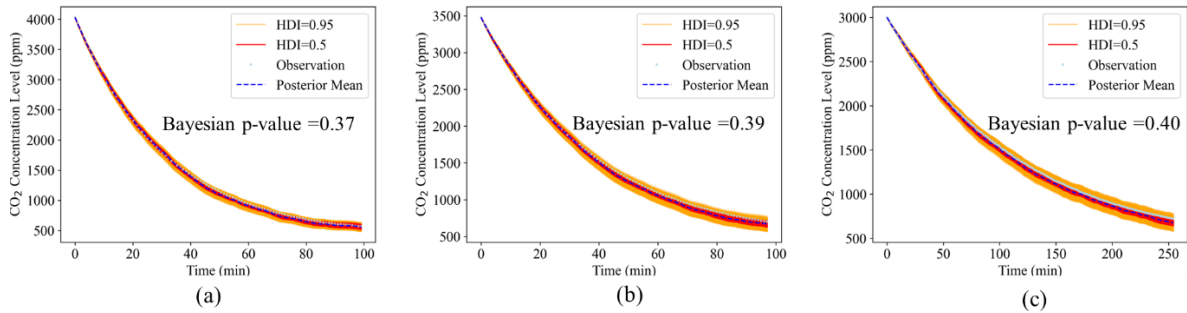
Figure 5-8 Posterior predictive simulations for decay scenarios (HDI =Highest Density Interval, indicating the probability that true value drops in this interval; (a) – (c): Test 1 – Test 3, details see Table 5-3)
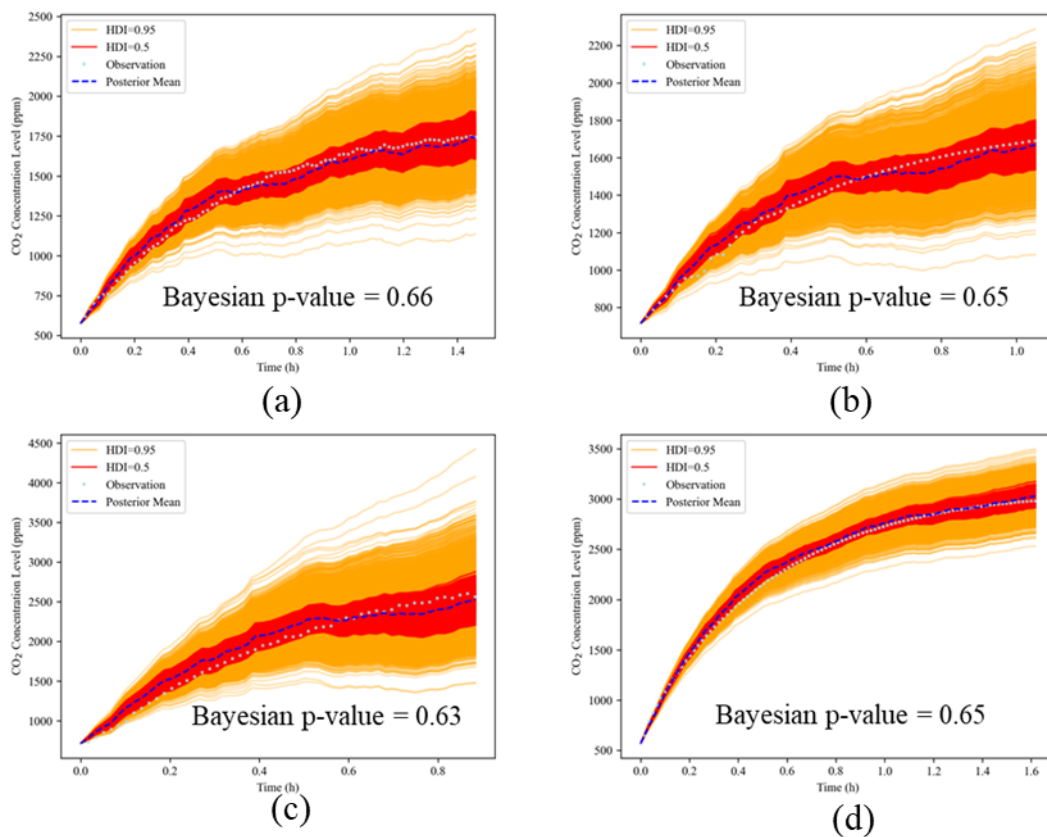
Figure 5-9 Posterior predictive simulations for constant injection scenarios (HDI =Highest Density Interval, indicating the probability that true value drops in this interval; (a) - (d): Test 4 – Test7, details see Table 5-4)

5.3.2.4 Noise level estimations in CO_2 trend predictions

In this section, the posterior means from the constant injection scenarios (Table 5-5) are taken as inputs for the ODE and SDE CO_2 mass-balance models (Eq. 5-1 and Eq.5-2), respectively. One hundred simulations were conducted for the SDE model. The CO_2 trend predictions and noise level estimations are illustrated in Figure 5-10. The SDE model could capture the variability in the observational data and make reasonable estimations for the CO_2 trend. Compared with the traditional ODE model, SDE predictions could consider real-life noise estimations and make unbiased predictions. The posterior distributions estimated for σ, which is the incremental variance in the Wiener process to scale the magnitude of the random fluctuation, were shown in Table 5-5. Correspondingly, the noise level estimations are shown in Figure 5-10 (b) (d) (f) (h).

For the scenarios with a CO_2 release rate of 0.013 L/s, the disturbances in the system illustrated similar magnitudes with σ estimations at 72.7 ± 5.8 (fan off) and 75.4 ±7.1(fan on), respectively. No significant differences were observed, and the predicted noise levels both fall in the range of -100 ppm to 100 ppm. In scenarios where the CO_2 release rate was 0.026 L/s, the disturbances were significantly reduced when the fan was on. For the fan-off condition, the σ was estimated to be 157.3 ± 16.9, whereas this estimation dropped to 48.6 ± 3.6 when the fan was turned on. The fan's operation appeared to reduce the variability in the observed data and this effect was not obvious when the CO_2 release rate was low. It should be noted that throughout the experiments, the fan was controlled remotely, ensuring its operation was the only altered condition. All other experimental conditions were kept constant during these tests. According to the manufacturers, the sensor measurement errors are ± 40 ppm, which is captured by the scenarios listed in Table 5-5.

Table 5-5 Posterior distributions estimated for the incremental variance

| Test number (for constant injection) | Experimental conditions | σ (ppm/$\sqrt{h}$) | | Relative ratio to steady-state CO_2 level in ppm (mean estimations from one hundred SDE simulations) |
		mean	sd	
Test 4	Ventilation 1, CO_2 release =0.013 L/s (0.8 L/min), fan off	72.7	5.8	± 1 %
Test 5	Ventilation 1, CO_2 release =0.013 L/s (0.8 L/min), fan on	75.4	7.1	± 2.2 %
Test 6	Ventilation 1, CO_2 release =0.026 L/s (1.6 L/min), fan off	157.3	16.9	± 1.1 %
Test 7	Ventilation 1, CO_2 release =0.026 L/s (1.6 L/min), fan on	48.6	3.6	± 0.9 %
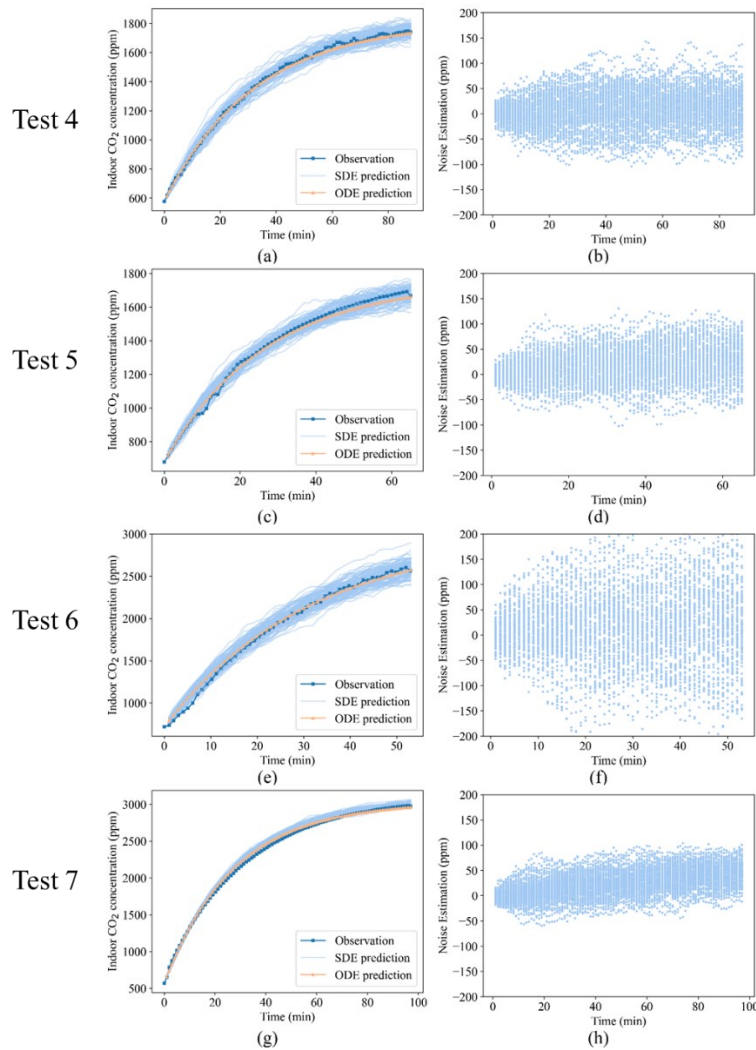
Figure 5-10 ODE- and SDE-based CO_2 trend predictions and noise level estimations

5.3.3 Case Study

Indoor whole-year field measurements of CO_2 levels from two Montreal primary schools (from 2020 to 2021) were used to employ the proposed approach in real-life settings. The selected classrooms have a floor area of 9.4 m × 6.6 m (Classroom 1) and 8.8 m × 7.1 m (Classroom 2), respectively, and both are naturally ventilated. The HOBO Bluetooth Low Energy Carbon Dioxide- Temp / RH Data Logger was installed in classrooms at 1.7 meters height on the west internal wall right above the thermostat (1.5 m height). The detailed information on the data logger is listed in Table 5-6.

Table 5-6 Detailed information for the HOBO Data Logger

Reading Type	Measurement range	Accuracy	Resolution
CO_2	0 – 5000 ppm	± 50 ppm	–
Relative Humidity	1% – 90% RH	± 2 % RH	0.01 %
Temperature	-20 – 70 ºC	± 0.21 ºC	0.024 °C at 25°C

Table 5-7 Measurements information in the classroom

Classroom	Location	Age	Dimensions (m)	Ventilation Type	Measurement Periods
Classroom 1	Montreal	5-8	9.4 × 6.6 ×3.47	Natural ventilation	2020/06/22 - 2021/06/21
Classroom 2	Montreal	5-8	8.8 × 7.1 × 3.2	Natural ventilation	2020/08/26 - 2021/08/25

Table 5-7 illustrates the measurement information for the two primary classrooms. One week of weekday data (from Monday to Friday, represented as Day 1 to Day 5 in later discussions) was selected from Autumn, Winter, and Spring for each of the classrooms (Figure 5-11). Since the classrooms remained unoccupied for most of the summer vacation, this period was not included in our analysis. For each day, the data was selected from the first class start to the first CO_2 peak to do the evaluation. It is based on the assumption that the ventilation conditions remain the same for the whole day, and the number of students who attend the first class will be considered as the maximum attendance on that day. The ventilation rate and CO_2 emission

rates were estimated using the developed approach, and occupancy was also calculated under the assumption that the average CO_2 generation rate per person was 0.0047 L/s [7].

Based on the estimated ventilation rates and occupancy levels, the equivalent clean airflow delivery rates per person were carried out (ECAi) and compared with the minimum values recommended by ASHRAE Standard 241 [292]. The ECAi sums the clean air supply rates contributed by indoor mitigation measures, including outdoor air ventilation, HVAC filtration, and air-cleaning devices such as portable air cleaners (PAC) or germicidal ultraviolet (GUV) [105, 257, 293]. This will assess the capability of the classroom to mitigate long-range aerosol exposures. In addition, it will help clarify the efforts required to achieve the infection risk management target established by ASHRAE 241 and figure out proper mitigation measures. The Equivalent Clean Air Calculator will be used for the assessment [292]. A steady-state CO_2 threshold that achieves minimum ECAi requirements was carried out for the evaluation periods and summarized with mean and pooled standard deviation for each classroom. Thresholds were established for scenarios involving pure ventilation, combined mitigation strategies, and various occupancy levels based on the summary of 2,000 runs of SDE model simulations for each scenario.
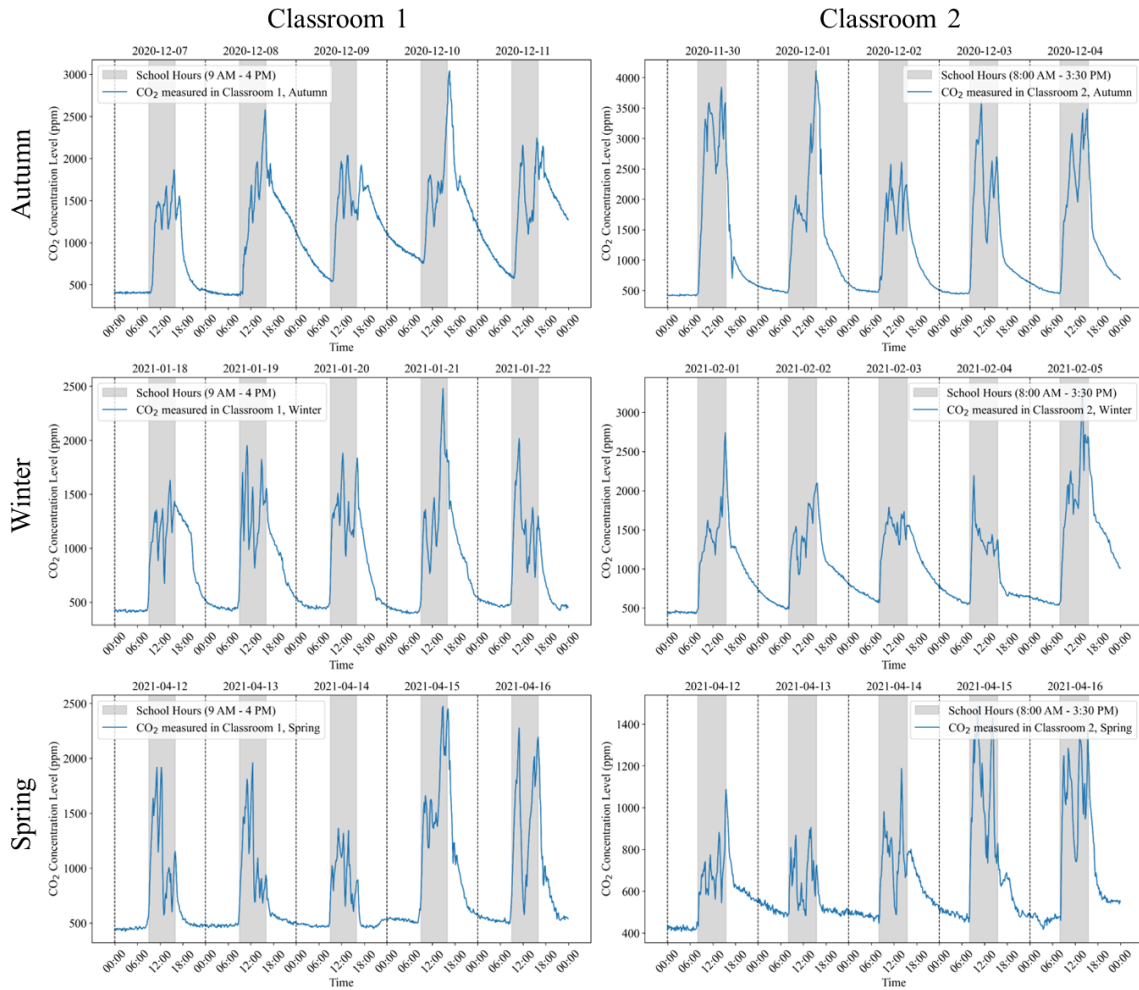
Figure 5-11 One-week CO_2 measurements selected from Autumn, Winter, and Spring for two classrooms

5.3.3.1 Estimated parameters and ECAi

The proposed approach was subsequently employed to evaluate the ventilation conditions of two classrooms from two Montreal primary schools. As illustrated in Table 5-8, it could be found that the ventilation rates for Classroom 1 and Classroom 2 were inferred to be in the range of 0.11 – 1.38 ACH and 0.11 – 3.66 ACH, respectively. In evaluated days, the largest ventilation rate appears in Spring for both classrooms, which turns out to be Day 3, Spring (2021-04-14) for Classroom 1 and Day 2, Spring (2021-04-13) for Classroom 2. The occupancy turns out to be ranging from 9 - 20 for Classroom 1 and 14 - 20 for Classroom 2, with one

exceptional day of only 3 students attending the class. The ECAi provided for each day was evaluated, ranging from 0.6 to 24.7 L/s/person. In the evaluated days, the ECAi provided in most of the days was significantly lower than the value recommended by ASHRAE 241 (20 L/s/person for Classroom) [292]. This suggests that, throughout the evaluation period, the clean air introduced into the two classrooms had limited capabilities in removing aerosols and failed to meet the ECAi requirements.

Table 5-8 Evaluation results for the two classrooms in Autumn, Winter, and Spring

Classroom1, Autumn	Day1	Day2	Day3	Day4	Day5
Ventilation rate (ACH)	0.35	0.63	0.24	0.34	0.25
Total CO_2 emission rate (L/s)	0.044	0.079	0.09	0.083	0.088
Estimated occupancy	9	17	19	18	19
ECAi provided (L/s/person)	2.3	2.2	0.8	1.1	0.8
Classroom1, Winter	Day1	Day2	Day3	Day4	Day5
Ventilation rate (ACH)	0.58	1.24	0.96	0.81	0.2
Total CO_2 emission rate (L/s)	0.044	0.069	0.078	0.081	0.091
Estimated occupancy	9	15	17	17	19
ECAi provided (L/s/person)	3.9	5.0	3.4	2.9	0.6
Classroom1, Spring	Day1	Day2	Day3	Day4	Day5
Ventilation rate (ACH)	0.11	0.44	1.38	0.48	0.14
Total CO_2 emission rate (L/s)	0.046	0.087	0.079	0.083	0.092
Estimated occupancy	10	19	17	18	20
ECAi provided (L/s/person)	0.7	1.4	4.9	1.6	0.4
Classroom2, Autumn	Day1	Day2	Day3	Day4	Day5
Ventilation rate (ACH)	0.21	0.26	0.3	0.24	0.11
Total CO_2 emission rate (L/s)	0.084	0.089	0.085	0.083	0.092
Estimated occupancy	18	19	18	18	20
ECAi provided (L/s/person)	0.6	3.2	0.9	0.7	0.3
Classroom2, Winter	Day1	Day2	Day3	Day4	Day5
Ventilation rate (ACH)	1.18	0.6	0.51	0.79	0.2
Total CO_2 emission rate (L/s)	0.071	0.083	0.085	0.071	0.09
Estimated occupancy	15	18	18	15	19
ECAi provided (L/s/person)	4.4	4.5	1.6	2.9	0.6
Classroom2, Spring	Day1	Day2	Day3	Day4	Day5
Ventilation rate (ACH)	1.33	3.66	0.81	0.88	1.74
Total CO_2 emission rate (L/s)	0.015	0.068	0.086	0.081	0.069
Estimated occupancy	3	14	18	17	15
ECAi provided (L/s/person)	24.7	17.9	2.5	2.9	6.5

Note. The average CO_2 generation rate per person was assumed to be 0.0047 L/s for Classrooms (5-8 years) [280].

5.3.3.2 Steady-state CO_2 threshold achieving minimum ECAi requirements

To satisfy the minimum ECAi requirements, the steady-state CO_2 threshold was determined with the stochastic CO_2 grey-box model, employing outdoor ventilation as the only air-cleaning

strategy. The minimum ECAi requirement of 20 L/s/person was used to determine the ventilation rate 'Q' in the model, alongside other parameters estimated from the previous evaluation phase. Two thousand CO_2 steady-state concentration simulations were conducted for each day evaluated in Table 5-8, and the summarized CO_2 steady-state concentration was shown in Figure 5-12 for each of the classrooms (Classroom 1: 688.2 ± 132.4 ppm, Classroom 2: 690.3 ± 158.2 ppm). Daily evaluation results are shown in Appendix 3. The cumulative distribution of school-hour CO_2 measurements in Autumn, Winter, and Spring for Classroom 1 and Classroom 2 were also demonstrated in Figure 5-12. In Classroom 1, only 25% of measurements fall into the established steady-state CO_2 threshold that achieves minimum ECAi requirements, while this number for Classroom 2 was 35%. This shows that during at least two-thirds of school hours, the minimum ECAi requirements are not met throughout the academic year. Natural ventilation alone is insufficient to ensure safe and healthy learning environments. Therefore, an increased supply of clean air in classrooms is necessary.
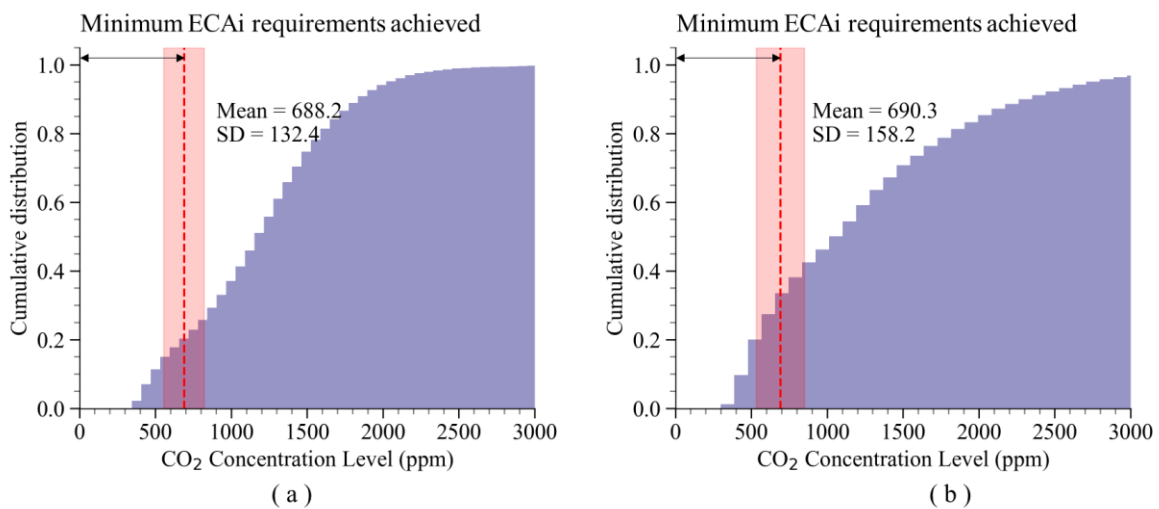
Figure 5-12 Whole year CO_2 measurements in two classrooms; a) Cumulative distribution of school-hour CO_2 measurements in Autumn, Winter, and Spring for Classroom 1; b) Cumulative distribution of school-hour CO_2 measurements in Autumn, Winter, and Spring for Classroom 2

5.3.3.3 Retrofits to achieve the minimum ECAi required by ASHRAE 241

The impact of different exposure mitigation measures, with clean air delivery rates (CADR)

ranging from 0.09 – 0.47 m^3/s on ECAi was investigated, and the results are presented in Table 5-9. Various combinations of in-room UV devices and air cleaners (fan filter type) were evaluated to achieve varying levels of CADR. The findings suggest that a supplement of air-cleaning devices with a CADR of 0.38 m^3/s or more ensures that ECAi requirements are consistently achieved in both classrooms.

Table 5-9 ECAi under different mitigation measures

Classroom 1, Autumn	Day1	Day2	Day3	Day4	Day5
In-room UV (0.09 m^3/s CADR)	12.8	7.8	5.7	6.4	5.8
In-room air cleaner (0.19 m^3/s CADR)	**23.3**	13.3	10.7	11.6	10.7
In-room UV + In-room air cleaner (0.27 m^3/s CADR)	**33.8**	18.9	15.7	16.9	15.7
2 × In-room air cleaner (0.38 m^3/s CADR)	**44.3**	**24.4**	**20.6**	**22.1**	**20.7**
In-room UV + 2 × In-room air cleaner (0.47 m^3/s CADR)	**54.8**	**30.0**	**25.6**	**27.4**	**25.6**
Classroom 1, Winter	Day1	Day2	Day3	Day4	Day5
In-room UV (0.09 m^3/s CADR)	14.4	11.2	8.9	8.4	5.6
In-room air cleaner (0.19 m^3/s CADR)	**24.8**	17.5	14.5	14.0	10.6
In-room UV + In-room air cleaner (0.27 m^3/s CADR)	**35.3**	**23.8**	**20.0**	19.5	15.5
2 × In-room air cleaner (0.38 m^3/s CADR)	**45.8**	**30.1**	**25.6**	**25.1**	**20.5**
In-room UV + 2 × In-room air cleaner (0.47 m^3/s CADR)	**56.3**	**36.4**	**31.2**	**30.6**	**25.5**
Classroom 1, Spring	Day1	Day2	Day3	Day4	Day5
In-room UV (0.09 m^3/s CADR)	10.1	6.4	10.4	6.8	5.1
In-room air cleaner (0.19 m^3/s CADR)	19.5	11.3	16.0	12.1	9.9
In-room UV + In-room air cleaner (0.27 m^3/s CADR)	**29.0**	16.3	**21.5**	17.3	14.6
2 × In-room air cleaner (0.38 m^3/s CADR)	**38.4**	**21.3**	**27.1**	**22.6**	19.3
In-room UV + 2 × In-room air cleaner (0.47 m^3/s CADR)	**47.9**	**26.2**	**32.6**	**27.8**	**24.0**
Classroom 2, Autumn	Day1	Day2	Day3	Day4	Day5
In-room UV (0.09 m^3/s CADR)	5.9	8.2	6.2	6.0	5.0
In-room air cleaner (0.19 m^3/s CADR)	11.1	13.2	11.4	11.2	9.7
In-room UV + In-room air cleaner (0.27 m^3/s CADR)	16.4	18.2	16.7	16.5	14.5
2 × In-room air cleaner (0.38 m^3/s CADR)	**21.6**	**23.1**	**21.9**	**21.7**	19.2
In-room UV + 2 × In-room air cleaner (0.47 m^3/s CADR)	**26.9**	**28.1**	**27.2**	**27.0**	**23.9**
Classroom 2, Winter	Day1	Day2	Day3	Day4	Day5
In-room UV (0.09 m^3/s CADR)	10.7	9.7	6.8	9.2	5.6
In-room air cleaner (0.19 m^3/s CADR)	17.0	15.0	12.1	15.5	10.5
In-room UV + In-room air cleaner (0.27 m^3/s CADR)	**23.3**	**20.2**	17.3	**21.8**	15.5
2 × In-room air cleaner (0.38 m^3/s CADR)	**29.6**	**25.5**	**22.6**	**28.1**	**20.5**
In-room UV + 2 × In-room air cleaner (0.47 m^3/s CADR)	**35.8**	**30.7**	**27.8**	**34.4**	**25.4**

Classroom 2, Spring	Day1	Day2	Day3	Day4	Day5
In-room UV (0.09 m^3/s)	**56.2**	**24.7**	7.7	8.4	12.8
In-room air cleaner (0.19 m^3/s CADR)	**87.6**	**31.4**	13.0	14.0	19.0
In-room UV + In-room air cleaner (0.27 m^3/s CADR)	**119.1**	**38.2**	18.2	19.5	25.3
2 × In-room air cleaner (0.38 m^3/s CADR)	**150.6**	**44.9**	**23.5**	**25.1**	**31.6**
In-room UV + 2 × In-room air cleaner (0.47 m^3/s CADR)	**182.0**	**51.6**	**28.7**	**30.6**	**37.9**

Note: The conditions that satisfy the EACi requirements in ASHRAE 241 (20 L/s/person) are in bold

5.3.3.4 Manage long-range indoor aerosol exposures using CO_2 as a proxy

For the purpose of creating a clean and healthy indoor environment, the CO_2 thresholds were established for potential future indoor ventilation designs and operations in the classrooms. The steady-state CO_2 levels were carried out using the stochastic CO_2-based grey-box model. Three aerosol exposure management levels were established from two thousand predictive outcomes of the model: C_{limit} (Mean + SD) as the maximum threshold indicating poor ventilation beyond this limit, C_{target} (Mean) as the expected CO_2 concentration limit, under which conditions are deemed acceptable and generally comply with ECAi, and C_{ideal} (Mean – SD) as the optimal threshold, recommended when infection risk of respiratory diseases in the classroom is a significant concern. These thresholds could help manage long-range indoor aerosol exposures by using CO_2 as a proxy while taking real-life uncertainties into consideration.

The design C_{target} levels were evaluated for classrooms under varying occupancy and CADR conditions (Figure 5-13). When no additional CADR is supplied, a ventilation rate of 20 L/s per person is required, resulting in an average C_{target} level of 683 ppm and 686 ppm for the classrooms respectively. Thus, it is suggested to set C_{target} below 690 ppm when managing indoor aerosol exposures is a priority. In scenarios where air-cleaning devices with sufficient CADR are adopted (0.38 m^3/s), the C_{target} stabilizes around 1000 ppm. Conversely, when limited CADR is supplemented such as 0.09 m^3/s, the C_{target} level initially rises with increased occupancy but subsequently falls as additional ventilation is needed to maintain the effective clean air level (ECAi).

Uncertainties in real-life operations can influence the estimated maximum CO_2 levels used to

indicate whether a room meets ECAi requirements. For instance, actual attendance may vary from the designed occupancy levels. As a result, the CO_2 thresholds (C_{limit}, C_{target}, and C_{ideal}) were carried out for different mitigation measures with CADR ranging from $0.09 – 0.47$ m^3/s. These thresholds are depicted in Figure 5-14 for Classroom 1 and Classroom 2, and generalized equations derived from the average of their coefficients are presented in Eq.5-6 to Eq.5-8. When the CADR is below 0.28 m^3/s, enhancing air-cleaning capacity improves ECAi, thereby reducing reliance on outdoor ventilation for achieving ECAi requirements. While the contribution from outdoor ventilation can decrease from the initial 20 L/s/person, it must still meet the minimum ventilation rate of 7.4 L/s/person recommended in ASHRAE 62.1 for classrooms [279]. Once air-cleaning devices provide sufficient ECAi, the steady-state CO_2 thresholds indicating ECAi satisfaction remain stable.
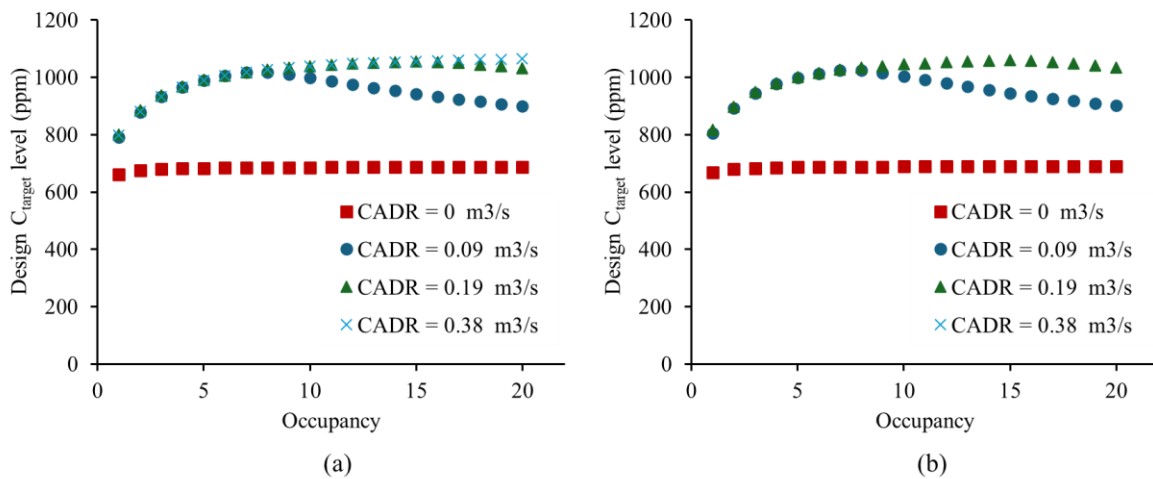
Figure 5-13 Design C_{target} level for different occupancy in two classrooms; a) Classroom 1; b) Classroom 2
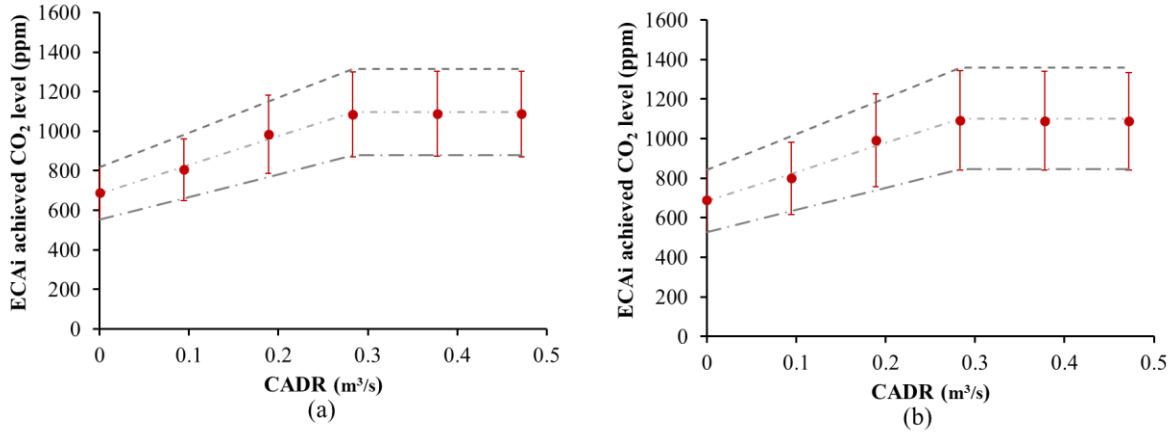
Figure 5-14 Steady-state CO_2 thresholds that achieve minimum ECAi requirements with the employment of air-cleaning devices under different CADR; a) Classroom 1; b) Classroom 2

$$C_{limit} = \begin{cases} 0.8 \times CADR + 829.1 & (CADR \leq 600) \\ 1309.1 & (CADR > 600) \end{cases} \quad \text{5-6}$$

$$C_{target} = \begin{cases} 0.7 \times CADR + 684.6 & (CADR \leq 600) \\ 1104.6 & (CADR > 600) \end{cases} \quad \text{5-7}$$

$$C_{ideal} = \begin{cases} 0.5 \times CADR + 540.1 & (CADR \leq 600) \\ 840.1 & (CADR > 600) \end{cases} \quad \text{5-8}$$

When the CADR level of air-cleaning devices introduced into classrooms is set, the C_{limit}, C_{target}, and C_{ideal} can be respectively calculated for classrooms with similar designs as the two Montreal primary classrooms investigated in this study. The 'similar designs' refer to aspects such as dimensions, occupancy, attendance, ventilation mode, etc. For other public indoor facilities with distinctive ventilation designs, measuring CO_2 concentrations during occupied hours is advised to obtain the data for inference. Subsequently, case-specific CO_2 thresholds can be determined using the methodology established in this study.

It should also be noted that the CO_2 thresholds established here aim at indicating whether the IAQ in classrooms complies with ASHRAE standard 241 [292] and ASHRAE standard 62.1 [279]. ASHRAE standard 241 outlines the clean-air requirements within an Infection Risk Management Mode (IRMM) during an outbreak, requiring higher cleaning air delivery levels

when compared with ASHRAE standard 62.1. In scenarios where air-cleaning devices are absent or limited, a considerable volume of outdoor ventilation is recommended to maintain air quality (e.g., when the CADR is 0.28 m^3/s, a ventilation rate of 20 L/s/person is advised). As the CADR available to the room increases, the requirement for outdoor ventilation decreases accordingly. Nonetheless, it needs to be realized that even when air-cleaning devices supply sufficient ECAi, the outdoor ventilation rates must still adhere to the minimum requirements outlined in ASHRAE standard 62.1 to ensure adequate air quality (for instance, when CADR is equal to or greater than 0.28 , a minimum ventilation rate of 7.4 L/s/person is still mandated). When the community infection risk of respiratory diseases is low, it is also appropriate to utilize the thresholds designed for scenarios with sufficient CADR, such as during the plateau periods when the CADR exceeds 0.28 m^3/s . These thresholds align with the ventilation requirements specified by ASHRAE standard 62.1 only.

5.4 Conclusions

In this study, we present an innovative method to quantify uncertainties in indoor ventilation conditions, aimed at enhancing future evaluations of Canadian primary schools. The approach proposed by this study has the potential to help interpret CO_2 recordings in real classroom settings and predict steady-state CO_2 levels considering uncertainties. Here are the main contributions of this study:

- By employing Bayesian inference on a CO_2-based grey-box SDE model, the ventilation rate and CO_2 emission rate can be accurately predicted. Uncertainties come from measurements, the randomness of air movements, and modeled or unmodelled parameters, which can be quantified using the incremental variance σ.

- The robustness and reliability of the model were validated with CO_2 tracer gas experiments in an airtight chamber. Prior sensitivity analysis was conducted to verify the rationality of assumed prior assumptions. Parameters inferred from the model were compared with chamber measurements to confirm its estimation accuracy. The PPC evaluations were

conducted to see whether the estimated parameters for the model could work well to represent the observations. The results suggested that the model is robust to its prior assumptions and can estimate the interested parameters with reliable accuracy.

- Applications were conducted to interpret the real-life CO_2 measurements in two classrooms in Montreal. Using the estimated ventilation and occupancy, the provided ECAi and the steady-state CO_2 threshold for achieving minimum ECAi requirements were calculated, suggesting natural ventilation is insufficient to achieve ECAi standards established by ASHRAE 241 for all three seasons.

- Adopting a CADR of 0.38 m^3/s can help the classrooms to effectively manage aerosol exposures. In addition, steady-state CO_2 thresholds (C_{limit}, C_{target}, and C_{ideal}) to indicate the ECAi satisfactory status were carried out for different mitigations using the stochastic CO_2 grey-box model and inferred parameters.

- To achieve the minimum ECAi level required by ASHRAE 241, the target CO_2 level is suggested to be below 690 ppm for similar classrooms without additional clean-air treatment. When sufficient clean air is supplemented, the design C_{target} is appropriately set at 1000 ppm. Empirical equations were also established for classrooms that share the ventilation design featured in this study. In real-life operations and management, it is recommended to reference Figure 5-14 to consider uncertainties.

Limitations do exist in this study because only two classrooms were investigated, and occupancy information was not available for further verifications of the model. For people who are interested in understanding the ECAi-compliant steady-state CO_2 thresholds for a specific indoor environment, it is advisable to conduct consistent field CO_2 measurements in occupied hours for the intended scenario and apply the approach developed in this study.

Chapter 6 Conclusions and Future Work

This study explored approaches to manage long-range indoor aerosol transmissions of respiratory diseases such as SARS-CoV-2. Initially, multizonal aerosol transmissions of SARS-CoV-2 were assessed using the CONTAM-quanta approach. This method was demonstrated with a DOE prototype Large Office building and subsequently applied to a Medium Office, Stand-Alone Retail, Small Hotel, and Secondary School. The effectiveness of various mechanical mitigation measures was analyzed and compared. Additionally, to control aerosol exposures in real-life settings using CO_2 monitoring records, Bayesian inference was applied to a stochastic CO_2-based grey-box model to estimate indoor ventilation conditions. The main contributions, limitations, and future work of this study are summarized below.

6.1 Major Contributions

In order to limit the indoor aerosol transmissions and guarantee safe occupants' exposures inside the building, this study developed methodologies to effectively compare mitigation strategies in multizone buildings and infer indoor ventilation conditions via CO_2 field monitoring. Here are the main findings and contributions in this study:

- This modeling approach allows for an evaluation of the whole building as a multizone structure, enabling an effective comparison of ventilation and air-cleaning components. The Large Office scenario simulated in this study served as an excellent example for implementing mitigation strategies. In the baseline case, while zone-to-zone and floor-to-floor spread was possible, the risk was significantly lower in all zones compared to the source zone. A duct-treatment strategy could approach the effectiveness of using 100% outdoor air, and adding room cleaning devices such as portable air cleaners and in-room germicidal UV light could further enhance air cleaning.

- The study also modeled layered mitigation strategies for long-range transmission of SARS-CoV-2 quanta in five DOE prototype commercial buildings. The results

indicated that duct-treatment air-cleaning strategies (upgrading MERV filter levels and using in-duct UV) are more effective in large rooms that can accommodate hundreds of occupants. In contrast, room-treatment strategies (adding portable air cleaners and in-room UV) are more effective in smaller spaces. The priority of mitigation strategies varies for different rooms depending on room volume, occupants' exposure time, and HVAC system designs.

- This study employs Bayesian inference on a CO_2-based grey-box SDE model to accurately predict ventilation and CO_2 emission rates, accounting for uncertainties from measurements, air movement randomness, and parameters. The model's robustness and reliability were validated through CO_2 tracer gas experiments in an airtight chamber, with prior sensitivity analysis and comparison with chamber measurements confirming its accuracy. Posterior predictive checks further validated the model's reliability. Real-life CO_2 measurements from two classrooms in Montreal were analyzed, revealing that natural ventilation alone is insufficient to meet ASHRAE 241 ECAi standards across seasons. The study found that adopting a CADR of 0.38 m^3/s effectively manages aerosol exposures, and steady-state CO_2 thresholds were established to indicate satisfactory ECAi status for different mitigation strategies using the stochastic CO_2 grey-box model.

6.2 Limitations

In multizonal aerosol transmission evaluations, this study established a relationship between infection risks and the ratio of duration (D) to the product of room volume (V) and equivalent air change rate (Q_e), facilitating quick estimations of Q_e for ventilation design. While this allows for rapid ventilation decision-making, each building's unique characteristics require individual analysis. The Q_e is calculated for the source zone containing the infector, but multizone buildings need a broader design goal to ensure no transmission risks throughout the building. The study's limitations include the need for more detailed analyses to address

questions about overall mitigation goals and transmission risk management. Besides, though the CONTAM-quanta approach realized the comparisons of different mechanical mitigation approaches, the level of quanta generation rate would lead to huge uncertainties to the risk assessment level. Additionally, the well-mixed assumption was made throughout the study, the influence of flow patterns inside the room was not taken into consideration.

For the CO_2-based ventilation designs in primary schools, this study only investigated two classrooms, and the steady-state CO_2 thresholds were obtained based on the measurements data. Occupancy information was also not available for further verifications of the model. Ventilation rates and CO_2 generation rates were assumed to be constant throughout the evaluation period for the model. Meanwhile, the air was assumed to be well-mixed in the room and the influence of the sensor location was neglected. As a result, the application of the proposed approach would be limited to the assumptions made in current investigated scenarios.

6.3 Future work

Despite the meaningful evaluation results obtained in the thesis, there are still several aspects that remain to be investigated, which are recommended for the future work.

For multizonal aerosol transmission mitigations:

- In case studies for the DOE prototype buildings, 100% outdoor air supply was found to be effective in removing airborne aerosols in most evaluated scenarios. However, in real-life situations, the adoption of 100% outdoor air supply can lead to huge energy consumptions. The selection of proper mechanical engineering mitigations may not only depend on the aerosol removal capabilities but also the energy consumption and economic budgets. As energy-efficient ventilation design was not the primary focus of this study, it can be investigated in future studies to nudge an optimal trade-off between energy costs and air-cleaning indoor environments.
- Multizonal aerosol modelling can be extended from prototype commercial buildings

to real-life building settings. Field measurements can be obtained from the buildings to establish multizone building models that are close to real-life. Practical ventilation designs can thus be established to guide real-life operations and prevent potential aerosol zonal transmissions. This will help retrofit existing buildings and prevent future outbreaks of respiratory diseases.

- Future research should evaluate more real-life scenarios using the CONTAM-quanta approach, consider local SARS-CoV-2 prevalence, apply occupancy schedules, account for increasing vaccination rates, and incorporate stochastic effects as seen in the Skagit Valley Chorale super-spreading event investigation. The influence of occupants' activities can be investigated in the future, for instance, the effects of door-opening and window-opening, the effects of toilet flushing, and the effects of different occupancy schedules. These changes inside the building could lead to different aerosol transmission patterns.

For using occupant-generated CO_2 as a tracer gas for indoor ventilation evaluations:

- CO_2 measurements from more classrooms and longer evaluation periods can be involved for further evaluations. Occupancy attendance and absenteeism can be recorded to further verify the model's prediction ability in real-life settings. The location of the CO_2 sensors may also influence the estimation results, which can be further discussed and evaluated.

- The developed evaluation approach could be extended to other public spaces such as auditoriums, shopping malls, offices, gyms, etc. The case-specific CO_2 metrics can thus be established for different contexts to manage the long-range aerosol indoor exposures, which is based on the parameters inferred from their field CO_2 measurements.

- The CO_2 generation rates from occupants can also be estimated for different settings and help establish the CO_2 metrics to indicate indoor ventilation conditions

Appendix

Appendix 1 Verification of CONTAM-quanta Approach

The CONTAM multizone contaminants transportation simulation has been validated by many previous studies in terms of both airflow/ventilation and pollutant predictions [61,62]. Therefore, this verification focused on applying the CONTAM-*quanta* model to the Skagit Valley Chorale superspreading event [44], and comparing results with those from the COVID-19 Aerosol Transmission Estimator [23]. The single-zone CONTAM case – FaTIMA [40] was used to model the quanta transmission. The verification details are illustrated in Table A1. It should be noted that the FaTIMA tool was not originally designed for modeling aerosols in terms of quanta, instead, it models the transmission of infective particles. In this study, we implemented the proposed CONTAM-*quanta* approach in FaTIMA and verified it in this section. Note a verification is to confirm the accuracy of a numerical approach when compared to the previous analytical approach with the same input parameters. This step is important because it ensures the numerical programming of a software tool is able to reproduce the results in the literature.

The transient airborne concentration predictions are compared as follows. Figure A1 shows that the predicted airborne concentrations agrees well with the values predicted using the formula underlying the COVID19 Aerosol Transmission Estimator [23]. In addition, the final airborne aerosol concentration levels were both at 0.56 quanta/m^3 and exposure risks at the end of the 2.5h event were predicted to be 88.6%. Thus, the proposed CONTAM-*quanta* approach can provide comparable results on estimating exposure as previous studies.

Table A 1 Comparison of CONTAM (FaTIMA)-*quanta* single-zone and COVID19 Aerosol Transmission Estimator [23]

	CONTAM (FaTIMA)-*quanta*		COVID19 Aerosol Transmission Estimator	
Zone volume	810 m³		810 m³	
Generation	Number of infector	1	Number of infector	1
	Particles/Quanta generation rate	970 quanta/h	Infective person	970 quanta/h
Removal	Supply air rate	567 m³/h	Ventilation with outside air	0.7 h⁻¹
	Return air rate	567 m³/h (0.7h⁻¹)		
	Exhaust air	567 m³/h (0.7h⁻¹)	Exhaust air	567 m³/h (0.7h⁻¹)
	Air cleaner (Filter)	0	Additional control measures	0
	Source deposition	0.3 h⁻¹	Source deposition	0.3 h⁻¹
	Decay of the virus	0.63 h⁻¹	Decay of the virus	0.63 h⁻¹
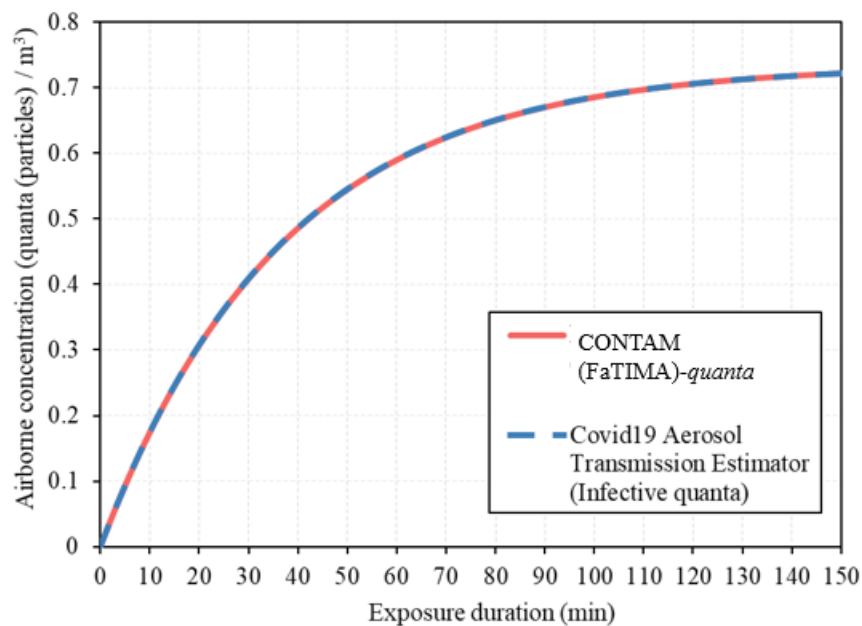
Figure A 1 Transient airborne contaminants concentration predictions during the 2.5h Choir duration (CONTAM-*quanta* vs COVID19 Aerosol Transmission Estimator)

Appendix 2 Comparisons between CONTAM-multizone and FaTIMA-singlezone modeling

The comparisons between CONTAM multizone simulations and single zone FaTIMA simulations of the baseline case (Baseline OA + MERV8) are illustrated as follows (Figure A2). The differences were due to zone-to-zone transmissions through air leakages and the central ventilation system (VAV in the Large Office). The single-zone FaTIMA only allows steady-state weather conditions while the multizone modeling adopts the Chicago TMY3 weather. The infiltration was also neglected by FaTIMA. In CONTAM modeling of the Large Office building, the VAV systems were modeled by a series of air-handling units across different floors, which reflects more realistically the multizone aerosol transmissions, e.g., via return grills. In comparison, one simple supply/return system was applied in FaTIMA. The comparison of the differences is summarized in Table A2 between the proposed CONTAM-quanta approach from this study and other single-zone models (i.e., COVID19 Estimator, REHVA calculator, FaTIMA), and multizone model (i.e., CONTAM).
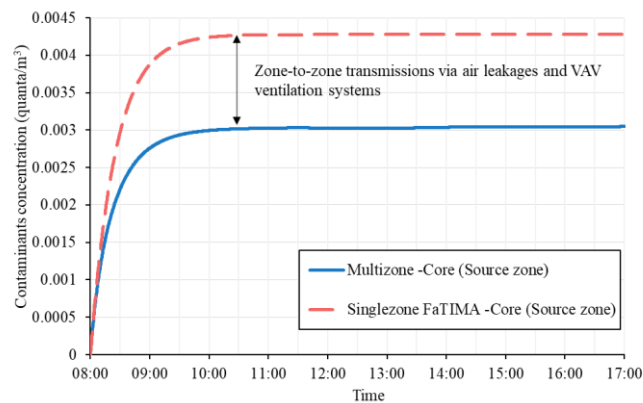
Figure A 2 Comparisons between single-zone and multi-zone simulations of the Large Office

Table A 2 Comparison between different tools for airborne aerosol modeling

	COVID19 Estimator [294]	REHVA calculator [295]	FaTIMA [296]	CONTAM [209]	CONTAM-quanta
Building details	-	-	-	√	√
HVAC details	-	-	√	√	√
Occupancy schedule	-	-	-	√	√
Weather impacts	-	-	-	√	√
Multi-zone analysis	-	-	-	√	√
Occupant exposure	√	√	√	√	√
Infection risk	√	√	-	-	√

Appendix 3 The daily steady-state CO_2 threshold for achieving minimum ECAi requirements
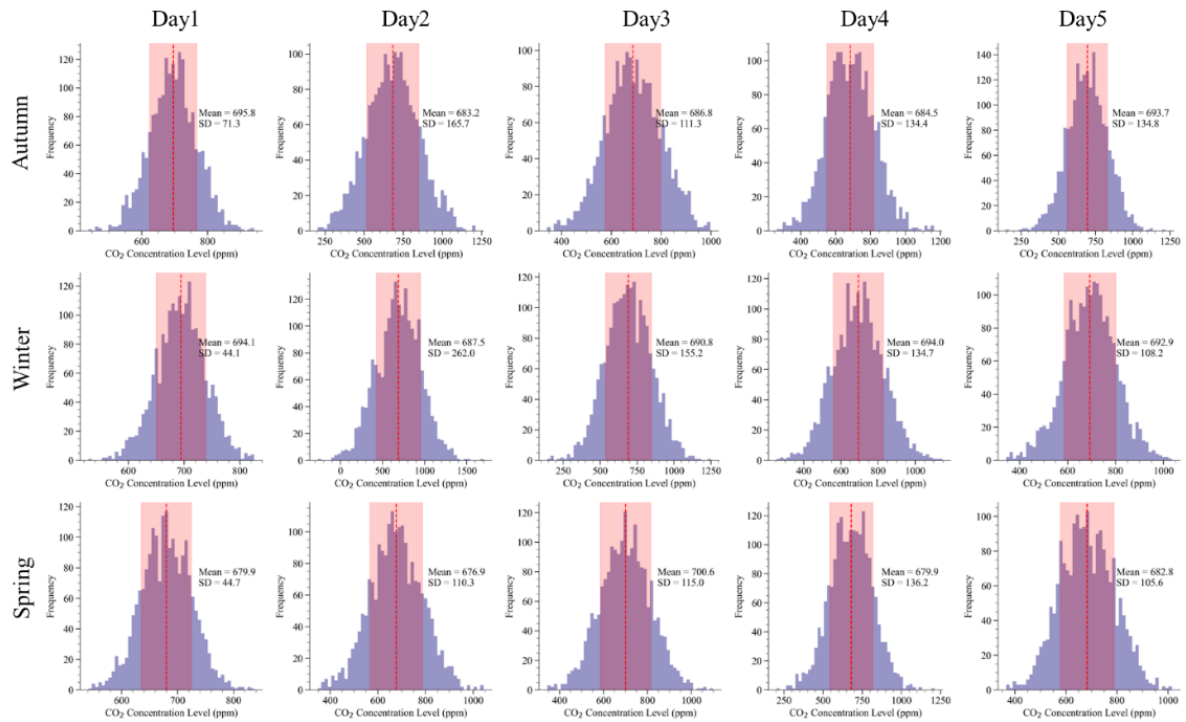
Figure A 3 The selected daily steady-state CO_2 threshold evaluated for Classroom 1 to achieve minimum ECAi requirement
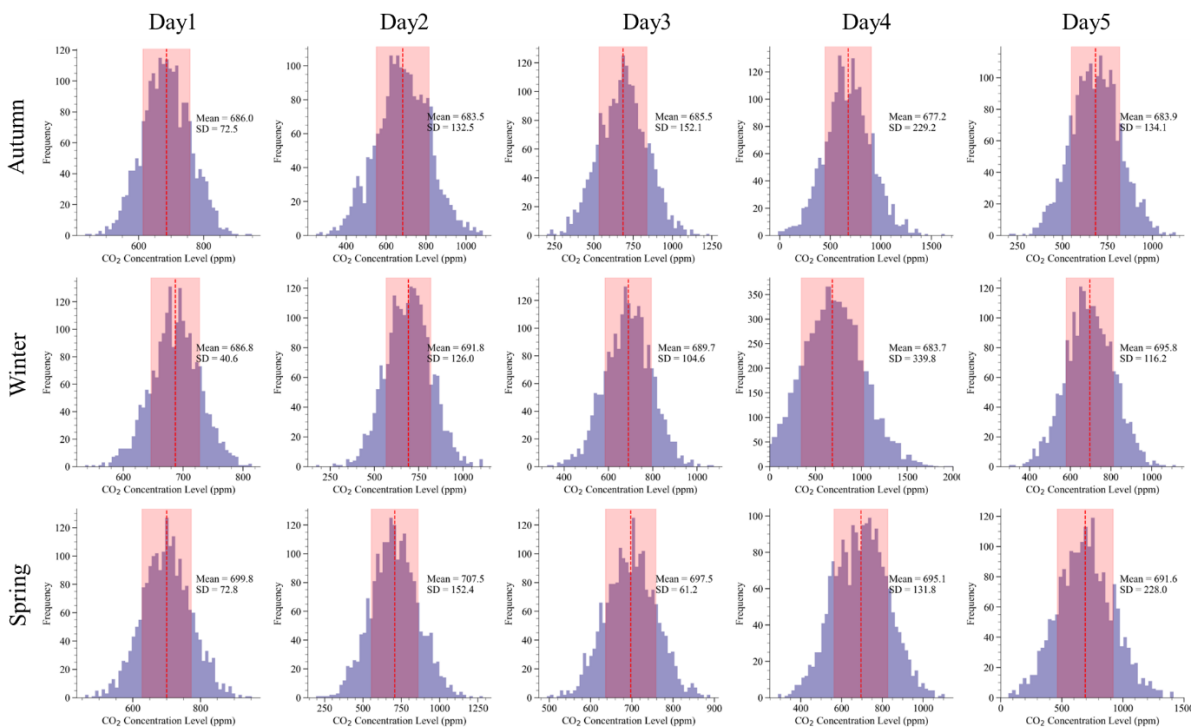
Figure A 4 The selected daily steady-state CO_2 threshold evaluated for Classroom 2 to achieve minimum ECAi requirement

References

[1] L. Morawska *et al.*, "How can airborne transmission of COVID-19 indoors be minimised?," *Environment international,* vol. 142, p. 105832, 2020.

[2] K. A. Prather, C. C. Wang, and R. T. Schooley, "Reducing transmission of SARS-CoV-2," *Science,* vol. 368, no. 6498, pp. 1422-1424, 2020.

[3] M. Klompas, M. A. Baker, and C. Rhee, "Airborne transmission of SARS-CoV-2: theoretical considerations and available evidence," *Jama,* vol. 324, no. 5, pp. 441-442, 2020.

[4] S. Asadi, N. Bouvier, A. S. Wexler, and W. D. Ristenpart, "The coronavirus pandemic and aerosols: Does COVID-19 transmit via expiratory particles?,"   vol. 54, ed: Taylor & Francis, 2020, pp. 635-638.

[5] T. Lipinski, D. Ahmad, N. Serey, and H. Jouhara, "Review of ventilation strategies to reduce the risk of disease transmission in high occupancy buildings," *International Journal of Thermofluids,* vol. 7, p. 100045, 2020.

[6] K. Azuma, U. Yanagi, N. Kagi, H. Kim, M. Ogata, and M. Hayashi, "Environmental factors involved in SARS-CoV-2 transmission: effect and role of indoor environmental quality in the strategy for COVID-19 infection control," *Environmental health and preventive medicine,* vol. 25, pp. 1-16, 2020.

[7] Y. Zhang, F. K. P. Hui, C. Duffield, and A. M. Saeed, "A review of facilities management interventions to mitigate respiratory infections in existing buildings," *Building and Environment,* vol. 221, p. 109347, 2022.

[8] L. O. Gostin and L. F. Wiley, "Governmental public health powers during the COVID-19 pandemic: stay-at-home orders, business closures, and travel restrictions," *Jama,* vol. 323, no. 21, pp. 2137-2138, 2020.

[9] G. Egorov, R. Enikolopov, A. Makarin, and M. Petrova, "Divided we stay home: Social distancing and ethnic diversity," *Journal of Public Economics,* vol. 194, p. 104328, 2021.

[10] K. B. Habersaat *et al.*, "Ten considerations for effectively managing the COVID-19 transition," *Nature human behaviour,* vol. 4, no. 7, pp. 677-687, 2020.

[11] R. C. Khanna, M. V. Cicinelli, S. S. Gilbert, S. G. Honavar, and G. V. Murthy, "COVID-19 pandemic: Lessons learned and future directions," *Indian journal of ophthalmology,* vol. 68, no. 5, pp. 703-710, 2020.

[12] J. Drury, M. B. Rogers, T. M. Marteau, L. Yardley, S. Reicher, and C. Stott, "Re-opening live events and large venues after Covid-19 'lockdown': Behavioural risks and their mitigations," *Safety Science,* vol. 139, p. 105243, 2021.

[13] B. Pavilonis, A. M. Ierardi, L. Levine, F. Mirer, and E. A. Kelvin, "Estimating aerosol transmission risk of SARS-CoV-2 in New York City public schools during reopening," *Environmental Research,* vol. 195, p. 110805, 2021.

[14] P. J. Bueno de Mesquita, W. W. Delp, W. R. Chan, W. P. Bahnfleth, and B. C. Singer, "Control of airborne infectious disease in buildings: Evidence and research priorities," *Indoor Air,* vol. 32, no. 1, p. e12965, 2022.

[15] A. Mikszewski, L. Stabile, G. Buonanno, and L. Morawska, "The airborne contagiousness of respiratory viruses: a comparative analysis and implications for mitigation," *Geoscience Frontiers,* vol. 13, no. 6, p. 101285, 2022.

[16] Z. Peng *et al.*, "Practical indicators for risk of airborne transmission in shared indoor environments and their application to COVID-19 outbreaks," *Environmental science & technology,* vol. 56, no. 2, pp. 1125-

1137, 2022.

[17] C. C. Wang *et al.*, "Airborne transmission of respiratory viruses," *Science,* vol. 373, no. 6558, p. eabd9149, 2021.

[18] M. M. Weiss, P. D. Weiss, D. E. Weiss, and J. B. Weiss, "Disrupting the transmission of influenza a: face masks and ultraviolet light as control measures," *American Journal of Public Health,* vol. 97, no. Supplement_1, pp. S32-S37, 2007.

[19] A. M. Elsaid, H. A. Mohamed, G. B. Abdelaziz, and M. S. Ahmed, "A critical review of heating, ventilation, and air conditioning (HVAC) systems within the context of a global SARS-CoV-2 epidemic," *Process Safety and Environmental Protection,* vol. 155, pp. 230-261, 2021.

[20] A. A. Aliabadi, S. N. Rogak, K. H. Bartlett, and S. I. Green, "Preventing airborne disease transmission: review of methods for ventilation design in health care facilities," *Advances in preventive medicine,* vol. 2011, no. 1, p. 124064, 2011.

[21] N. Izadyar and W. Miller, "Ventilation strategies and design impacts on indoor airborne transmission: A review," *Building and Environment,* vol. 218, p. 109158, 2022.

[22] A. M. Elsaid and M. S. Ahmed, "Indoor air quality strategies for air-conditioning and ventilation systems with the spread of the global coronavirus (COVID-19) epidemic: Improvements and recommendations," *Environmental Research,* vol. 199, p. 111314, 2021.

[23] Z. Alqarni, Y. Rezgui, I. Petri, and A. Ghoroghi, "Viral infection transmission and indoor air quality: A systematic review," *Science of The Total Environment,* p. 171308, 2024.

[24] S. J. Emmerich, "Validation of multizone IAQ modeling of residential-scale buildings: a review," *Transactions-American Society of Heating Refrigerating and Air Conditioning Engineers,* vol. 107, no. 2, pp. 619-628, 2001.

[25] J. Guo, J. Liu, D. Tu, J. Zhang, J. Xu, and P. Xue, "Multizone modeling of pressure difference control analyses for an infectious disease hospital," *Building and Environment,* vol. 206, p. 108341, 2021.

[26] G. Mavromatidis, K. Orehounig, and J. Carmeliet, "A review of uncertainty characterisation approaches for the optimal design of distributed energy systems," *Renewable and Sustainable Energy Reviews,* vol. 88, pp. 258-277, 2018.

[27] N. Ma, D. Aviv, H. Guo, and W. W. Braham, "Measuring the right factors: A review of variables and models for thermal comfort and indoor air quality," *Renewable and Sustainable Energy Reviews,* vol. 135, p. 110436, 2021.

[28] F. W. Lipfert and R. E. Wyzga, "Air pollution and mortality: issues and uncertainties," *Journal of the Air & Waste Management Association,* vol. 45, no. 12, pp. 949-966, 1995.

[29] G. Li, J. Xiong, R. Tang, S. Sun, and C. Wang, "In-situ sensor calibration for building HVAC systems with limited information using general regression improved Bayesian inference," *Building and Environment,* vol. 234, p. 110161, 2023.

[30] C. A. Faulkner, J. E. Castellini Jr, W. Zuo, and M. D. Sohn, "Comprehensive analysis of model parameter uncertainty influence on evaluation of HVAC operation to mitigate indoor virus: A case study for an office building in a cold and dry climate," *Building and Environment,* vol. 238, p. 110314, 2023.

[31] A.-T. Nguyen, S. Reiter, and P. Rigo, "A review on simulation-based optimization methods applied to building performance analysis," *Applied energy,* vol. 113, pp. 1043-1058, 2014.

[32] Y. Chen, J. Wen, O. Pradhan, L. J. Lo, and T. Wu, "Using discrete Bayesian networks for diagnosing and isolating cross-level faults in HVAC systems," *Applied Energy,* vol. 327, p. 120050, 2022.

[33] N. R. Kristensen, H. Madsen, and S. B. Jørgensen, "A method for systematic improvement of stochastic

grey-box models," *Computers & chemical engineering,* vol. 28, no. 8, pp. 1431-1449, 2004.

[34]   X. Yu, L. Georges, and L. Imsland, "Data pre-processing and optimization techniques for stochastic and deterministic low-order grey-box models of residential buildings," *Energy and Buildings,* vol. 236, p. 110775, 2021.

[35]   U. Von Toussaint, "Bayesian inference in physics," *Reviews of Modern Physics,* vol. 83, no. 3, p. 943, 2011.

[36]   G. E. Box and G. C. Tiao, *Bayesian inference in statistical analysis*. John Wiley & Sons, 2011.

[37]   J. Axley, "Multizone airflow modeling in buildings: History and theory," *HVAC&R Research,* vol. 13, no. 6, pp. 907-928, 2007.

[38]   H. E. Feustel, "COMIS—an international multizone air-flow and contaminant transport model," *Energy and Buildings,* vol. 30, no. 1, pp. 3-18, 1999.

[39]   C. H. Lozinsky and M. F. Touchie, "Inter-zonal airflow in multi-unit residential buildings: A review of the magnitude and interaction of driving forces, measurement techniques and magnitudes, and its impact on building performance," *Indoor Air,* vol. 30, no. 6, pp. 1083-1108, 2020.

[40]   H. E. Feustel and M. H. Sherman, "A simplified model for predicting air flow in multizone structures," *Energy and Buildings,* vol. 13, no. 3, pp. 217-230, 1989.

[41]   J. E. Edinger, D. K. Brady, and J. C. Geyer, "Heat exchange and transport in the environment," 1974.

[42]   J. P. Cockroft, "Heat transfer and air flow in buildings," University of Glasgow, 1979.

[43]   G. N. Walton, "Airflow network models for element-based building airflow modeling," 1989.

[44]   J. Axley, "Multi-zone IAQ model: The development of models for the prediction of indoor air quality in buildings," *Building Research and Practice,* vol. 17, no. 4, pp. 228-235, 1989.

[45]   A. K. Persily, "Multizone Modeling of Three Residential Indoor Air Quality Control Options," 1996.

[46]   G. Walton, "CONTAM96 User Manual, Report NISTIR 6056," *National Institute for Standards and Technology, Gaithersburg, MD,* 1997.

[47]   G. N. Walton, "CONTAM93 user manual," National Inst. of Standards and Technology (BFRL), Gaithersburg, MD (United …, 1994.

[48]   P. Tuomaala and J. Rahola, "Combined air flow and thermal simulation of buildings," *Building and Environment,* vol. 30, no. 2, pp. 255-265, 1995/04/01/ 1995, doi: https://doi.org/10.1016/0360-1323(94)00044-S.

[49]   P. Smith Schneider, J.-J. Roux, and J. Brau, "Strategies for solving the air flow—Thermal problem in multiroom buildings," *Building and Environment,* vol. 30, no. 2, pp. 277-286, 1995/04/01/ 1995, doi: https://doi.org/10.1016/0360-1323(94)00042-Q.

[50]   L. L. Wang, W. S. Dols, and Q. Chen, "Using CFD capabilities of CONTAM 3.0 for simulating airflow and contaminant transport in and around buildings," *Hvac&R Research,* vol. 16, no. 6, pp. 749-763, 2010.

[51]   L. Wang and N. H. Wong, "Coupled simulations for naturally ventilated rooms between building simulation (BS) and computational fluid dynamics (CFD) for better prediction of indoor thermal environment," *Building and Environment,* vol. 44, no. 1, pp. 95-112, 2009/01/01/ 2009, doi: https://doi.org/10.1016/j.buildenv.2008.01.015.

[52]   J. Richmond-Bryant, A. D. Eisner, L. A. Brixey, and R. W. Wiener, "Short-term dispersion of indoor aerosols: can it be assumed the room is well mixed?," *Building and Environment,* vol. 41, no. 2, pp. 156-163, 2006/02/01/ 2006, doi: https://doi.org/10.1016/j.buildenv.2004.12.016.

[53]   S. T. Parker, D. M. Lorenzetti, and M. D. Sohn, "Implementing state-space methods for multizone contaminant transport," *Building and Environment,* vol. 71, pp. 131-139, 2014/01/01/ 2014, doi:

https://doi.org/10.1016/j.buildenv.2013.09.021.

[54]   L. L. Wang and Q. Chen, "Evaluation of some assumptions used in multizone airflow network models," *Building and Environment,* vol. 43, no. 10, pp. 1671-1677, 2008.

[55]   Q. Chen *et al.*, "Ventilation performance prediction for buildings: Model assessment," *Building and Environment,* vol. 45, no. 2, pp. 295-303, 2010/02/01/ 2010, doi: https://doi.org/10.1016/j.buildenv.2009.06.008.

[56]   B. P. P. Barbosa and N. d. C. L. Brum, "Validation and assessment of the CFD-0 module of CONTAM software for airborne contaminant transport simulation in laboratory and hospital applications," *Building and Environment,* vol. 142, pp. 139-152, 2018/09/01/ 2018, doi: https://doi.org/10.1016/j.buildenv.2018.06.013.

[57]   F. Haghighat and A. C. Megri, "A comprehensive validation of two airflow models—COMIS and CONTAM," *Indoor air,* vol. 6, no. 4, pp. 278-288, 1996.

[58]   K. Verijkazemi, N. Mansouri, F. Moattar, and S. M. Khezri, "Evaluation of indoor PM distribution by CONTAM airflow model and real time measuring: Model description and validation," *Avicenna Journal of Environmental Health Engineering,* vol. 5, no. 1, pp. 42-49, 2018.

[59]   A. Musser and A. K. Persily, "Multizone modeling approaches to contaminant-based design," *Transactions-American Society of Heating Refrigerating and Air Conditioning Engineers,* vol. 108, no. 2, pp. 803-810, 2002.

[60]   S. Cui, M. Cohen, P. Stabat, and D. Marchio, "CO2 tracer gas concentration decay method for measuring air change rate," *Building and Environment,* vol. 84, pp. 162-169, 2015/01/01/ 2015, doi: https://doi.org/10.1016/j.buildenv.2014.11.007.

[61]   L. F. Pease *et al.*, "Investigation of potential aerosol transmission and infectivity of SARS-CoV-2 through central ventilation systems," *Building and Environment,* vol. 197, p. 107633, 2021/06/15/ 2021, doi: https://doi.org/10.1016/j.buildenv.2021.107633.

[62]   L. C. Ng, A. Musser, A. K. Persily, and S. J. Emmerich, "Multizone airflow models for calculating infiltration rates in commercial reference buildings," *Energy and Buildings,* vol. 58, pp. 11-18, 2013.

[63]   C. Balocco and L. Leoncini, "Energy cost for effective ventilation and air quality for healthy buildings: Plant proposals for a historic building school reopening in the covid-19 era," *Sustainability,* vol. 12, no. 20, p. 8737, 2020.

[64]   Q. Zhen *et al.*, "A Markov chain-based approach for assessing respiratory infection risk in a multi-zone office building," *Journal of Building Engineering,* vol. 90, p. 109328, 2024.

[65]   Y. Chang, Z. Ai, J. Ye, and G. Ma, "A cost-effectiveness assessment of the operational parameters of central HVAC systems during pandemics," in *Building Simulation*, 2023, vol. 16, no. 5: Springer, pp. 667-682.

[66]   B. Poirier, G. Guyot, M. Woloszyn, H. Geoffroy, M. Ondarts, and E. Gonze, "Development of an assessment methodology for IAQ ventilation performance in residential buildings: An investigation of relevant performance indicators," *Journal of Building Engineering,* vol. 43, p. 103140, 2021.

[67]   R. Becker, I. Goldberger, and M. Paciuk, "Improving energy performance of school buildings while ensuring indoor air quality ventilation," *Building and Environment,* vol. 42, no. 9, pp. 3261-3276, 2007.

[68]   Y. Liu *et al.*, "Aerodynamic analysis of SARS-CoV-2 in two Wuhan hospitals," *Nature,* Article vol. 582, no. 7813, pp. 557-560, 2020, doi: 10.1038/s41586-020-2271-3.

[69]   H. Qian, Y. Li, W. Seto, P. Ching, W. Ching, and H. Sun, "Natural ventilation for reducing airborne infection in hospitals," *Building and Environment,* vol. 45, no. 3, pp. 559-565, 2010.

[70]   C. A. Faulkner, J. E. Castellini Jr, W. Zuo, D. M. Lorenzetti, and M. D. Sohn, "Investigation of HVAC operation strategies for office buildings during COVID-19 pandemic," *Building and Environment,* vol. 207, p. 108519, 2022.

[71]   T. Ben-David, S. Wang, A. Rackes, and M. S. Waring, "Measuring the efficacy of HVAC particle filtration over a range of ventilation rates in an office building," *Building and Environment,* vol. 144, pp. 648-656, 2018.

[72]   M. López-García, M. F. King, and C. J. Noakes, "A multicompartment SIS stochastic model with zonal ventilation for the spread of nosocomial infections: Detection, outbreak management, and infection control," *Risk Analysis,* vol. 39, no. 8, pp. 1825-1842, 2019.

[73]   C. H. Lozinsky and M. F. Touchie, "Inter-zonal airflow in multi-unit residential buildings: A review of the magnitude and interaction of driving forces, measurement techniques and magnitudes, and its impact on building performance," *Indoor Air,* vol. 30, no. 6, pp. 1083-1108, 2020, doi: https://doi.org/10.1111/ina.12712.

[74]   A. J. Aguilar, M. L. de la Hoz-Torres, M. D. Martínez-Aires, and D. P. Ruiz, "Monitoring and assessment of indoor environmental conditions after the implementation of COVID-19-based ventilation strategies in an educational building in southern Spain," *Sensors,* vol. 21, no. 21, p. 7223, 2021.

[75]   S. Altomonte *et al.*, "Ten questions concerning well-being in the built environment," *Building and Environment,* vol. 180, p. 106949, 2020.

[76]   D. R. M. Smith *et al.*, "Predicting consequences of COVID-19 control measure de-escalation on nosocomial transmission and mortality: a modelling study in a French rehabilitation hospital," *Journal of Hospital Infection,* vol. 147, pp. 47-55, 2024/05/01/ 2024, doi: https://doi.org/10.1016/j.jhin.2024.02.020.

[77]   C. Xu, W. Liu, X. Luo, X. Huang, and P. V. Nielsen, "Prediction and control of aerosol transmission of SARS-CoV-2 in ventilated context: from source to receptor," *Sustainable Cities and Society,* vol. 76, p. 103416, 2022/01/01/ 2022, doi: https://doi.org/10.1016/j.scs.2021.103416.

[78]   Q. Qiao, C. Cheung, A. Yunusa-Kaltungo, P. Manu, R. Cao, and Z. Yuan, "An interactive agent-based modelling framework for assessing COVID-19 transmission risk on construction site," *Safety Science,* vol. 168, p. 106312, 2023/12/01/ 2023, doi: https://doi.org/10.1016/j.ssci.2023.106312.

[79]   M. Al-Mustanjid *et al.*, "Systems biology models to identify the influence of SARS-CoV-2 infections to the progression of human autoimmune diseases," *Informatics in Medicine Unlocked,* vol. 32, p. 101003, 2022/01/01/ 2022, doi: https://doi.org/10.1016/j.imu.2022.101003.

[80]   K.-W. Shi, Y.-H. Huang, H. Quon, Z.-L. Ou-Yang, C. Wang, and S. C. Jiang, "Quantifying the risk of indoor drainage system in multi-unit apartment building as a transmission route of SARS-CoV-2," *Science of The Total Environment,* vol. 762, p. 143056, 2021/03/25/ 2021, doi: https://doi.org/10.1016/j.scitotenv.2020.143056.

[81]   E. Ransome *et al.*, "Evaluating the transmission risk of SARS-CoV-2 from sewage pollution," *Science of The Total Environment,* vol. 858, p. 159161, 2023/02/01/ 2023, doi: https://doi.org/10.1016/j.scitotenv.2022.159161.

[82]   E. C. Riley, G. Murphy, and R. L. Riley, "AIRBORNE SPREAD OF MEASLES IN A SUBURBAN ELEMENTARY SCHOOL," *American Journal of Epidemiology,* vol. 107, no. 5, pp. 421-432, 1978, doi: 10.1093/oxfordjournals.aje.a112560.

[83]   A. Aganovic, G. Cao, J. Kurnitski, and P. Wargocki, "New dose-response model and SARS-CoV-2 quanta emission rates for calculating the long-range airborne infection risk," *Building and Environment,* vol.

228, p. 109924, 2023/01/15/ 2023, doi: https://doi.org/10.1016/j.buildenv.2022.109924.

[84] B. Jones, C. Iddon, and M. Sherman, "Quantifying quanta: determining emission rates from clinical data," *Indoor Environments,* p. 100025, 2024/06/21/ 2024, doi: https://doi.org/10.1016/j.indenv.2024.100025.

[85] B. E. Cummings, C. N. Haas, L. J. Lo, C. M. Sales, J. Fox, and M. S. Waring, "Airborne disease transmission risks on public transit buses: Impacts of ridership, duration, and mechanical filtration using a relative risk metric," *Building and Environment,* vol. 255, p. 111303, 2024/05/01/ 2024, doi: https://doi.org/10.1016/j.buildenv.2024.111303.

[86] G. A. Somsen, M. M. Winter, I. I. Tulevski, S. Kooij, and D. Bonn, "Risk of aerosol transmission of SARS-CoV-2 in a clinical cardiology setting," *Building and Environment,* vol. 220, p. 109254, 2022/07/15/ 2022, doi: https://doi.org/10.1016/j.buildenv.2022.109254.

[87] H. Dai and B. Zhao, "Association of the infection probability of COVID-19 with ventilation rates in confined spaces," *Building Simulation,* Article vol. 13, no. 6, pp. 1321-1327, 2020, doi: 10.1007/s12273-020-0703-5.

[88] J. Shen, M. Kong, B. Dong, M. J. Birnkrant, and J. Zhang, "A systematic approach to estimating the effectiveness of multi-scale IAQ strategies for reducing the risk of airborne infection of SARS-CoV-2," *Building and Environment,* vol. 200, p. 107926, 2021/08/01/ 2021, doi: https://doi.org/10.1016/j.buildenv.2021.107926.

[89] B. P. P. Barbosa and N. de Carvalho Lobo Brum, "Ventilation mode performance against airborne respiratory infections in small office spaces: limits and rational improvements for Covid-19," *Journal of the Brazilian Society of Mechanical Sciences and Engineering,* vol. 43, no. 6, p. 316, 2021.

[90] Z. Peng *et al.*, "Practical indicators for risk of airborne transmission in shared indoor environments and their application to covid-19 outbreaks," *Environmental science & technology,* vol. 56, no. 2, pp. 1125-1137, 2022.

[91] W. Bahnfleth, J. DeGraw, and O. R. T. N. Oak Ridge National Lab, "Reducing Airborne Infectious Aerosol Exposure," *ASHRAE Transactions,* vol. 63, no. 5, 2021.

[92] S. H. Taylor and C. M. Scofield, "Improving IEQ to reduce transmission of airborne pathogens in cold climates," *ASHRAE Journal,* vol. 62, no. 9, pp. 30-47, 2020.

[93] T. A. Yates *et al.*, "The transmission of Mycobacterium tuberculosis in high burden settings," *The Lancet Infectious Diseases,* Review vol. 16, no. 2, pp. 227-238, 2016, doi: 10.1016/S1473-3099(15)00499-5.

[94] U. Igwe, O. J. Okolie, S. U. Ismail, and E. Adukwu, "Effectiveness of Infection Prevention and Control Interventions in Healthcare Facilities in Africa: A Systematic Review," *American Journal of Infection Control,* 2024/06/12/ 2024, doi: https://doi.org/10.1016/j.ajic.2024.06.004.

[95] P. Shrestha, J. W. DeGraw, M. Zhang, and X. Liu, "Multizonal modeling of SARS-CoV-2 aerosol dispersion in a virtual office building," *Building and Environment,* vol. 206, p. 108347, 2021/12/01/ 2021, doi: https://doi.org/10.1016/j.buildenv.2021.108347.

[96] M. A. Waltenburg *et al.*, "Update: COVID-19 among workers in meat and poultry processing facilities — United States, April–May 2020," *Morbidity and Mortality Weekly Report,* Article vol. 69, no. 27, pp. 887-892, 2020, doi: 10.15585/MMWR.MM6927E2.

[97] L. F. Moriarty *et al.*, "Public health responses to covid-19 outbreaks on cruise ships - Worldwide, February-March 2020," *Morbidity and Mortality Weekly Report,* Review vol. 69, no. 12, pp. 347-352, 2020, doi: 10.15585/MMWR.MM6912E3.

[98] REHVA, "REHVA Covid-19 Guidance Document," 2020.

[99]   M. Guo, P. Xu, T. Xiao, R. He, M. Dai, and S. L. Miller, "Review and comparison of HVAC operation guidelines in different countries during the COVID-19 pandemic," *Building and Environment,* vol. 187, p. 107368, 2021/01/01/ 2021, doi: https://doi.org/10.1016/j.buildenv.2020.107368.

[100]   M. Esrafilian-Najafabadi and F. Haghighat, "Occupancy-based HVAC control systems in buildings: A state-of-the-art review," *Building and Environment,* vol. 197, p. 107810, 2021/06/15/ 2021, doi: https://doi.org/10.1016/j.buildenv.2021.107810.

[101]   W. Jung and F. Jazizadeh, "Human-in-the-loop HVAC operations: A quantitative review on occupancy, comfort, and energy-efficiency dimensions," *Applied Energy,* vol. 239, pp. 1471-1508, 2019.

[102]   S. He, Y. Peng, and K. Sun, "SEIR modeling of the COVID-19 and its dynamics," *Nonlinear Dynamics,* Article vol. 101, no. 3, pp. 1667-1680, 2020, doi: 10.1007/s11071-020-05743-y.

[103]   Y. Pan, D. Zhang, P. Yang, L. L. M. Poon, and Q. Wang, "Viral load of SARS-CoV-2 in clinical samples," *The Lancet Infectious Diseases,* Letter vol. 20, no. 4, pp. 411-412, 2020, doi: 10.1016/S1473-3099(20)30113-4.

[104]   M.-E. Dubuis *et al.*, "High and low flowrate sampling of airborne influenza in hospital rooms during three outbreaks," *Journal of Aerosol Science,* vol. 158, p. 105824, 2021.

[105]   S. Rayegan *et al.*, "A review on indoor airborne transmission of COVID-19– modelling and mitigation approaches," *Journal of Building Engineering,* vol. 64, p. 105599, 2023/04/01/ 2023, doi: https://doi.org/10.1016/j.jobe.2022.105599.

[106]   N. Dias, C. Jayakody, D. Amaratunga, C. Abenayake, and A. Jayasinghe, "Health resilient cities in a post Covid world," in *COVID 19: Impact, Mitigation, Opportunities and Building Resilience: From Adversity to Serendipity*: National Science Foundation of Sri Lanka, 2021, pp. 621-635.

[107]   G. Guyot, S. Sayah, S. Guernouti, and A. Mélois, "Role of ventilation on the transmission of viruses in buildings, from a single zone to a multizone approach," *Indoor Air,* vol. 32, no. 8, p. e13097, 2022, doi: https://doi.org/10.1111/ina.13097.

[108]   A. K. Persily, "Field measurement of ventilation rates," *Indoor Air,* vol. 26, no. 1, pp. 97-111, 2016.

[109]   M. H. Sherman, "Tracer-gas techniques for measuring ventilation in a single zone," *Building and environment,* vol. 25, no. 4, pp. 365-374, 1990.

[110]   G. Remion, B. Moujalled, and M. El Mankibi, "Review of tracer gas-based methods for the characterization of natural ventilation performance: Comparative analysis of their accuracy," *Building and Environment,* vol. 160, p. 106180, 2019.

[111]   M. Sherman, "On the estimation of multizone ventilation rates from tracer gas measurements," *Building and Environment,* vol. 24, no. 4, pp. 355-362, 1989.

[112]   M. Santamouris and P. Wouters, "Building ventilation: the state of the art," 2006.

[113]   D. W. Etheridge and M. Sandberg, *Building ventilation: theory and measurement*. John Wiley & Sons Chichester, UK, 1996.

[114]   A. Kabirikopaei and J. Lau, "Uncertainty analysis of various CO2-Based tracer-gas methods for estimating seasonal ventilation rates in classrooms with different mechanical systems," *Building and Environment,* vol. 179, p. 107003, 2020/07/15/ 2020, doi: https://doi.org/10.1016/j.buildenv.2020.107003.

[115]   W. W. Nazaroff, "Residential air-change rates: A critical review," *Indoor Air,* vol. 31, no. 2, pp. 282-313, 2021.

[116]   K. P. Andrew, "Tracer gas techniques for studying building air exchange," ed: , National Institute of Standards and Technology, Gaithersburg, MD, 1988.

[117] K. Cheong, "Airflow measurements for balancing of air distribution system—tracer-gas technique as an alternative?," *Building and Environment,* vol. 36, no. 8, pp. 955-964, 2001.

[118] P. W. Grieve, "Measuring ventilation using tracer gases," 1989.

[119] L. Shao and S. B. Riffat, "Tracer-gas mixing with air: Effect of tracer species," *Applied Energy,* vol. 49, no. 2, pp. 197-211, 1994/01/01/ 1994, doi: https://doi.org/10.1016/0306-2619(94)90037-X.

[120] L. D. Harvey, "A guide to global warming potentials (GWPs)," *Energy Policy,* vol. 21, no. 1, pp. 24-34, 1993.

[121] M. Bivolarova, J. Ondráček, A. Melikov, and V. Ždímal, "A comparison between tracer gas and aerosol particles distribution indoors: The impact of ventilation rate, interaction of airflows, and presence of objects," *Indoor air,* vol. 27, no. 6, pp. 1201-1212, 2017.

[122] N. Edouard, J. Mosquera, H. J. C. van Dooren, L. B. Mendes, and N. W. M. Ogink, "Comparison of CO2- and SF6- based tracer gas methods for the estimation of ventilation rates in a naturally ventilated dairy barn," *Biosystems Engineering,* vol. 149, pp. 11-23, 2016/09/01/ 2016, doi: https://doi.org/10.1016/j.biosystemseng.2016.06.001.

[123] T. Zhang, W. Zhang, R. Yang, Y. Liu, and M. Jafari, "CO2 capture and storage monitoring based on remote sensing techniques: A review," *Journal of Cleaner Production,* vol. 281, p. 124409, 2021.

[124] C. Ghazi and J. Marshall, "A CO2 tracer-gas method for local air leakage detection and characterization," *Flow Measurement and Instrumentation,* vol. 38, pp. 72-81, 2014.

[125] J. L. Verkerke, D. J. Williams, and E. Thoma, "Remote sensing of CO2 leakage from geologic sequestration projects," *International Journal of Applied Earth Observation and Geoinformation,* vol. 31, pp. 67-77, 2014.

[126] A. Keats, E. Yee, and F.-S. Lien, "Bayesian inference for source determination with applications to a complex urban environment," *Atmospheric environment,* vol. 41, no. 3, pp. 465-479, 2007.

[127] W. Tian *et al.*, "A review of uncertainty analysis in building energy assessment," *Renewable and Sustainable Energy Reviews,* vol. 93, pp. 285-301, 2018.

[128] A. Booth, R. Choudhary, and D. Spiegelhalter, "A hierarchical Bayesian framework for calibrating micro-level models with macro-level data," *Journal of Building Performance Simulation,* vol. 6, no. 4, pp. 293-318, 2013.

[129] X. Li and F. Xue, "Bayesian inversion of inflow direction and speed in urban dispersion simulations," *Building and Environment,* vol. 144, pp. 555-564, 2018.

[130] A. Gelman, J. B. Carlin, H. S. Stern, D. B. Dunson, A. Vehtari, and D. B. Rubin, *Bayesian data analysis*, Third edition ed. Boca Raton: CRC Press, 2014. [Online]. Available: http://public.ebookcentral.proquest.com/choice/publicfullrecord.aspx?p=1438153.

[131] J. K. Kruschke, *Doing Bayesian data analysis : a tutorial with R and BUGS*. Burlington, MA: Academic Press (in English), 2011.

[132] M. Richey, "The evolution of Markov chain Monte Carlo methods," *The American Mathematical Monthly,* vol. 117, no. 5, pp. 383-413, 2010.

[133] S. Chib, "Markov chain Monte Carlo methods: computation and inference," *Handbook of econometrics,* vol. 5, pp. 3569-3649, 2001.

[134] D. Luengo, L. Martino, M. Bugallo, V. Elvira, and S. Särkkä, "A survey of Monte Carlo methods for parameter estimation," *EURASIP Journal on Advances in Signal Processing,* vol. 2020, pp. 1-62, 2020.

[135] J. Sokol, C. C. Davila, and C. F. Reinhart, "Validation of a Bayesian-based method for defining residential archetypes in urban building energy models," *Energy and Buildings,* vol. 134, pp. 11-24, 2017.

[136] T. Hong, Y. Chen, X. Luo, N. Luo, and S. H. Lee, "Ten questions on urban building energy modeling," *Building and Environment,* vol. 168, p. 106508, 2020.

[137] Y. Q. Ang, Z. M. Berzolla, and C. F. Reinhart, "From concept to application: A review of use cases in urban building energy modeling," *Applied Energy,* vol. 279, p. 115738, 2020.

[138] Y. Heo, R. Choudhary, and G. A. Augenbroe, "Calibration of building energy models for retrofit analysis under uncertainty," *Energy and Buildings,* vol. 47, pp. 550-560, 2012.

[139] J. Kim, S. Schiavon, and G. Brager, "Personal comfort models–A new paradigm in thermal comfort for occupant-centric environmental control," *Building and Environment,* vol. 132, pp. 114-124, 2018.

[140] R. E. Hedegaard, M. H. Kristensen, T. H. Pedersen, A. Brun, and S. Petersen, "Bottom-up modelling methodology for urban-scale analysis of residential space heating demand response," *Applied Energy,* vol. 242, pp. 181-204, 2019.

[141] Y. Zhong, A. D. Knefaty, G. Chen, J. Yao, and R. Zheng, "Forecast of air-conditioning duration in office buildings in summer using machine learning and Bayesian theories," *Journal of Building Engineering,* vol. 61, p. 105218, 2022.

[142] T. Zhao, J. Li, P. Wang, S. Yoon, and J. Wang, "Improvement of virtual in-situ calibration in air handling unit using data preprocessing based on Gaussian mixture model," *Energy and Buildings,* vol. 256, p. 111735, 2022.

[143] Z. Wang and T. Hong, "Learning occupants' indoor comfort temperature through a Bayesian inference approach for office buildings in United States," *Renewable and Sustainable Energy Reviews,* vol. 119, p. 109593, 2020.

[144] D. Hou, I. Hassan, and L. Wang, "Review on building energy model calibration by Bayesian inference," *Renewable and Sustainable Energy Reviews,* vol. 143, p. 110930, 2021.

[145] H. Lim and Z. J. Zhai, "Influences of energy data on Bayesian calibration of building energy model," *Applied Energy,* vol. 231, pp. 686-698, 2018.

[146] H. Lim and Z. J. Zhai, "Comprehensive evaluation of the influence of meta-models on Bayesian calibration," *Energy and Buildings,* vol. 155, pp. 66-75, 2017.

[147] F. Wang, X. Zhou, J. Huang, H. Wang, H. Kikumoto, and C. Deng, "Natural gas leakage estimation in underground utility tunnels using Bayesian inference based on flow fields with gas jet disturbance," *Process Safety and Environmental Protection,* vol. 165, pp. 532-544, 2022.

[148] F. Wang, X. Zhou, and H. Kikumoto, "Improvement of optimization methods in indoor time-variant source parameters estimation combining unsteady adjoint equations and flow field information," *Building and Environment,* vol. 226, p. 109710, 2022.

[149] F. Septier, P. Armand, and C. Duchenne, "A bayesian inference procedure based on inverse dispersion modelling for source term estimation in built-up environments," *Atmospheric Environment,* vol. 242, p. 117733, 2020.

[150] D. Hou *et al.*, "Development of a Bayesian inference model for assessing ventilation condition based on CO_2 meters in primary schools," *Building Simulation,* vol. 16, no. 1, pp. 133-149, 2023/01/01 2023, doi: 10.1007/s12273-022-0926-8.

[151] H. Rahman and H. Han, "Bayesian estimation of occupancy distribution in a multi-room office building based on CO_2 concentrations," in *Building Simulation*, 2018, vol. 11: Springer, pp. 575-583.

[152] B. Kamiński, "Interval metamodels for the analysis of simulation Input–Output relations," *Simulation Modelling Practice and Theory,* vol. 54, pp. 86-100, 2015.

[153] Y. Lei, S. Zhou, J. Filar, and N. Ye, "Multi-pass Bayesian estimation: a robust Bayesian method,"

Computational Statistics, vol. 39, no. 4, pp. 2183-2216, 2024.

[154]   S. M. Ross, *Introduction to Probability Models, ISE*. Academic press, 2006.

[155]   D. C. Montgomery and G. C. Runger, *Applied statistics and probability for engineers*. John wiley & sons, 2010.

[156]   H. Liu, C. Yang, M. Huang, D. Wang, and C. Yoo, "Modeling of subway indoor air quality using Gaussian process regression," *Journal of hazardous materials,* vol. 359, pp. 266-273, 2018.

[157]   L. Chatzidiakou, D. Mumovic, and A. Summerfield, "Is CO2 a good proxy for indoor air quality in classrooms? Part 1: The interrelationships between thermal conditions, CO2 levels, ventilation rates and selected indoor pollutants," *Building Services Engineering Research and Technology,* vol. 36, no. 2, pp. 129-161, 2015.

[158]   M. Santamouris *et al.*, "Experimental investigation of the air flow and indoor carbon dioxide concentration in classrooms with intermittent natural ventilation," *Energy and Buildings,* vol. 40, no. 10, pp. 1833-1843, 2008.

[159]   M. Pinsky and S. Karlin, *An introduction to stochastic modeling*. Academic press, 2010.

[160]   A. Afram and F. Janabi-Sharifi, "Review of modeling methods for HVAC systems," *Applied thermal engineering,* vol. 67, no. 1-2, pp. 507-519, 2014.

[161]   R. Goodman, *Introduction to stochastic models*. Courier Corporation, 2006.

[162]   T. N. Palmer *et al.*, "Stochastic parametrization and model uncertainty," 2009.

[163]   T. P. Bohlin, *Practical grey-box process identification: theory and applications*. Springer Science & Business Media, 2006.

[164]   Y. Balali, A. Chong, A. Busch, and S. O'Keefe, "Energy modelling and control of building heating and cooling systems with data-driven and hybrid models—A review," *Renewable and Sustainable Energy Reviews,* vol. 183, p. 113496, 2023.

[165]   K. Sharma, Z. Papamitsiou, and M. Giannakos, "Building pipelines for educational data using AI and multimodal analytics: A "grey-box" approach," *British Journal of Educational Technology,* vol. 50, no. 6, pp. 3004-3031, 2019.

[166]   Y. Li, Z. O'Neill, L. Zhang, J. Chen, P. Im, and J. DeGraw, "Grey-box modeling and application for building energy simulations-A critical review," *Renewable and Sustainable Energy Reviews,* vol. 146, p. 111174, 2021.

[167]   O. M. Brastein, D. W. U. Perera, C. Pfeifer, and N.-O. Skeie, "Parameter estimation for grey-box models of building thermal behaviour," *Energy and Buildings,* vol. 169, pp. 58-68, 2018.

[168]   N. R. Kristensen, H. Madsen, and S. B. Jørgensen, "Parameter estimation in stochastic grey-box models," *Automatica,* vol. 40, no. 2, pp. 225-237, 2004.

[169]   F. Haghighat, P. Fazio, and T. Unny, "A predictive stochastic model for indoor air quality," *Building and Environment,* vol. 23, no. 3, pp. 195-201, 1988.

[170]   P. E. Kloeden, E. Platen, P. E. Kloeden, and E. Platen, *Stochastic differential equations*. Springer, 1992.

[171]   M. Macarulla, M. Casals, M. Carnevali, N. Forcada, and M. Gangolells, "Modelling indoor air carbon dioxide concentration using grey-box models," *Building and Environment,* vol. 117, pp. 146-153, 2017.

[172]   M. Macarulla, M. Casals, N. Forcada, M. Gangolells, and A. Giretti, "Estimation of a room ventilation air change rate using a stochastic grey-box modelling approach," *Measurement,* vol. 124, pp. 539-548, 2018/08/01/ 2018, doi: https://doi.org/10.1016/j.measurement.2018.04.029.

[173]   "WHO Coronavirus (COVID-19) dashboard " World Health Organization 2023 data. https://data.who.int/dashboards/covid19/data (accessed Dec 31, 2023).

[174] S. S. Abdool Karim and T. de Oliveira, "New SARS-CoV-2 variants — Clinical, public health, and vaccine implications," *New England Journal of Medicine,* Letter vol. 384, no. 19, pp. 1866-1868, 2021, doi: 10.1056/NEJMc2100362.

[175] J. P. Moore and P. A. Offit, "SARS-CoV-2 Vaccines and the Growing Threat of Viral Variants," *JAMA - Journal of the American Medical Association,* Note vol. 325, no. 9, pp. 821-822, 2021, doi: 10.1001/jama.2021.1114.

[176] R. P. Walensky, H. T. Walke, and A. S. Fauci, "SARS-CoV-2 Variants of Concern in the United States-Challenges and Opportunities," *JAMA - Journal of the American Medical Association,* Note vol. 325, no. 11, pp. 1037-1038, 2021, doi: 10.1001/jama.2021.2294.

[177] P. Rodrigo and C. Hu, "Brazil: Covid-19 Caused One in Three Deaths in the Country So Far This Year - CNN," Article 2021.

[178] S. Menon, "India covid: how bad is the second wave?," Article 2021.

[179] M. Scudellari, "How the pandemic might play out in 2021 and beyond," *Nature,* Article vol. 584, no. 7819, pp. 22-25, 2020, doi: 10.1038/d41586-020-02278-5.

[180] N. Zhu *et al.*, "A novel coronavirus from patients with pneumonia in China, 2019," *New England Journal of Medicine,* Article vol. 382, no. 8, pp. 727-733, 2020, doi: 10.1056/NEJMoa2001017.

[181] G. Mallach *et al.*, "Aerosol SARS-CoV-2 in hospitals and long-term care homes during the COVID-19 pandemic," *PLoS ONE,* Article vol. 16, no. 9 September, 2021, Art no. e0258151, doi: 10.1371/journal.pone.0258151.

[182] J. A. Lednicky *et al.*, "Isolation of SARS-CoV-2 from the air in a car driven by a COVID patient with mild illness," *International Journal of Infectious Diseases,* Article vol. 108, pp. 212-216, 2021, doi: 10.1016/j.ijid.2021.04.063.

[183] J. L. Santarpia *et al.*, "The size and culturability of patient-generated SARS-CoV-2 aerosol," *Journal of Exposure Science and Environmental Epidemiology,* Article vol. 32, no. 5, pp. 706-711, 2022, doi: 10.1038/s41370-021-00376-8.

[184] J. L. Santarpia *et al.*, "Aerosol and surface contamination of SARS-CoV-2 observed in quarantine and isolation care," *Scientific Reports,* Article vol. 10, no. 1, 2020, Art no. 12732, doi: 10.1038/s41598-020-69286-3.

[185] B. U. Lee, "Minimum sizes of respiratory particles carrying SARS-CoV-2 and the possibility of aerosol generation," *International Journal of Environmental Research and Public Health,* Review vol. 17, no. 19, pp. 1-8, 2020, Art no. 6960, doi: 10.3390/ijerph17196960.

[186] G. Buonanno, L. Stabile, and L. Morawska, "Estimation of airborne viral emission: Quanta emission rate of SARS-CoV-2 for infection risk assessment," *Environment International,* Article vol. 141, 2020, Art no. 105794, doi: 10.1016/j.envint.2020.105794.

[187] L. Morawska *et al.*, "How can airborne transmission of COVID-19 indoors be minimised?," *Environment International,* Letter vol. 142, 2020, Art no. 105832, doi: 10.1016/j.envint.2020.105832.

[188] J. W. Tang *et al.*, "Dismantling myths on the airborne transmission of severe acute respiratory syndrome coronavirus-2 (SARS-CoV-2)," *Journal of Hospital Infection,* Review vol. 110, pp. 89-96, 2021, doi: 10.1016/j.jhin.2020.12.022.

[189] M. Kapsalaki, "ASHRAE Resources Available to Address COVID-19 Concerns," 2020.

[190] M. Kapsalaki, "AIVC Newsletter, Special Issue COVID-19, July 2021," 2021.

[191] ASHRAE, "GUIDANCE FOR RE-OPENING BUILDINGS," *GUIDANCE FOR RE-OPENING BUILDINGS,* Article 2021.

[192]   J. Kurnitski, F. Franchimon, and J. Hogeling, "How to Operate and Use Building Services in Order to Prevent the Spread of the Coronavirus Disease (COVID-19) in Workplaces," *REHVA,* Article vol. 2020, 2020.

[193]   "ISO 16890-1:2016 Air filters for general ventilation. Technical specifications, requirements and classification system based upon particulate matter efficiency (ePM)," Article vol. 1, pp. 1-27, 2016.

[194]   V. W. Group, "Support Document for the Advisory Committee onCOVID-19 Transmission in School and Healthcare Environments and on the Role of Ventilation," 2021.

[195]   Z. Peng *et al.*, "Practical Indicators for Risk of Airborne Transmission in Shared Indoor Environments and Their Application to COVID-19 Outbreaks," *Environmental Science and Technology,* Article vol. 56, no. 2, pp. 1125-1137, 2022, doi: 10.1021/acs.est.1c06531.

[196]   J. Lelieveld *et al.*, "Aerosol transmission of COVID-19 and infection risk in indoor environments," *MedRxiv,* Article 2020.

[197]   J. Zhang, "Integrating IAQ control strategies to reduce the risk of asymptomatic SARS CoV-2 infections in classrooms and open plan offices," *Science and Technology for the Built Environment,* Editorial pp. 1013-1018, 2020, doi: 10.1080/23744731.2020.1794499.

[198]   C. Sun and Z. Zhai, "The efficacy of social distance and ventilation effectiveness in preventing COVID-19 transmission," *Sustainable Cities and Society,* Article vol. 62, 2020, Art no. 102390, doi: 10.1016/j.scs.2020.102390.

[199]   J. Shen, M. Kong, B. Dong, M. J. Birnkrant, and J. Zhang, "A systematic approach to estimating the effectiveness of multi-scale IAQ strategies for reducing the risk of airborne infection of SARS-CoV-2," *Building and Environment,* Article vol. 200, 2021, Art no. 107926, doi: 10.1016/j.buildenv.2021.107926.

[200]   M. E. Dubuis *et al.*, "High and low flowrate sampling of airborne influenza in hospital rooms during three outbreaks," *Journal of Aerosol Science,* Article vol. 158, 2021, Art no. 105824, doi: 10.1016/j.jaerosci.2021.105824.

[201]   T. Han *et al.*, "COVID-19 Cluster Linked to Aerosol Transmission of SARS-CoV-2 via Floor Drains," *Journal of Infectious Diseases,* Article vol. 225, no. 9, pp. 1554-1560, 2022, doi: 10.1093/infdis/jiab598.

[202]   "Coronavirus: How infected air can flow from one apartment to another." https://elpais.com/especiales/coronavirus-covid-19/how-infected-air-can-flow-from-one-apartment-to-another/ (accessed April 13, 2022).

[203]   S. J. Emmerich, D. Heinzerling, J. I. Choi, and A. K. Persily, "Multizone modeling of strategies to reduce the spread of airborne infectious agents in healthcare facilities," *Building and Environment,* Article vol. 60, pp. 105-115, 2013, doi: 10.1016/j.buildenv.2012.11.013.

[204]   L. F. Pease *et al.*, "Investigation of potential aerosol transmission and infectivity of SARS-CoV-2 through central ventilation systems," *Building and Environment,* vol. 197, 2021, Art no. 107633, doi: 10.1016/j.buildenv.2021.107633.

[205]   P. Shrestha, J. W. DeGraw, M. Zhang, and X. Liu, "Multizonal modeling of SARS-CoV-2 aerosol dispersion in a virtual office building," *Building and Environment,* Article vol. 206, 2021, Art no. 108347, doi: 10.1016/j.buildenv.2021.108347.

[206]   J. Guo, J. Liu, D. Tu, J. Zhang, J. Xu, and P. Xue, "Multizone modeling of pressure difference control analyses for an infectious disease hospital," *Building and Environment,* Article vol. 206, 2021, Art no. 108341, doi: 10.1016/j.buildenv.2021.108341.

[207]   C. A. Faulkner, J. E. Castellini, W. Zuo, D. M. Lorenzetti, and M. D. Sohn, "Investigation of HVAC operation strategies for office buildings during COVID-19 pandemic," *Building and Environment,*

Article vol. 207, 2022, Art no. 108519, doi: 10.1016/j.buildenv.2021.108519.

[208]   M. López-García, M. F. King, and C. J. Noakes, "A Multicompartment SIS Stochastic Model with Zonal Ventilation for the Spread of Nosocomial Infections: Detection, Outbreak Management, and Infection Control," *Risk Analysis,* Article vol. 39, no. 8, pp. 1825-1842, 2019, doi: 10.1111/risa.13300.

[209]   W. S. Dols and B. J. Polidoro, "CONTAM User Guide and Program Documentation – Version 3.2," *CONTAM User Guide and Program Documentation Version 3.2,* Article 2015.

[210]   "EnergyPlus Engineering Reference, Washington," *EnergyPlus Engineering Reference,* Article 2012.

[211]   G. N. Walton, "AIRNET – a computer program for building airflow network modeling," *AIRNET - A Computer Program for Building Airflow Network Modeling,* Article 1989.

[212]   H. E. Feustel, "COMIS-an international multizone air-flow and contaminant transport model," *Energy and Buildings,* Article vol. 30, no. 1, pp. 3-18, 1999, doi: 10.1016/S0378-7788(98)00043-7.

[213]   W. S. Dols, B. J. Polidoro, D. G. Poppendieck, and S. J. Emmerich, "Tool to Model the Fate and Transport of Indoor Microbiological Aerosols (FaTIMA)," *NIST Technical Note 2095 A Tool to Model the Fate and Transport of Indoor Microbiological Aerosols (FaTIMA),* Article 2020.

[214]   L. Wang, W. S. Dols, and Q. Chen, "Using CFD capabilities of CONTAM 3.0 for simulating airflow and contaminant transport in and around buildings," *HVAC and R Research,* Article vol. 16, no. 6, pp. 749-763, 2010, doi: 10.1080/10789669.2010.10390932.

[215]   L. Wang and Q. Chen, "Validation of a coupled multizone-CFD program for building airflow and contaminant transport simulations," *HVAC and R Research,* Article vol. 13, no. 2, pp. 267-281, 2007, doi: 10.1080/10789669.2007.10390954.

[216]   W. F. Wells, "Airborne contagion and air hygiene: An ecological study of droplet infections," *JAMA,* Article vol. 159, no. 1, 1955.

[217]   T. L. Thatcher, A. C. K. Lai, R. Moreno-Jackson, R. G. Sextro, and W. W. Nazaroff, "Effects of room furnishings and air speed on particle deposition rates indoors," *Atmospheric Environment,* Article vol. 36, no. 11, pp. 1811-1819, 2002, doi: 10.1016/S1352-2310(02)00157-7.

[218]   N. Van Doremalen *et al.*, "Aerosol and surface stability of SARS-CoV-2 as compared with SARS-CoV-1," *New England Journal of Medicine,* Letter vol. 382, no. 16, pp. 1564-1567, 2020, doi: 10.1056/NEJMc2004973.

[219]   G. R. Johnson *et al.*, "Modality of human expired aerosol size distributions," *Journal of Aerosol Science,* Article vol. 42, no. 12, pp. 839-851, 2011, doi: 10.1016/j.jaerosci.2011.07.009.

[220]   "Methods of Testing General Ventilation Air-Cleaning Devices for Removal Efficiency by Particle Size," *Method of Testing General Ventilation Air-Cleaning Devices for Removal Efficiency by Particle Size,* Article 2018.

[221]   S. Miller-Leiden, C. Lohascio, W. W. Nazaroff, and J. M. Macher, "Effectiveness of In-Room Air Filtration and Dilution Ventilation for Tuberculosis Infection Control," *Journal of the Air and Waste Management Association,* Article vol. 46, no. 9, pp. 869-882, 1996, doi: 10.1080/10473289.1996.10467523.

[222]   "Commercial Prototype Building Models | Building Energy Codes Program, U.S. Dep. Energy," Article 2013.

[223]   A. ASHRAE, "Standard 62.1-2013 Ventilation for acceptable indoor air quality," *American Society of Heating, Refrigerating and Air-Conditioning Engineers, Inc., Atlanta, GA,* vol. 40, 2013.

[224]   S. N. Rudnick and D. K. Milton, "Risk of indoor airborne infection transmission estimated from carbon dioxide concentration," *Indoor Air,* Article vol. 13, no. 3, pp. 237-245, 2003, doi: 10.1034/j.1600-

0668.2003.00189.x.

[225]   T. Moreno *et al.*, "Tracing surface and airborne SARS-CoV-2 RNA inside public buses and subway trains," *Environment International,* Article vol. 147, 2021, Art no. 106326, doi: 10.1016/j.envint.2020.106326.

[226]   L. Ng, A. Musser, A. Persily, and S. Emmerich, "Airflow and Indoor Air Quality Models of DOE Prototype Commercial Buildings," ed: Technical Note (NIST TN), National Institute of Standards and Technology, Gaithersburg, MD, 2019.

[227]   A. ASHRAE, "Standard 90.1-2013 Energy Standard for Buildings except Low-Rise Residential Buildings," *American Society of Heating, Refrigerating and Air-Conditioning Engineers, Inc., Atlanta, GA,* vol. 40, 2013.

[228]   B. Polidoro, L. C. Ng, W. S. Dols, and S. J. Emmerich, "NIST Technical Note 1873: CONTAM To EnergyPlus Infiltration Features of the CONTAM Results Export Tool," Article 2015.

[229]   L. C. Ng, A. Musser, S. J. Emmerich, and A. K. Persily, "Airflow and Indoor Air Quality Models of DOE Reference Commercial Buildings," *Airflow and Indoor Air Quality Models of DOE Reference Commercial Buildings,* Article 2012.

[230]   *Exposure Factors Handbook,* Article 2011.

[231]   E. Diapouli, A. Chaloulakou, and P. Koutrakis, "Estimating the concentration of indoor particles of outdoor origin: A review," *Journal of the Air and Waste Management Association,* Article vol. 63, no. 10, pp. 1113-1129, 2013, doi: 10.1080/10962247.2013.791649.

[232]   S. L. Miller and J. M. MacHer, "Evaluation of a Methodology for Quantifying the Effect of Room Air Ultraviolet Germicidal Irradiation on Airborne Bacteria," *Aerosol Science and Technology,* vol. 33, no. 3, pp. 274-295, 2000/09/01 2000, doi: 10.1080/027868200416259.

[233]   E. Kujundzic, M. Hernandez, and S. L. Miller, "Ultraviolet germicidal irradiation inactivation of airborne fungal spores and bacteria in upper-room air and HVAC in-duct configurations," *Journal of Environmental Engineering and Science,* vol. 6, no. 1, pp. 1-9, 2007.

[234]   J. Pan, C. Harb, W. Leng, and L. C. Marr, "Inward and outward effectiveness of cloth masks, a surgical mask, and a face shield," *Aerosol Science and Technology,* Article vol. 55, no. 6, pp. 718-733, 2021, doi: 10.1080/02786826.2021.1890687.

[235]   J. L. Jimenez and et al., "2020_COVID-19_Aerosol_Transmission_Estimator - Google Sheets," ed, 2020.

[236]   H. Qian, T. Miao, L. Liu, X. Zheng, D. Luo, and Y. Li, "Indoor transmission of SARS-CoV-2," *Indoor Air,* Article vol. 31, no. 3, pp. 639-645, 2021, doi: 10.1111/ina.12766.

[237]   D. Weissberg *et al.*, "Does respiratory co-infection facilitate dispersal of SARS-CoV-2? investigation of a super-spreading event in an open-space office," *Antimicrobial Resistance and Infection Control,* Article vol. 9, no. 1, 2020, Art no. 191, doi: 10.1186/s13756-020-00861-z.

[238]   B. Atkinson *et al.*, "An outbreak of SARS-CoV-2 in a public-facing office in England, 2021," *MedRxiv,* Article 2022.

[239]   B. L. Augenbraun *et al.*, "Assessment and mitigation of aerosol airborne SARS-CoV-2 transmission in laboratory and office environments," *Journal of Occupational and Environmental Hygiene,* Article vol. 17, no. 10, pp. 447-456, 2020, doi: 10.1080/15459624.2020.1805117.

[240]   S. L. Miller *et al.*, "Transmission of SARS-CoV-2 by inhalation of respiratory aerosol in the Skagit Valley Chorale superspreading event," *Indoor Air,* Article 2020.

[241]   L. Comber *et al.*, "Airborne transmission of SARS-CoV-2 via aerosols," *Reviews in Medical Virology,* vol. 31, no. 3, 2021, Art no. e2184, doi: 10.1002/rmv.2184.

[242] "Omicron Variant: What You Need to Know." Centers for Disease Control and Prevention. https://www.cdc.gov/coronavirus/2019-ncov/variants/omicron-variant.html (accessed 01/10, 2022).

[243] "Map of COVID-19 case trends and restrictions." USATODAY. https://www.usatoday.com/storytelling/coronavirus-reopening-america-map/ (accessed 03/18, 2022).

[244] "COVID-19 Restrictions Easing Next Week, Fully Lifted on March 21." https://novascotia.ca/news/release/?id=20220223008 (accessed 03/18, 2022).

[245] "COVID-19 in Europe: England ends all restrictions and removes isolation rule." https://www.euronews.com/2022/02/23/covid-19-in-europe-italy-to-end-state-of-emergency-and-ease-restrictions-in-april (accessed 03/18, 2022).

[246] J. Kurnitski *et al.*, "Respiratory infection risk-based ventilation design method," *Building and Environment,* vol. 206, p. 108387, 2021.

[247] Y. Li *et al.*, "Role of ventilation in airborne transmission of infectious agents in the built environment–a multidisciplinary systematic review," *Indoor air,* vol. 17, no. 1, 2007.

[248] L. Stabile, A. Pacitto, A. Mikszewski, L. Morawska, and G. Buonanno, "Ventilation procedures to minimize the airborne transmission of viruses in classrooms," *Building and Environment,* vol. 202, p. 108042, 2021/09/01/ 2021, doi: https://doi.org/10.1016/j.buildenv.2021.108042.

[249] M. Bertone *et al.*, "Assessment of SARS-CoV-2 airborne infection transmission risk in public buses," *Geoscience Frontiers,* vol. 13, no. 6, 2022, Art no. 101398, doi: 10.1016/j.gsf.2022.101398.

[250] M. Kennedy, S. J. Lee, and M. Epstein, "Modeling aerosol transmission of SARS-CoV-2 in multi-room facility," *Journal of Loss Prevention in the Process Industries,* vol. 69, 2021, Art no. 104336, doi: 10.1016/j.jlp.2020.104336.

[251] Z. J. Cotman, M. J. Bowden, B. P. Richter, J. H. Phelps, and C. J. Dibble, "Factors affecting aerosol SARS-CoV-2 transmission via HVAC systems; a modeling study," *PLoS Computational Biology,* vol. 17, no. 10, 2021, Art no. e1009474, doi: 10.1371/journal.pcbi.1009474.

[252] E. J. Stewart *et al.*, "ASHRAE position document on infectious aerosols," *ASHRAE: Atlanta, GA, USA,* 2020.

[253] Rehva, "REHVA COVID-19 Guidance Document," *REHVA COVID-19 guidance document,* 2020.

[254] J. W. Axley, "Multi-zone dispersal analysis by element assembly," *Building and Environment,* vol. 24, no. 2, pp. 113-130, 1989.

[255] Y. Li, S. Duan, I. Yu, and T. Wong, "Multi-zone modeling of probable SARS virus transmission by airflow between flats in Block E, Amoy Gardens," *Indoor air,* vol. 15, no. 2, pp. 96-111, 2005.

[256] M. Deru *et al.*, "US department of energy commercial reference building models of the national building stock," *U.S. Department of Energy Commercial Reference Building Models of the National Building Stock,* Article 2015.

[257] S. Yan, L. Wang, M. J. Birnkrant, J. Zhai, and S. L. Miller, "Evaluating SARS-CoV-2 airborne quanta transmission and exposure risk in a mechanically ventilated multizone office building," *Building and Environment,* vol. 219, p. 109184, 2022/07/01/ 2022, doi: https://doi.org/10.1016/j.buildenv.2022.109184.

[258] A. Aganovic, Y. Bi, G. Cao, F. Drangsholt, J. Kurnitski, and P. Wargocki, "Estimating the impact of indoor relative humidity on SARS-CoV-2 airborne transmission risk using a new modification of the Wells-Riley model," *Building and Environment,* vol. 205, 2021, Art no. 108278, doi: 10.1016/j.buildenv.2021.108278.

[259] S. Yan, L. L. Wang, M. J. Birnkrant, J. Zhai, and S. L. Miller, "Evaluating SARS-CoV-2 airborne quanta

transmission and exposure risk in a mechanically ventilated multizone office building," *Building and Environment,* vol. 219, 2022, Art no. 109184, doi: 10.1016/j.buildenv.2022.109184.

[260] W. F. Wells, "Airborne Contagion and Air Hygiene. An Ecological Study of Droplet Infections," *Airborne Contagion and Air Hygiene. An Ecological Study of Droplet Infections.,* 1955.

[261] A. Aganovic, Y. Bi, G. Cao, F. Drangsholt, J. Kurnitski, and P. Wargocki, "Estimating the impact of indoor relative humidity on SARS-CoV-2 airborne transmission risk using a new modification of the Wells-Riley model," *Building and environment,* vol. 205, p. 108278, 2021.

[262] M. Deru *et al.*, "US Department of Energy commercial reference building models of the national building stock," 2011.

[263] L. C. Ng, A. Musser, A. K. Persily, and S. J. Emmerich, "Airflow and indoor air quality models of DOE reference commercial buildings," *Gaithersburg, MD, National Institute of Standards and Technology,* vol. 163, 2012.

[264] G. Buonanno, L. Morawska, and L. Stabile, "Quantitative assessment of the risk of airborne transmission of SARS-CoV-2 infection: Prospective and retrospective applications," *Environment International,* Article vol. 145, 2020, Art no. 106112, doi: 10.1016/j.envint.2020.106112.

[265] Y. Liu *et al.*, "Aerodynamic analysis of SARS-CoV-2 in two Wuhan hospitals," *Nature,* vol. 582, no. 7813, pp. 557-560, 2020/06/01 2020, doi: 10.1038/s41586-020-2271-3.

[266] *Method of Testing General Ventilation Air-Cleaning Devices for Removal Efficiency by Particle Size*, N. T. Committee, NAFA Technical Committee, 2018.

[267] S. Miller-Leiden, C. Lohascio, W. W. Nazaroff, and J. M. Macher, "Effectiveness of In-Room Air Filtration and Dilution Ventilation for Tuberculosis Infection Control," *Journal of the Air & Waste Management Association,* vol. 46, no. 9, pp. 869-882, 1996/09/01 1996, doi: 10.1080/10473289.1996.10467523.

[268] *U.S.EPA.Exposure Factors Handbook 2011 Edition (Final Report)*, Washington, DC, EPA/600/R-09/052F,2011.

[269] D. K. W. Chu *et al.*, "SARS-CoV-2 Superspread in Fitness Center, Hong Kong, China, March 2021," (in eng), *Emerging infectious diseases,* vol. 27, no. 8, pp. 2230-2232, 2021, doi: 10.3201/eid2708.210833.

[270] Y. Li *et al.*, "Probable airborne transmission of SARS-CoV-2 in a poorly ventilated restaurant," *Building and Environment,* vol. 196, p. 107788, 2021/06/01/ 2021, doi: https://doi.org/10.1016/j.buildenv.2021.107788.

[271] ASHRAE, "ASHRAE Position Document on Infectious Aerosols," 2020.

[272] Y. Shen *et al.*, "Community Outbreak Investigation of SARS-CoV-2 Transmission among Bus Riders in Eastern China," *JAMA Internal Medicine,* Article vol. 180, no. 12, pp. 1665-1671, 2020, doi: 10.1001/jamainternmed.2020.5225.

[273] S. J. Emmerich, D. Heinzerling, J.-i. Choi, and A. K. Persily, "Multizone modeling of strategies to reduce the spread of airborne infectious agents in healthcare facilities," *Building and Environment,* vol. 60, pp. 105-115, 2013.

[274] L. Wang and Q. Chen, "Validation of a coupled multizone-CFD program for building airflow and contaminant transport simulations," *HVAC&R Research,* vol. 13, no. 2, pp. 267-281, 2007.

[275] "WHO Coronavirus (COVID-19) dashboard " World Health Organization 2023 data. https://data.who.int/dashboards/covid19/data (accessed April 7, 2024).

[276] Y. Wang *et al.*, "Characterization of an Asymptomatic Cohort of Severe Acute Respiratory Syndrome Coronavirus 2 (SARS-CoV-2) Infected Individuals Outside of Wuhan, China," *Clinical Infectious*

Diseases, Article vol. 71, no. 16, pp. 2132-2138, 2020, doi: 10.1093/cid/ciaa629.

[277] I. Garg, R. Shekhar, A. B. Sheikh, and S. Pal, "Impact of COVID-19 on the changing patterns of respiratory syncytial virus infections," *Infectious Disease Reports,* vol. 14, no. 4, pp. 558-568, 2022.

[278] L. Chatzidiakou, D. Mumovic, and A. J. Summerfield, "What do we know about indoor air quality in school classrooms? A critical review of the literature," *Intelligent Buildings International,* vol. 4, no. 4, pp. 228-259, 2012.

[279] *Ventilation and Acceptable Indoor Air Quality*, ASHRAE-62.1, 2022.

[280] A. Persily, "Development and application of an indoor carbon dioxide metric," *Indoor Air,* vol. 32, no. 7, p. e13059, 2022.

[281] M. St-Jean *et al.*, "Indoor air quality in Montréal area day-care centres, Canada," *Environmental Research,* vol. 118, pp. 1-7, 2012/10/01/ 2012, doi: https://doi.org/10.1016/j.envres.2012.07.001.

[282] M. M. Andamon, P. Rajagopalan, and J. Woo, "Evaluation of ventilation in Australian school classrooms using long-term indoor CO2 concentration measurements," *Building and Environment,* vol. 237, p. 110313, 2023/06/01/ 2023, doi: https://doi.org/10.1016/j.buildenv.2023.110313.

[283] J. Lofaro. "Education ministry says 90,000 CO2 readers to be installed in classrooms across Quebec." CTVNewsMontreal. https://montreal.ctvnews.ca/education-ministry-says-90-000-co2-readers-to-be-installed-in-classrooms-across-quebec-1.5581304 (accessed 04/16, 2024).

[284] S. Batterman, "Review and extension of CO2-based methods to determine ventilation rates with application to school classrooms," *International journal of environmental research and public health,* vol. 14, no. 2, p. 145, 2017.

[285] B. K. Øksendal, *Stochastic differential equations : an introduction with applications*, 6th , corr. ed. (Universitext). Berlin ;: Springer, 2007.

[286] S. Madhira and S. Deshmukh, "Brownian Motion Process," in *Introduction to Stochastic Processes Using R*: Springer, 2023, pp. 487-545.

[287] X. Mao, "The truncated Euler–Maruyama method for stochastic differential equations," *Journal of Computational and Applied Mathematics,* vol. 290, pp. 370-384, 2015.

[288] A. Gelman, J. B. Carlin, H. S. Stern, and D. B. Rubin, *Bayesian data analysis*. Chapman and Hall/CRC, 1995.

[289] J. Rockström *et al.*, "Planetary Boundaries Exploring the Safe Operating Space for Humanity," *Ecology and Society,* vol. 14, no. 2, 2009. [Online]. Available: http://www.jstor.org/stable/26268316.

[290] A. Patil, D. Huard, and C. J. Fonnesbeck, "PyMC: Bayesian stochastic modelling in Python," *Journal of statistical software,* vol. 35, no. 4, p. 1, 2010.

[291] *Thermal environmental conditions for human occupancy*, ASHRAE-55, 2023.

[292] *Control of Infectious Aerosols*, ASHRAE-241, 2023.

[293] S. Yan, L. Wang, M. J. Birnkrant, Z. Zhai, and S. L. Miller, "Multizone Modeling of Airborne SARS-CoV-2 Quanta Transmission and Infection Mitigation Strategies in Office, Hotel, Retail, and School Buildings," *Buildings*, vol. 13, no. 1, doi: 10.3390/buildings13010102.

[294] J. Jimenez, "2020_COVID-19_Aerosol_Transmission_Estimator-Google Sheets. 2020," ed, 2020.

[295] J. Kurnitski, "COVID-19 Ventilation Calculator V2.1," REHVA, 2020.

[296] W. S. Dols, B. Polidoro, D. Poppendieck, and S. J. Emmerich, "A tool to model the Fate and Transport of Indoor Microbiological Aerosols (FaTIMA)," 2020.